Summer 9-1-2014

DAPK3 Suppresses Mammary Acini Morphogenesis and is Required for Mouse Development

Brandon Kocher
Washington University in St. Louis

WASHINGTON UNIVERSITY IN ST. LOUIS

Division of Biology and Biomedical Sciences
Molecular Cell Biology

Dissertation Examination Committee:
David Piwnica-Worms, Chair
Deborah Novack, Co-chair
David Denardo
Fanxin Long
Sheila Stewart
Zhongsheng You

DAPK3 Suppresses Mammary Acini Morphogenesis and is Required for Mouse Development

by

Brandon Anthony Miller Kocher

A dissertation presented to the
Graduate School of Arts and Sciences
of Washington University
in partial fulfillment of the
requirements for the degree
of Doctor of Philosophy

August 2014

St Louis, Missouri

TABLE OF CONTENTS

LIST OF FIGURES

LIST OF TABLES

ACKNOWLEDGEMENTS

Throughout my graduate career I have had the pleasure of being surrounded by a collection of truly wonderful people and scientists. I'd like to thank Dr. David Piwnica-Worms for his mentorship, guidance and overall scientific insight and support. My projects have taken many twists and turns and I greatly appreciate his everlasting encouragement, criticisms and optimism. I want to thank my many lab mates, past and present, for their many discussions and years of friendship. I want to also thank many members of the BRIGHT Institute for their technical assistance, expertise and input. I'd also like to thank my family and friends for supporting my curiosity and passion for science. Finally, I want to thank my wife for her sacrifices, love and support.

ABSTRACT OF DISSERTATION

DAPK3 Suppresses Mammary Acini Morphogenesis and is Required for Mouse Development

by

Brandon Anthony Miller Kocher

Doctor of Philosophy in Biological and Biomedical Sciences

Molecular Cell Biology

Washington University in Saint Louis, 2014

Dr. David Piwnica-Worms, Chairperson

Over the past decade several lines of research have indicated that DAPK3, a member of the serine/threonine death associated protein kinase (DAPK) family, plays an important role in various signaling pathways important to tissue homeostasis and mammalian biology. Considered to be a putative tumor suppressor, the molecular mechanisms by which DAPK3 exerts its tumor suppressor functions are not fully understood. Furthermore, unlike other DAPK family members, DAPK3 has received little attention regarding its physiological roles *in vivo* due to the lack of knockout animals. To address these gaps in our fundamental understanding of DAPK3 we utilized the MCF10A 3D tumorigenesis model *in vitro* and generated a constitutive DAPK3 knockout mouse. Using the MCF10A 3D morphogenesis model we identified that loss of DAPK3 through lenti-viral mediated knockdown accelerates MCF10A acini proliferation and apoptosis while maintaining acini polarity relative to negative control. Furthermore, depletion of DAPK3 leads to enhanced growth factor–dependent mTOR activation and enlarged DAPK3 structures are uniquely sensitive to low doses of rapamycin treatment compared to negative control. Simultaneous knockdown of RAPTOR (a key mTORC1 component) rescues the

augmented acinar size in DAPK3 depleted structures indicating an epistatic interaction. To identify the overall physiological contribution of DAPK3 we generated a constitutive DAPK3 knockout mouse using a gene trap embryonic stem cell line from the International Gene Trap Consortium. Described herein we have identified that DAPK3 is vital for early mouse development and that the Dapk3 promoter exhibits spatio-temporal activity in the developing heart and nervous system in addition to the gastrointestinal myenteric plexus of adult mice. Importantly, our data suggests that DAPK3 is expressed in the breast epithelia of adult mice and that potential ablation of *DAPK3* expression can facilitate the development of breast cancer as observed in primary patient biopsies. Our studies shed light on the growth inhibitory mechanisms of DAPK3 and provide direct evidence that DAPK3 plays an underappreciated role in mouse development, warranting further studies.

CHAPTER 1: INTRODUCTION

1.1 Death-associated protein kinase family (DAPK)

The death-associated protein kinase (DAPK) family is a relatively novel group of serine/ threonine kinases characterized by shared kinase domain homology as well as a pronounced cell death phenotypes upon overexpression. DAPK1, the prototypical family member, was first identified as a positive regulator of interferon gamma-induced cell death in HeLa cells using an anti-sense cDNA library screen (1). Additional studies indicated that the intrinsic cell death promoting activities of DAPK1 were dependent on its kinase activity; a characteristic soon found true for all DAPK family members (2). The DAPK family is phylogenetically related to the CaM-regulated kinases and includes 5 members: DAPK1, DAPK2 (DRP1), DAPK3 (ZIPK), DRAK1 (STK17A), and DRAK2 (STK17B) (**Figure 1.1**) (3). In addition to the similar overexpression phenotypes, the family is defined by amino acid sequence homology that exists between each member's N-terminal kinase domain. Despite similar kinase domains, family members differ drastically through the presence of additional regulatory domains. DAPK1 has a Ca^2+/ CaM regulatory domain, ankyrin repeats, a cytoskeletal binding and death domain. DAPK2 also contains a Ca^2+/ CaM regulator domain but lacks these additional domains similar to DAPK3, DRAK1 and 2. Overall, this family has diverse roles in inflammation, stress-response, muscle contraction, tumor suppression and cell death.

1.2 DAPK3

While DAPK1 has received the most attention regarding biochemical function and phenotypes, relatively little is known about DAPK3. DAPK3 shares 83% amino acid homology within its kinase domain but lacks the additionally regulatory domains observed in DAPK1. DAPK3 also contains three putative C-terminal nuclear localization signals in addition to a leucine zipper motif (**Figure 1.1)**. DAPK3 was first identified as an ATF4 interaction partner through a yeast two-hybrid screen using respective leucine zipper domains from a mouse cDNA library (4). The leucine zipper domain of DAPK3 is also required for homodimerization. Currently no clear regulation of DAPK3 endogenous activity has been determined. However, upon overexpression, DAPK3 and DAPK1 interact via their kinase domains resulting in trans-phosphorylation of DAPK3 by DAPK1 at various sites. This DAPK1-DAPK3 signaling cascade is required for the activation of a translational inhibitory gene expression program (5).

Functional DAPK3 studies are limited by the lack of a knockout mouse (constitutive or conditional knockout). One group reportedly attempted to generate a conditional DAPK3 knockout mouse but admitted its failure through personal communications (*Hagerty L & Haystead T. Unpublished Thesis Dissertation, 2007*). Commonly used model systems such as *Caenorhabditis elegans, Saccharomyces cerevisiae*, and *Drosophila melanogaster* lack clear DAPK3 orthologues, thereby hindering traditional genetic interrogation. Uncovering the physiological contributions of DAPK3 is crucial to understanding the relevancy of previous clinical and basic research observations. Furthermore, DAPK1 and DAPK3 inhibitors are currently under development for use in smooth muscle related disorders and a DAPK3 deficient

animal may indicate potentially deleterious phenotypes associated with loss of a functional DAPK3 protein (6,7).

Further hampering the functional understanding of DAPK3, many groups have published conflicting reports concerning the localization and respective molecular functions of DAPK3. One group of research indicates that ectopically expressed DAPK3 resides mainly within the cytoplasm and induces membrane blebbing, cell rounding and actin filament assembly (8,9). DAPK3 cytoplasmic subcellular localization has also been shown to correlate with its death inducing function in certain animal cell lines (3). These phenotypes have been attributed to DAPK3's direct phosphorylation of myosin light chain II (MLC) (8) and/ or GTP-dependent RhoD-mediated actin reorganization and actomyosin contraction (9). An additional cytoplasmic function of DAPK3 involves Ca^{2+} sensitization and smooth muscle contraction that is dependent on DAPK3 mediated phosphorylation of MLC and inactivation of smooth muscle myosin phosphatase (SMMP-1M) and CPI17 (7,10).

Contrasting with these cytoplasmic observations, other groups have indicated a nuclear specific localization and subsequent molecular action of DAPK3. Upon ectopic expression of DAPK3 by other groups, DAPK3 was observed to display nuclear localization with a 'speckled pattern' considered to be promyelocytic leukemia oncogenic bodies (PODs) (4,11–14). Subsequent research indicated that DAPK3 participates in the translocation of pro-cell death proteins DAXX (Fas death domain-associated protein) and PAR-4 (prostate apoptosis response-4) to PODs (13,15,16).

These discrepancies regarding DAPK3 subcellular localization and resulting overexpression phenotypes have recently been resolved. Through overexpression and sequence alignment studies in various cell lines *Shoval et al* revealed that ectopically expressed human and zebrafish DAPK3 resides in the cytoplasm while rat DAPK3 localizes specifically to the nucleus (17). Indeed, the majority of DAPK3 nuclear localization studies were performed using rat DAPK3 in established rat cell lines while cytoplasmic studies were performed using human DAPK3 in human cell lines such as HEK293T and HeLa. These studies shed light on additional questions regarding protein interaction partners. Rat DAPK3 was found to strongly interact with PAR-4 while human and zebrafish do not bind PAR-4. The authors also hypothesized that mouse DAPK3 is localized to the nucleus based upon amino acid sequence similarities but did not report any actual localization studies. These studies have identified a phylogenetic specific divergence for localization and potentially function of DAPK3 but questions still remain regarding the localization-dependent function of mouse DAPK3.

1.3 DAPK3 & Cancer

Two clear lines of research regarding DAPK3 related phenotypes exist: cell death and cytoskeletal regulation. From a fundamental cell biology perspective these cell death or 'tumor suppressive' observations are mainly inferred through ectopic expression of DAPK3 and other DAPK family members. Specifically, members of the DAPK family are considered to be involved in 'apoptotic' and/ or autophagy-related cell death programs with varying degrees of experimental support for each member. However, despite various reports regarding the role of DAPK members in autophagy (via LC3 punctate structures or processing) no additional

autophagy –rescue experiments (chemical or genetic) have been published that would satisfy the official Nomenclature Committee on Cell Death of 2012 (18). Additionally, notable discrepancies regarding their role in apoptosis exist, largely due to the old-world misinterpretation of ‘apoptotic’ cells displaying ‘characteristic apoptotic’ morphology. These ‘apoptotic morphologies’ include membrane blebbing (commonly observed in dividing, mobile and apoptotic cells) (19), loss of membrane integrity (20) and DNA condensation or fragmentation (sub G1 content). Ectopic overexpression of DAPK1 or DAPK3 does not lead to caspase-dependent apoptosis as seen by the lack of apoptotic caspase activation and PARP cleavage, but DNA degradation has been observed (21–23). Collectively, these results suggest that overexpression of DAPK1/ DAPK3 causes a form of cell death similar to caspase-independent or necrotic cell death as cells detach and lose membrane integrity. Since the majority of exploratory DAPK-mediated cell death experiments have occurred in the context of ectopic overexpression, it is possible that the observed cell death is secondary to cell detachment due to forced cytoskeletal contraction and rearrangement. Indeed, it is well known that various members of the DAPK family participate in cytoskeletal dynamics through phosphorylation and direct interaction with MLC, ROCK1, RhoD, MLCK, and CPI-17 (3). However, notable biochemical features of anoikis as determined by the Nomenclature Committee on Cell Death of 2012, such as caspase activation, are not observed in ectopic expression experiments. While the type of cell death observed upon ectopic expression of DAPK3 remains to be determined, several clinical observations suggest these growth inhibitory properties are inactivated in various cancers.

Alterations within the *DAPK3* coding sequence and its expression have been observed in several types of cancers prompting investigation into the tumor suppressive mechanisms of DAPK3. Heterozygous *loss-of-function* mutations were identified in various cancers that influenced cell survival, proliferation, aggregation and chemotherapy resistance (23). Additionally, reduced *DAPK3* mRNA expression correlated with tumor invasion, metastasis and was a poor prognostic factor in a population of over 160 gastric cancer patients (24). These observations are not specific to gastric cancer as knockdown of DAPK3 increases proliferation of various malignant cell lines *in vitro* (23). Abrogation of *DAPK3* mRNA expression was shown to significantly decrease cisplatin sensitivity in lung cancer cell lines and its downregulation may impact overall survival of non-small cell lung cancer patients treated with platinum-based therapy (25). DAPK3 is also considered a potentially novel breast cancer gene as recurrent DAPK3 alterations were observed in BRCA1 mutant and BRCA-1 non-mutant breast cancers (26). Additionally, DAPK3 has been shown to interact with and/ or phosphorylate various proteins *in vitro* that are involved in cancer including ATF4, AATF, Daxx, Par-4, STAT3, NLK, and AR (4,14,27–32). These basic research and clinical observations have spurred further interest into defining the key molecular pathways regulated by DAPK3 in the hopes of identifying novel anti-cancer therapies.

These observations are not unique to DAPK3 and are similarly observed for DAPK1, the most well characterized tumor suppressor of the DAPK family. Originally identified as a potential mediator of interferon gamma -induced cell death, DAPK1 has since been regarded as a *bona fide* tumor suppressor in large part through the efforts of the Dr. Adi Kimchi Lab (1). It was first posited that DAPK1 is a tumor suppressor after identification of non-existent DAPK1

protein expression in various human cancer cell lines that could be partially restored by DNA demethylation (33). Since these initial studies it has been shown that DAPK1 ectopic expression can reduce metastasis and soft agar colony formation (34). Others have shown that DAPK1 overexpression activates p19ARF/p53 dependent 'apoptosis' in a kinase-dependent manner and that DAPK1 is required for p53 induction following oncogene activation (via overexpression of c-Myc and E2F-1) (35). Another group showed that *DAPK1* mRNA expression is induced upon DNA damage in a p53-dependent manner (36). Indeed, it appears that DAPK1 is mainly regulated through epigenetic repression of *DAPK1* mRNA expression via promoter hypermethylation. The *DAPK1* promoter is hypermethylated in various cancers including lung, bladder, head and neck, kidney, breast and B cell malignancies relative to normal tissues (37–42). Interestingly, despite these hypermethylation observations, several studies have shown that DAPK1 protein remains largely unaffected in certain patient cohorts (42). Given that no *loss-of-function* mutations have been reported for DAPK1, research performed to date indicates mRNA expression as a crucial means of regulating DAPK1 and potentially other DAPK members such as DAPK3.

1.4 The mTOR Pathway

My research has identified DAPK3 mediated inhibition of the mTOR pathway as a novel growth inhibitory or tumor suppressive mechanism and further discussion requires an introduction to the mTOR pathway.

The 'mechanistic target of rapamycin' or mTOR protein kinase was initially identified as a crucial mediator of the profound anti-proliferative effects exerted by rapamycin, a macrolide

produced by *Streptomyces hygroscopicus.* mTOR was first purified and determined to be a functional target of rapamycin in the early 1990s (43–45). Since its initial discovery the mTOR pathway has been implicated as a major regulator of cellular and tissue energy metabolism, growth and proliferation (46). As a member of the phosphoinositide 3-kinase (PI3K)-related kinase family, mTOR is considered to be an atypical serine/ threonine non-lipid protein kinase. mTOR interacts with a variety of protein binding partners and ultimately forms two distinct and massive protein complexes (mTORC1 and mTORC2) that respond to and regulate a diverse array of upstream and downstream signaling (**Figure 1.2**). Both complexes respond to a variety of stimuli and regulate a number of key processes including cell growth, metabolism autophagy and many other biologic programs.

The large mTORC1 and mTORC2 complexes are composed of a unique set of interaction partners that help regulate the diversity of functions controlled by the mTOR pathways. mTORC1 is comprised of six known subunits including the catalytic mTOR subunit, mammalian lethal with sec-12 protein 9 (mLST8/ GβL) (47), DEP domain containing mTOR-interacting protein (DEPTOR) (48), the scaffold protein complex Tti1/Tel2 (31), regulatory-associated protein of mammalian target of rapamycin (raptor) (49,50), and proline-rich Akt substrate 40 kDa (PRAS40) (51–54). Similarly, the relatively rapamycin insensitive mTORC2 shares mTOR, mLST8 (55), DEPTOR (48) and Tti1/ Tel2 (31) but differs through interactions with rapamycin-insensitive companion of mTOR (rictor) (55,56), mammalian stress-activated map kinase-interacting protein 1 (mSin1) (57,58) and protein observed with rictor 1 and 2 (protor1/2) (52,59,60). Rapamycin directly inhibits mTOR when it is associated with mTORC1 through allosteric kinase inhibition (61–63) and/ or structural disruption (49,64).

mTORC1 is the most well understood of the two mTOR complexes and it responds to a diversity of signals including growth factors, stress, energy status, oxygen and amino acids. Using the epidermal growth factor (EGF) pathway as a representative example, mTORC1 is activated by two major signaling pathways downstream of the EGF receptor (EGFR): PI3K-AKT and RAS-ERK (65). Extracellular binding of EGF to the receptor tyrosine kinase EGFR induces receptor homo- and/or heterodimerization of EGFR monomers resulting in cytoplasmic trans- and/ or autophosphorylation and subsequent activation of PI3K-AKT and RAS-ERK pathways. The initial stages of activation for both pathways involve proximity-based activation through phosphatidylinositol-phosphoinositide dependent kinase 1 (PDPK1) (66) and growth factor receptor-bound protein 2 (GRB2) -son of sevenless (SOS) for AKT and RAS-ERK, respectively (67). The effector components of both pathways ultimately converge on phosphorylation and inhibition of the tuberous sclerosis complex (TSC) which is made up of TSC1, TSC2 and Tre2-Bub2-Cdc16 (TBC) 1 domain family member 7 (TBC1D7). This effectively activates mTORC1 through an as of yet not well understood mechanism (68).

Once activated, downstream components of mTORC1 signaling regulate cell growth (cell mass), macromolecular biosynthesis, autophagy, and cell cycle progression. mTORC1 regulation of protein synthesis is the most fundamental and well understood mechanism by which mTORC1 influences these multiple cell processes. Once activated, mTORC1 directly phosphorylates two key protein translational and synthesis regulators: eukaryotic initiation factor 4E-binding protein 1 (4E-BP1) and S6 kinase (S6K) (69). Overall, regulation of these components ultimately controls translation of key transcripts involved in ribosome biogenesis, cell cycle, anti-apoptosis, metastasis, angiogenesis and glycolysis. mTORC1 mediated

phosphorylation of 4E-BP1 prevents it from inhibiting the assembly of eIF4E at the 5' mRNA cap thereby effectively facilitating the formation of the pre-initiation complex at the ribosome. mTORC1 initiates S6K activation through phosphorylation of T389 which creates a docking site for PDPK1 allowing it to phosphorylate S6K at T229 (69). Once activated by mTORC1, S6K phosphorylates a variety of translational regulator substrates including eukaryotic elongation factor 2 kinase (eEF2K), S6 Aly/ REF-like target (SKAR) and ribosomal protein S6 (S6) which ultimately facilitates translation initiation and elongation (70). An increase in the translation of cell cycle progression, ribosomal protein and translational elongation factor mRNA transcripts correlates with the phosphorylation of S6 (71). Interestingly, primary mouse embryonic fibroblasts (MEFs) produced from mice with homozygous knock-in S->A mutations at key S6 phosphorylation sites, display decreased cell size but augmented protein synthesis and cell division (72). Moreover, MEFs produced from mice devoid of all three 4E-BPs (1-3) display increased proliferation (73). While these observations suggest S6 positively regulates cell growth and 4E-BPs negatively regulate proliferation, it is generally accepted that phosphorylation of 4E-BP1 and S6K-S6 serve as representative mTORC1 specific markers. And, that these markers are indicative of other mTORC1 specific translational programs that might be directly involved in the regulation of proliferation and cell growth, independent of these markers. Indeed, it is anticipated that phospho-S6 and phospho-4E-BP1 will serve as pharmacodynamic markers for mTORC1 activity in oncology clinical trials (74).

While much is known about mTORC1, only a handful of studies in the past 10 years have shed light on the mTORC2 pathway. mTORC2 integrates signals mainly from growth factors to control cell metabolism, cytoskeletal organization and cell survival. mTORC2 activates several

members of the AGC subfamily of kinases (AKT, and SGK1 or serum-and glucocorticoid-induced protein kinase 1) thereby regulating the phosphorylation of forkhead box O1/3a (FoxO1/3a) and the subsequent transcription of genes required for metabolism, cell cycle arrest and apoptosis (75,76). mTORC2 also activates protein kinase C-α (PKC-α) thereby playing a pivotal role in cell shape and actin cytoskeleton dynamics (55,56).

1.5 mTOR & Cancer

Pre-clinical and clinical observations indicate that mTORC1 and 2 are crucial for the development of cancer and as such have become attractive anti-cancer targets. Activating mutations in PI3K or deletion of the PI3K inhibitory protein, phosphatase and tensin homologue (PTEN), are commonly observed in human cancer resulting in hyperactivation of mTOR and AKT (77). Several negative regulators of the mTOR pathway are *bona fide* tumor suppressors and are widely deregulated in various human cancers. Inherited mutations in TSC1 and 2 causes tuberous sclerosis, a familial cancer that results in hamartomas and benign tumors in various organs (78). Conditional loss of TSC1 in the liver of mice results in hyperactive mTORC1 signaling and hepatocellular carcinoma, the development of which recapitulates human liver carcinogenesis (79). Another familial cancer syndrome, Peutz Jegher's syndrome, is caused by the loss of the tumor suppressor liver kinase B1 (LKB1) which results in the development of intestinal polyps and dramatically increases a patients risk for other cancers (80). LKB1 is deleted in 58% of lung cancers and is known to be a major negative regulator of mTORC1 signaling through AMPK mediated activation of the TSC complex (81).

Given these profound clinical oncology observations, mTOR inhibition has become a key therapeutic focus for anti-cancer therapies including combination therapy. This is supported by two recent studies that determined several tumors develop resistance to PI3K and BRAF inhibitors through mTORC1 signaling (82,83). Over the past decade rapamycin and several next-generation mTORC-specific inhibitors (rapalogues and mTOR kinase inhibitors) have witnessed improved clinical safety profiles but limited clinical efficacy (74). These targeted therapies have failed due to activation of compensatory mechanisms and partial inhibition of the mTORC2-AKT pathway (74). Interestingly, out of 750 human cancer samples only 3 mTOR activating mutations with functional significance have been identified (84). Indeed, many regulators of the mTORC1 pathway that promote growth factor-independent activation of mTORC1 are upregulated in 80% of human cancers (85). Collectively, this indicates that alternative strategies to effectively inhibiting the mTOR pathway are required

While many of the major regulators of the mTOR pathway have been elucidated, new regulators are continually being identified which will undoubtedly shed light on the complexities of the mTOR pathway, its many negative feedback loops and potentially new anti-cancer therapeutic targets. Taking a different approach, we hypothesize that rather than therapeutically inhibiting mTOR, an alternative strategy might include supporting the negative regulation of intrinsic mTOR-suppressive pathways.

1.6 DAPK and mTOR Pathway Interactions

As discussed above, the mTOR pathway is a critical regulator of various pathways found to be influenced by the DAPK family including proliferation, ‘autophagy’, survival, cell death

and cell cycle regulation. Interestingly, several members of the DAPK tumor suppressor family are known to regulate translation and regulate or be regulated by the mTOR pathway. Recent work has uncovered conflicting roles with regards to DAPK1-mediated regulation of the mTOR pathway. One group revealed that DAPK1 positively regulates mTOR activity through disruption of TSC1-TSC2 interactions (86). Another group revealed that DAPK1 negatively regulates protein translation through an inhibitory phosphorylation at S235/236 of S6 (87). However, research by *Roux et al.* revealed that phosphorylation of S235/236 on S6 by RSK actually promotes translation through enhanced assembly of the translational pre-initiation complex (88). DRAK2 was shown to phosphorylate S6K *in vitro* and play a functionally significant role in islet cell apoptosis (89). Overall, while some precedent exists, more work is required to identify and understand the functional connections between the DAPK family and mTOR regulation.

1.7 Three-Dimensional Cell Culture as a Powerful Model of Breast Cancer for Elucidating Novel DAPK3 Functions

It is clear that further research regarding the tumor suppressive functions of DAPK3 is warranted. Specifically, little is known about the functional tumor suppressive mechanisms regulated by DAPK3. Research on DAPK3 is further hampered by the lack of reliable immunohistochemical and immunofluorescence antibodies that can specifically recognize endogenous levels of mouse or human DAPK3 protein. These limitations are exacerbated by the lack of a knockout mouse model as well as inadequate cell culture models that cannot recapitulate the physiological context of tissue development or carcinogenesis.

Given these setbacks we have utilized a well-established three-dimensional (3D) *in vitro* epithelial tumor system that has been extensively used by other groups to study tumor suppressors and oncogenes. Studying tumor suppressors, such as DAPK3, in two-dimensional (2D) cell culture omits many of the complex external factors that are crucial to tissue homeostasis and carcinogenesis. Culturing cancer cells in or on an extracellular matrix (ECM) such as Matrigel (a protein mixture collected from Engelbreth-Holm-Swarm mouse sarcoma cells) or collagen supports the development of cell spheroids that closely resemble the architecture of glandular epithelial structures (90). 3D epithelial tumor structures form through coordinated series of biochemically-regulated events that are commonly deregulated in cancer including polarization, proliferation, survival, invasion, and apoptosis (**Figure 1.3 A**). Examining the relative contribution of tumor suppressor and oncogenes to the morphogenic phenotypes observed in 3D tumor systems serves as an accurate and approachable model for studying histopathological idiosyncrasies observed in human epithelial cancers *in vivo*. Furthermore, each structure represents a simplified tumor that can be studied and quantified in a relatively high throughput manner. Given the financial constraints of the current scientific research budget, the variability and still costly mouse models of cancer, 3D *in vitro* tumor systems are a highly attractive model for current basic cancer research.

One of the most well characterized 3D epithelial tumor systems utilizes the non-transformed, immortalized breast epithelial MCF10A cell line. When seeded as a single cell suspension atop solidified Matrigel, MCF10A cells eventually develop in to hollow acinar structures that cease to proliferate after 2 weeks (**Figure 1.3 A**). These structures undergo a coordinated series of biochemical and phenotypic processes and mimic true mammary acini

development. Early in the development of these hollow acini apical-basolateral cell polarity is established. After 5-6 days a population of cells loses contact with the ECM and eventually undergoes apoptosis. Cells that maintain contact with the ECM exhibit survival signaling through AKT and continue to proliferate. As the internal cells overcome pro-survival autophagy, they begin to undergo apoptosis and form a hollow lumen that closely resembles the glandular architecture seen in the human breast (91,92). This system allows dissection of the biochemical pathways and the respective functional contributions of novel regulatory proteins to the well-established 3D phenotypes of commonly deregulated oncogenic and tumor suppressive pathways. Indeed, the phenotypes of many cancer-associated genes have been characterized in detail, including HPV16 E7, ERBB2, AKT , CSF, LKB1, c-Myc, p38, PI3K, ERK1/2, Notch, STAT3, NF-κB and importantly mTORC1 (90,93–100) (**Figure 1.3 B**).

1.8 Figures

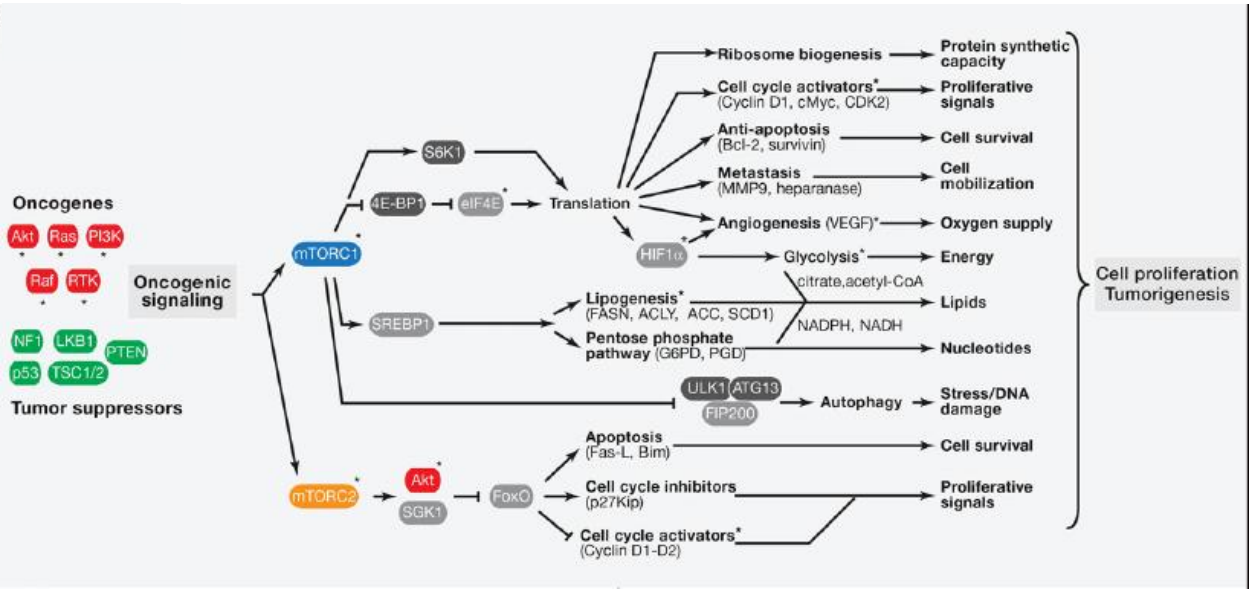

Figure 1.1 mTOR pathway and its contribution to tumorigenesis. Image amended from *Laplante, M, & Sabatini, D. 2012* (46).

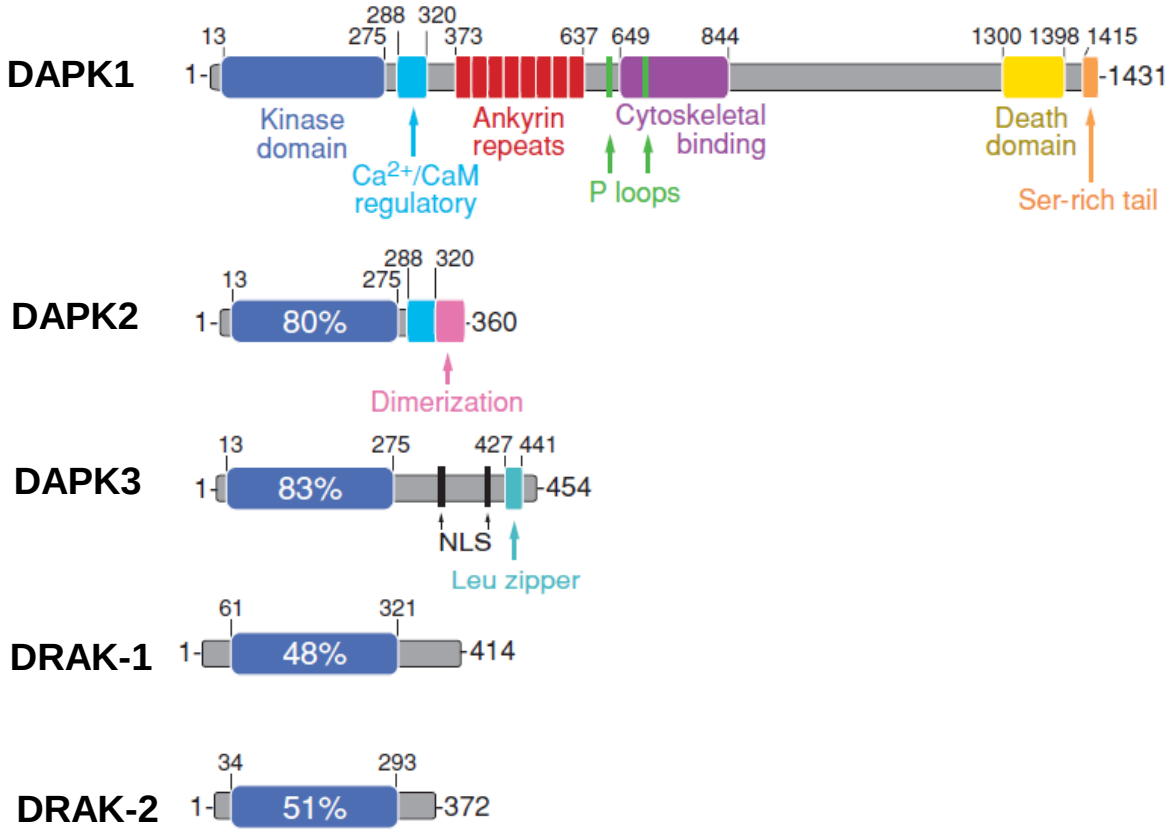

Figure 1.2 Schematic representation of the death associated protein kinase family (DAPK). Various regulatory domains are highlighted in addition to the amino acid homology relative to DAPK1. Image amended from *Bialik, S. & Kimchi A. 2006* (3).

A

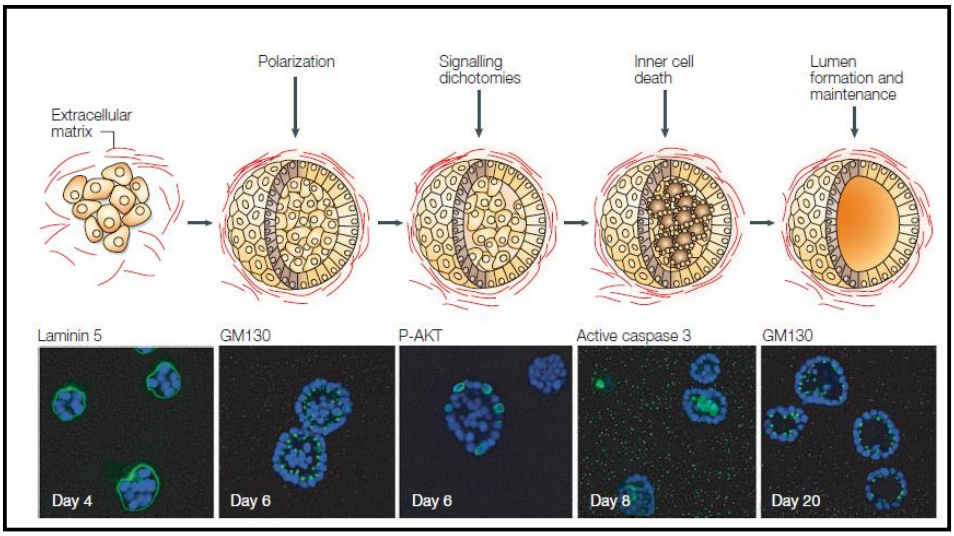

B

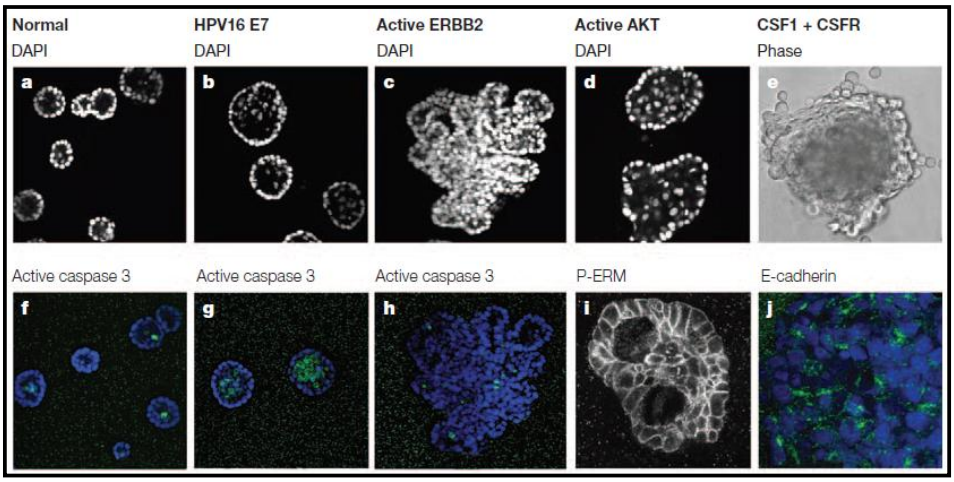

Figure 1.3 MCF10A morphogenesis (A) Schematic representation of the timeline of MCF10A acini development when grown on Matrigel. Apical-basolateral polarity is initiated by days 4 -6 (Lamini5 and GM130). Two clear populations of cells, proliferative and apoptotic, start to emerge at days 6-8. Cells that have lost contact with the Matrigel undergo apoptosis/ anoikis while the peripheral cells display increased AKT signaling. Eventually these structures cease to proliferate at day ~15 forming hollow structures. (B) The well characterized contribution of oncogenes to MCF10A morphogenesis.

1.9 References

1. Deiss LP, Feinstein E, Berissi H, Cohen O, Kimchi a. Identification of a novel serine/threonine kinase and a novel 15-kD protein as potential mediators of the gamma interferon-induced cell death. Genes Dev. 1995;9:15–30.

2. Cohen O, Feinstein E, Kimchi a. DAP-kinase is a Ca2+/calmodulin-dependent, cytoskeletal-associated protein kinase, with cell death-inducing functions that depend on its catalytic activity. EMBO J. 1997;16:998–1008.

3. Bialik S, Kimchi A. The death-associated protein kinases: structure, function, and beyond. Annu Rev Biochem. 2006;75:189–210.

4. Kawai T, Matsumoto M, Takeda K, Sanjo H. ZIP Kinase , a Novel Serine / Threonine Kinase Which Mediates Apoptosis ZIP Kinase , a Novel Serine / Threonine Kinase Which Mediates Apoptosis. 1998;18.

5. Mukhopadhyay R, Ray PS, Arif A, Brady AK, Kinter M, Fox PL. DAPK-ZIPK-L13a axis constitutes a negative-feedback module regulating inflammatory gene expression. Mol Cell. Elsevier Inc.; 2008;32:371–82.

6. Carlson D a, Franke AS, Weitzel DH, Speer BL, Hughes PF, Hagerty L, et al. Fluorescence linked enzyme chemoproteomic strategy for discovery of a potent and selective DAPK1 and ZIPK inhibitor. ACS Chem Biol. 2013;8:2715–23.

7. Haystead T a J. ZIP kinase, a key regulator of myosin protein phosphatase 1. Cell Signal. 2005;17:1313–22.

8. Murata-Hori M, Fukuta Y, Ueda K, Iwasaki T, Hosoya H. HeLa ZIP kinase induces diphosphorylation of myosin II regulatory light chain and reorganization of actin filaments in nonmuscle cells. Oncogene. 2001;20:8175–83.

9. Nehru V, Almeida FN, Aspenström P. Interaction of RhoD and ZIP kinase modulates actin filament assembly and focal adhesion dynamics. Biochem Biophys Res Commun. Elsevier Inc.; 2013;433:163–9.

10. Hagerty L, Weitzel DH, Chambers J, Fortner CN, Brush MH, Loiselle D, et al. ROCK1 phosphorylates and activates zipper-interacting protein kinase. J Biol Chem. 2007;282:4884–93.

11. Temmerman K, Simon B, Wilmanns M. Structural and functional diversity in the activity and regulation of DAPK-related protein kinases. FEBS J. 2013;280:5533–50.

12. Kögel D, Plöttner O, Landsberg G, Christian S, Scheidtmann KH. Cloning and characterization of Dlk, a novel serine/threonine kinase that is tightly associated with chromatin and phosphorylates core histones. Oncogene. 1998;17:2645–54.

13. Kögel D, Bierbaum H, Preuss U, Scheidtmann KH. C-terminal truncation of Dlk/ZIP kinase leads to abrogation of nuclear transport and high apoptotic activity. Oncogene. 1999;18:7212–8.

14. Kawai T, Akira S, Reed JC. ZIP Kinase Triggers Apoptosis from Nuclear PML Oncogenic Domains ZIP Kinase Triggers Apoptosis from Nuclear PML Oncogenic Domains. 2003;23.

15. Vetterkind S, Illenberger S, Kubicek J, Boosen M, Appel S, Naim HY, et al. Binding of Par-4 to the actin cytoskeleton is essential for Par-4/Dlk-mediated apoptosis. Exp Cell Res. 2005;305:392–408.

16. Page G, Kögel D, Rangnekar V, Scheidtmann KH. Interaction partners of Dlk/ZIP kinase: co-expression of Dlk/ZIP kinase and Par-4 results in cytoplasmic retention and apoptosis. Oncogene. 1999;18:7265–73.

17. Shoval Y, Pietrokovski S, Kimchi A. ZIPK: a unique case of murine-specific divergence of a conserved vertebrate gene. PLoS Genet. 2007;3:1884–93.

18. Galluzzi L, Vitale I, Abrams JM, Alnemri ES, Baehrecke EH, Blagosklonny M V, et al. Molecular definitions of cell death subroutines: recommendations of the Nomenclature Committee on Cell Death 2012. Cell Death Differ. 2012;19:107–20.

19. Bovellan M, Fritzsche M, Stevens C, Charras G. Death-associated protein kinase (DAPK) and signal transduction: blebbing in programmed cell death. FEBS J. 2010;277:58–65.

20. Llambi F, Lourenço FC, Gozuacik D, Guix C, Pays L, Del Rio G, et al. The dependence receptor UNC5H2 mediates apoptosis through DAP-kinase. EMBO J. 2005;24:1192–201.

21. Inbal B, Bialik S, Sabanay I, Shani G, Kimchi A. DAP kinase and DRP-1 mediate membrane blebbing and the formation of autophagic vesicles during programmed cell death. J Cell Biol. 2002;157:455–68.

22. Shani G, Marash L, Gozuacik D, Bialik S, Shohat G, Kimchi A, et al. Death-Associated Protein Kinase Phosphorylates ZIP Kinase , Forming a Unique Kinase Hierarchy To Activate Its Cell Death Functions Death-Associated Protein Kinase Phosphorylates ZIP Kinase , Forming a Unique Kinase Hierarchy To Activate Its Cell Death Fun. 2004;

23. Brognard J, Zhang Y-W, Puto L a, Hunter T. Cancer-associated loss-of-function mutations implicate DAPK3 as a tumor-suppressing kinase. Cancer Res. 2011;71:3152–61.

24. Bi J, Lau S-H, Hu L, Rao H-L, Liu H-B, Zhan W-H, et al. Downregulation of ZIP kinase is associated with tumor invasion, metastasis and poor prognosis in gastric cancer. Int J Cancer. 2009;124:1587–93.

25. Tan X-L, Moyer AM, Fridley BL, Schaid DJ, Niu N, Batzler AJ, et al. Genetic variation predicting cisplatin cytotoxicity associated with overall survival in lung cancer patients receiving platinum-based chemotherapy. Clin Cancer Res. 2011;17:5801–11.

26. Natrajan R, Mackay A, Lambros MB, Weigelt B, Wilkerson PM, Manie E, et al. A whole-genome massively parallel sequencing analysis of BRCA1 mutant oestrogen receptor-negative and -positive breast cancers. 2012;227:29–41.

27. Page G, Lödige I, Kögel D, Scheidtmann KH. AATF, a novel transcription factor that interacts with Dlk/ZIP kinase and interferes with apoptosis. FEBS Lett. 1999;462:187–91.

28. Boosen M, Vetterkind S, Kubicek J, Scheidtmann K, Illenberger S, Preuss U. Par-4 Is an Essential Downstream Target of DAP-like Kinase (Dlk) in Dlk / Par-4 – mediated Apoptosis. 2009;20:4010–20.

29. Sato N, Kawai T, Sugiyama K, Muromoto R, Imoto S, Sekine Y, et al. Physical and functional interactions between STAT3 and ZIP kinase. 2005;17:1543–52.

30. Togi S, Ikeda O, Kamitani S, Nakasuji M, Sekine Y, Muromoto R, et al. Zipper-interacting protein kinase (ZIPK) modulates canonical Wnt/beta-catenin signaling through interaction with Nemo-like kinase and T-cell factor 4 (NLK/TCF4). J Biol Chem. 2011;286:19170–7.

31. Kaizuka T, Hara T, Oshiro N, Kikkawa U, Yonezawa K, Takehana K, et al. Tti1 and Tel2 are critical factors in mammalian target of rapamycin complex assembly. J Biol Chem. 2010;285:20109–16.

32. Leister P, Felten a, Chasan a I, Scheidtmann KH. ZIP kinase plays a crucial role in androgen receptor-mediated transcription. Oncogene. 2008;27:3292–300.

33. Kissil JL, Feinstein E, Cohen O, Jones P a, Tsai YC, Knowles M a, et al. DAP-kinase loss of expression in various carcinoma and B-cell lymphoma cell lines: possible implications for role as tumor suppressor gene. Oncogene. 1997;15:403–7.

34. Inbal B, Cohen O, Polak-charcon S, Kopolovic J, Vadai E, Eisenbach L, et al. DAP kinase links the control of apoptosis to metastasis. Nature. 1997;390:180–4.

35. Raveh T, Droguett G, Horwitz MS, DePinho R a, Kimchi a. DAP kinase activates a p19ARF/p53-mediated apoptotic checkpoint to suppress oncogenic transformation. Nat Cell Biol. 2001;3:1–7.

36. Martoriati A, Doumont G, Alcalay M, Bellefroid E, Pelicci PG, Marine J-C. dapk1, encoding an activator of a p19ARF-p53-mediated apoptotic checkpoint, is a transcription target of p53. Oncogene. 2005;24:1461–6.

37. Christoph F, Kempkensteffen C, Weikert S, Köllermann J, Krause H, Miller K, et al. Methylation of tumour suppressor genes APAF-1 and DAPK-1 and in vitro effects of demethylating agents in bladder and kidney cancer. Br J Cancer. 2006;95:1701–7.

38. Christoph F, Hinz S, Kempkensteffen C, Schostak M, Schrader M, Miller K. mRNA expression profiles of methylated APAF-1 and DAPK-1 tumor suppressor genes uncover clear cell renal cell carcinomas with aggressive phenotype. J Urol. 2007;178:2655–9.

39. Zöchbauer-müller S, Fong KM, Virmani AK, Cancers L, Zo S. Aberrant Promoter Methylation of Multiple Genes in Non-Small Cell Lung Cancers Aberrant Promoter Methylation of Multiple Genes in Non-Small Cell. 2001;249–55.

40. Lehmann U, Celikkaya G, Hasemeier B, La F, Kreipe H. Promoter Hypermethylation of the Death-associated Protein Kinase Gene in Breast Cancer Is Associated with the Invasive Lobular Subtype Promoter Hypermethylation of the Death-associated Protein Kinase Gene in Breast Cancer Is Associated with the Invasive L. 2002;6634–8.

41. Katzenellenbogen R a, Baylin SB, Herman JG. Hypermethylation of the DAP-kinase CpG island is a common alteration in B-cell malignancies. Blood. 1999;93:4347–53.

42. Michie AM, McCaig AM, Nakagawa R, Vukovic M. Death-associated protein kinase (DAPK) and signal transduction: regulation in cancer. FEBS J. 2010;277:74–80.

43. Sabatini DM, Erdjument-Bromage H, Lui M, Tempst P, Snyder SH. RAFT1: a mammalian protein that binds to FKBP12 in a rapamycin-dependent fashion and is homologous to yeast TORs. Cell. 1994;78:35–43.

44. C. Sabers, M., Martin, G. Brunn, J. Williams, F. Dumont, G. Weiderrecht RA. Isolation of a Protein Target of the FKBP12-Rapamycin Complex in Mammalian Cells. J Biol Chem. 1995;270:815–22.

45. E. Brown, M. Albers, T. Shin, K. Ichikawa, C. Keith, W. Lane SS. A mammalian protein targeted by G1-arresting rapamycin-receptor complex. Nature. 1994;

46. Laplante M, Sabatini DM. mTOR signaling in growth control and disease. Cell. Elsevier; 2012;149:274–93.

47. Kim D-H, Sarbassov DD, Ali SM, Latek RR, Guntur KVP, Erdjument-Bromage H, et al. GbetaL, a positive regulator of the rapamycin-sensitive pathway required for the nutrient-sensitive interaction between raptor and mTOR. Mol Cell. 2003;11:895–904.

48. Peterson TR, Laplante M, Thoreen CC, Sancak Y, Kang S a, Kuehl WM, et al. DEPTOR is an mTOR inhibitor frequently overexpressed in multiple myeloma cells and required for their survival. Cell. Elsevier Ltd; 2009;137:873–86.

49. Kim D-H, Sarbassov DD, Ali SM, King JE, Latek RR, Erdjument-Bromage H, et al. mTOR interacts with raptor to form a nutrient-sensitive complex that signals to the cell growth machinery. Cell. 2002;110:163–75.

50. Hara K, Maruki Y, Long X, Yoshino K, Oshiro N, Hidayat S, et al. Raptor, a binding partner of target of rapamycin (TOR), mediates TOR action. Cell. 2002;110:177–89.

51. Sancak Y, Thoreen CC, Peterson TR, Lindquist R a, Kang S a, Spooner E, et al. PRAS40 is an insulin-regulated inhibitor of the mTORC1 protein kinase. Mol Cell. 2007;25:903–15.

52. Thedieck K, Polak P, Kim ML, Molle KD, Cohen A, Jenö P, et al. PRAS40 and PRR5-like protein are new mTOR interactors that regulate apoptosis. PLoS One. 2007;2:e1217.

53. Vander Haar E, Lee S-I, Bandhakavi S, Griffin TJ, Kim D-H. Insulin signalling to mTOR mediated by the Akt/PKB substrate PRAS40. Nat Cell Biol. 2007;9:316–23.

54. Wang L, Harris TE, Roth R a, Lawrence JC. PRAS40 regulates mTORC1 kinase activity by functioning as a direct inhibitor of substrate binding. J Biol Chem. 2007;282:20036–44.

55. Jacinto E, Loewith R, Schmidt A, Lin S, Rüegg M a, Hall A, et al. Mammalian TOR complex 2 controls the actin cytoskeleton and is rapamycin insensitive. Nat Cell Biol. 2004;6:1122–8.

56. Sarbassov DD, Ali SM, Kim D, Guertin DA, Latek RR, Erdjument-bromage H, et al. Rictor , a Novel Binding Partner of mTOR , Defines a Rapamycin-Insensitive and Raptor-Independent Pathway that Regulates the Cytoskeleton. 2004;14:1296–302.

57. Jacinto E, Facchinetti V, Liu D, Soto N, Wei S, Jung SY, et al. SIN1/MIP1 maintains rictor-mTOR complex integrity and regulates Akt phosphorylation and substrate specificity. Cell. 2006;127:125–37.

58. Frias M a, Thoreen CC, Jaffe JD, Schroder W, Sculley T, Carr S a, et al. mSin1 is necessary for Akt/PKB phosphorylation, and its isoforms define three distinct mTORC2s. Curr Biol. 2006;16:1865–70.

59. Pearce LR, Huang X, Boudeau J, Pawłowski R, Wullschleger S, Deak M, et al. Identification of Protor as a novel Rictor-binding component of mTOR complex-2. Biochem J. 2007;405:513–22.

60. Pearce LR, Sommer EM, Sakamoto K, Wullschleger S, Alessi DR. Protor-1 is required for efficient mTORC2-mediated activation of SGK1 in the kidney. Biochem J. 2011;436:169–79.

61. E. Brown, P. Beal, C. Keith, J. Chen, T. Shin SS. Control of p70 S6 kinase by kinase activity of FRAP in vivo. Nature. 1995;377:441–6.

62. Brunn GJ. Phosphorylation of the Translational Repressor PHAS-I by the Mammalian Target of Rapamycin. Science (80-). 1997;277:99–101.

63. P. Burnett, R. Barrow, N. Cohen, S. Snyder DS. RAFT1 phosphorylation of the translational regulators p70 S6 kinase and 4E-BP1. PNAS. 1998;95:1432–7.

64. Yip CK, Murata K, Walz T, Sabatini DM, Kang S a. Structure of the human mTOR complex I and its implications for rapamycin inhibition. Mol Cell. Elsevier Ltd; 2010;38:768–74.

65. Dibble CC, Manning BD. Signal integration by mTORC1 coordinates nutrient input with biosynthetic output. Nat Cell Biol. Nature Publishing Group; 2013;15:555–64.

66. Toker a, Newton a C. Cellular signaling: pivoting around PDK-1. Cell. 2000;103:185–8.

67. Zarich N, Oliva L, Martı N, Ballester A, Garcı S, Rojas M. Grb2 Is a Negative Modulator of the Intrinsic Ras-GEF Activity of hSos1 □. 2006;17:3591–7.

68. Beauchamp EM, Platanias LC. The evolution of the TOR pathway and its role in cancer. Oncogene. Nature Publishing Group; 2013;32:3923–32.

69. Ma XM, Blenis J. Molecular mechanisms of mTOR-mediated translational control. Nat Rev Mol Cell Biol. 2009;10:307–18.

70. Beauchamp EM, Platanias LC. The evolution of the TOR pathway and its role in cancer. Oncogene. Nature Publishing Group; 2013;32:3923–32.

71. Peterson RT, Schreiber SL. Translation control: connecting mitogens and the ribosome. Curr Biol. 1998;8:R248–50.

72. Ruvinsky I, Sharon N, Lerer T, Cohen H, Stolovich-Rain M, Nir T, et al. Ribosomal protein S6 phosphorylation is a determinant of cell size and glucose homeostasis. Genes Dev. 2005;19:2199–211.

73. Dowling RJO, Topisirovic I, Alain T, Bidinosti M, Fonseca BD, Petroulakis E, et al. mTORC1-mediated cell proliferation, but not cell growth, controlled by the 4E-BPs. Science. 2010;328:1172–6.

74. Fruman D a, Rommel C. PI3K and cancer: lessons, challenges and opportunities. Nat Rev Drug Discov. Nature Publishing Group; 2014;13:140–56.

75. Sarbassov DD, Guertin D a, Ali SM, Sabatini DM. Phosphorylation and regulation of Akt/PKB by the rictor-mTOR complex. Science. 2005;307:1098–101.

76. García-Martínez JM, Alessi DR. mTOR complex 2 (mTORC2) controls hydrophobic motif phosphorylation and activation of serum- and glucocorticoid-induced protein kinase 1 (SGK1). Biochem J. 2008;416:375–85.

77. Vivanco I, Sawyers CL. The phosphatidylinositol 3-Kinase AKT pathway in human cancer. Nat Rev Cancer. 2002;2:489–501.

78. Green AJ, Johnson PH, Yates JRW. The tuberous sclerosis gene on chromosome 9q34 acts as a growth suppressor. Hum Mol Genet. 1994;3:1833–4.

79. Menon S, Yecies JL, Zhang HH, Howell JJ, Nicholatos J, Harputlugil E, et al. Chronic activation of mTOR complex 1 is sufficient to cause hepatocellular carcinoma in mice. Sci Signal. 2012;5:ra24.

80. Hemminki a, Avizienyte E, Roth S, Loukola a, Aaltonen L a, Järvinen H, et al. [A serine/threonine kinase gene defective in Peutz-Jeghers syndrome]. Duodecim. 1998;114:667–8.

81. Korsse SE, Peppelenbosch MP, van Veelen W. Targeting LKB1 signaling in cancer. Biochim Biophys Acta. Elsevier B.V.; 2013;1835:194–210.

82. Elkabets M, Vora S, Juric D, Morse N, Mino-Kenudson M, Muranen T, et al. mTORC1 inhibition is required for sensitivity to PI3K p110α inhibitors in PIK3CA-mutant breast cancer. Sci Transl Med. 2013;5:196ra99.

83. Corcoran RB, Rothenberg SM, Hata AN, Faber AC, Piris A, Nazarian RM, et al. TORC1 suppression predicts responsiveness to RAF and MEK inhibition in BRAF-mutant melanoma. Sci Transl Med. 2013;5:196ra98.

84. Sato T, Nakashima a, Guo L, Coffman K, Tamanoi F. Single amino-acid changes that confer constitutive activation of mTOR are discovered in human cancer. Oncogene. Nature Publishing Group; 2010;29:2746–52.

85. Menon S, Manning BD. Common corruption of the mTOR signaling network in human tumors. Oncogene. Nature Publishing Group; 2008;27 Suppl 2:S43–51.

86. Stevens C, Lin Y, Harrison B, Burch L, Ridgway R a, Sansom O, et al. Peptide combinatorial libraries identify TSC2 as a death-associated protein kinase (DAPK) death domain-binding protein and reveal a stimulatory role for DAPK in mTORC1 signaling. J Biol Chem. 2009;284:334–44.

87. Schumacher AM, Velentza A V, Watterson DM, Dresios J. Death-associated protein kinase phosphorylates mammalian ribosomal protein S6 and reduces protein synthesis. Biochemistry. 2006;45:13614–21.

88. Roux PP, Shahbazian D, Vu H, Holz MK, Cohen MS, Taunton J, et al. RAS/ERK signaling promotes site-specific ribosomal protein S6 phosphorylation via RSK and stimulates cap-dependent translation. J Biol Chem. 2007;282:14056–64.

89. Mao J, Luo H, Han B, Bertrand R, Wu J. Drak2 is upstream of p70S6 kinase: its implication in cytokine-induced islet apoptosis, diabetes, and islet transplantation. J Immunol. 2009;182:4762–70.

90. Debnath J, Brugge JS. Modelling glandular epithelial cancers in three-dimensional cultures. Nat Rev Cancer. 2005;5:675–88.

91. Fung C, Lock R, Gao S, Salas E, Debnath J, Francisco S, et al. Induction of Autophagy during Extracellular Matrix Detachment Promotes Cell Survival. 2008;19:797–806.

92. Debnath J, Mills KR, Collins NL, Reginato MJ, Muthuswamy SK, Brugge JS, et al. The Role of Apoptosis in Creating and Maintaining Luminal Space within Normal and Oncogene-Expressing Mammary Acini Brigham and Women ' s Hospital. 2002;111:29–40.

93. Debnath J, Walker SJ, Brugge JS. Akt activation disrupts mammary acinar architecture and enhances proliferation in an mTOR-dependent manner. J Cell Biol. 2003;163:315–26.

94. Avivar-Valderas a, Bobrovnikova-Marjon E, Alan Diehl J, Bardeesy N, Debnath J, Aguirre-Ghiso J a. Regulation of autophagy during ECM detachment is linked to a selective inhibition of mTORC1 by PERK. Oncogene. Nature Publishing Group; 2013;32:4932–40.

95. Ben-Hur V, Denichenko P, Siegfried Z, Maimon A, Krainer A, Davidson B, et al. S6K1 alternative splicing modulates its oncogenic activity and regulates mTORC1. Cell Rep. The Authors; 2013;3:103–15.

96. Chua HL, Bhat-Nakshatri P, Clare SE, Morimiya a, Badve S, Nakshatri H. NF-kappaB represses E-cadherin expression and enhances epithelial to mesenchymal transition of mammary epithelial cells: potential involvement of ZEB-1 and ZEB-2. Oncogene. 2007;26:711–24.

97. Mazzone M, Selfors LM, Albeck J, Overholtzer M, Sale S, Carroll DL, et al. Dose-dependent induction of distinct phenotypic responses to Notch pathway activation in mammary epithelial cells. Proc Natl Acad Sci U S A. 2010;107:5012–7.

98. Pearson GW, Hunter T. PI-3 kinase activity is necessary for ERK1/2-induced disruption of mammary epithelial architecture. Breast Cancer Res. 2009;11:R29.

99. Wen H-C, Avivar-Valderas A, Sosa MS, Girnius N, Farias EF, Davis RJ, et al. p38α Signaling Induces Anoikis and Lumen Formation During Mammary Morphogenesis. Sci Signal. 2011;4:ra34.

100. Partanen JI, Nieminen AI, Mäkelä TP, Klefstrom J. Suppression of oncogenic properties of c-Myc by LKB1-controlled epithelial organization. Proc Natl Acad Sci U S A. 2007;104:14694–9.

CHAPTER 2: DAPK3 INHIBITION OF mTOR SIGNALING SUPPRESSES MAMMARY ACINI MORPHOGENESIS

2.1 Introduction

Death-associated protein kinase 3 (DAPK3, also known as ZIPK) is a member of the DAPK serine/ threonine protein kinase family and is known to regulate smooth muscle contraction, cell-cell adhesion, cytoskeleton dynamics, inflammation, and cardiovascular functions. It is also considered a putative tumor suppressor through regulation of caspase-dependent and -independent apoptosis, proliferation and autophagy (1). The DAPK family contains 4 other members, including DAPK1, DRP-1 (DAPK-related protein 1), DRAK-1 and DRAK-2 (DAPK-related apoptosis-inducing protein kinase-1 and -2), which all share homology within their kinase domain. DAPK3 contains an N-terminal kinase domain that shares 80% amino acid homology with the prototypical DAPK1. It differs from other family members by the presence of a C-terminal leucine zipper motif and the absence of a calmodulin-regulated (CaM) domain and death domain. Similar to other family members, DAPK3 is considered to be a tumor suppressor. Overexpression of DAPK3 in mammalian cells results in cell death and cell cycle inhibition while kinase inactivating mutations along with recurrent deleterious somatic mutations are observed in lung and breast cancers, respectively (2-4). Knockdown of DAPK3 increases proliferation of various cell lines (2). Clinically, reduced *DAPK3* mRNA correlated with increased tumor invasion, metastasis and overall survival in a cohort of gastric carcinoma patients (5). Abrogation of *DAPK3* mRNA expression was shown to significantly decrease cisplatin sensitivity in various lung cancer cell lines and may impact overall survival of non-small cell lung cancer patients treated with platinum-based therapy (6). DAPK3 is also considered a potentially novel breast cancer gene as recurrent DAPK3 alterations were observed

in BRCA1 mutant and BRCA-1 non-mutant breast cancers (3). Additionally, human DAPK3 regulates a variety of signaling pathways commonly deregulated in cancer. For example, DAPK3 negatively regulates the canonical Wnt/ β-catenin pathway by disrupting the interaction between Nemo-like kinase (NLK) and T-cell Factor 4 (TCF4) in colon cancer cell lines (7). DAPK3 regulates androgen receptor-mediated transcription via ubiquitination and degradation of AR in various cancer cell lines (8). DAPK3 also interacts with and/ or phosphorylated various cancer-associated proteins *in vitro*, including ATF4, AATF, Daxx, Par-4 and STAT-3 (4,9-12).

Despite these *in vitro* and clinical observations, the full physiological significance of DAPK3 is not well understood. Compared to the prototypical DAPK family member DAPK1, relatively little is known about the functional tumor suppressive mechanisms regulated by DAPK3. These limitations are potentially exacerbated by the lack of a knockout mouse model as well as inadequate cell culture models that cannot recapitulate the physiological context of tissue development or carcinogenesis.

3-dimensional (3D) *in vitro* tumor systems provide the ability to functionally investigate the contribution of tumor suppressors and oncogenes to the complex development and architecture of tumor spheroids (13). Given the utility of 3D tumor systems and the clinically observed mutations of DAPK3 in breast cancer (3), we chose to further explore the functional significance of DAPK3 in a MCF10A 3D morphogenesis model. When grown on an extracellular enriched matrix (Matrigel), the immortalized MCF10A epithelial cell line forms hollow spheroids that undergo a regulated and coordinated series of events similar to developing mammary acini (14). This model has been used to investigate the contribution of *loss-of-function* (LOF) alterations to acini development and early events in tumor formation.

Herein, we describe the functional significance of DAPK3 in MCF10A acini morphogenesis. We have identified that DAPK3 negatively regulates MCF10A morphogenesis through a mTORC1-S6K1-S6 pathway. We also identified that DAPK3 is downregulated in aggressive breast cancer relative to less aggressive and normal patient samples.

2.2 Materials & Methods

Cell culture and reagents

MCF10A and 293T cells were obtained from the American Type Culture Collection. MCF10A cells were cultured as described elsewhere (14) and 293T were cultured in DMEM supplemented with 10%FBS and L-glutamine. 3D morphogenesis assays were conducted as described elsewhere (14).

Plasmids and viral production

For DAPK3 overexpression, the DAPK3 ORF was PCR amplified (from Addgene plasmid 23436) and subcloned into pLVX-IRES-Hyg (Clonetech). PCR primers, forward: 5'-GAGAGA**CTCGAG**GCCACCATGTCCACGTTCAGGCAGGAG, and reverse: 5'-GAGAGA**GGATCC**TTACTAGCGCAGCCCGCACTCCACGCCCTGC, were used to create the restriction enzyme sites XhoI and BamHI (in bold) that allowed for ligation into the corresponding sites in pLVX-IRES-Hyg. For $HRas^{V12}$ overexpression, $HRas^{V12}$ was amplified and subcloned into pLVX-IRES-Hyg. PCR primers, forward: 5'-GAGAGA**CTCGAG**GCCACCATGACGGAATATAAGCTGGTGGTGGTGG, and reverse: 5'-GAGAGA**GGATCC**TTATCAGGAGAGCACACACTTGCAGCTCATG, were used to create the restriction enzyme sites XhoI and BamHI (in bold) that allowed for ligation into the corresponding sites in pLVX-IRES-Hyg.

pLKO.1-puro constructs obtained from the Genome Institute at Washington University were used for RNA interference (RNAi) against DAPK3. Sequences for the short hairpin RNAs are: 5'- CGTTCACTACCTGCACTCTAA (herein referred to as sh1), 5'- CCCAAGCGGAGAATGACCATT (herein referred to as sh2) and shNeg (15). For lentiviral production, 8 x 10^5 293T cells were co-transfected with pCMV-VSV-G, pCMVΔR8.2, and pLKO.1-puro constructs using Fugene 6 (Promega). Forty-eight hours post-transfection, viral supernatants were collected. PLKO.1 hygro shRNA constructs against Rictor and Raptor were generated by subcloning hygromycin in place of puromycin within the pLKO.1-constructs.

Immunofluorescence and confocal microscopy

MCF10A acini were grown in 8 well chamberslides and at the indicated time point were fixed with 4% paraformaldehyde (PFA) in PBS for 30 minutes at room temperature. Slides were washed three times (15 minutes each wash) at room temperature in 100 mM glycine in PBS and subsequently permeabilized with 0.05% Tween 20 in PBS, pH 7.4 for 20 minutes. Fixed acini were blocked in IF buffer (0.2% Triton X-100, 0.1% BSA-radioimmunoassay grade from Sigma Aldrich, 0.05% Tween 20 in PBS, pH 7.4) and 10% goat serum for 1.5 hours at room temperature and then blocked in secondary block containing IF buffer + 10% goat serum + 20ug/mL goat anti-mouse IgG F(ab')2 fragment specific (Jackson ImmunoResearch, Cat. 115-006-006) in a humidified chamber for 30 minutes. Fixed acini were then stained with 1:100 primary antibody in IF buffer + 10% goat serum + 20ug/mL goat anti-mouse IgG $F(ab')_2$. Primary antibodies were as follows: rabbit anti-Ki67 (Cell Signaling, 9129), rabbit-anti cleaved caspase 3 (Cell Signaling, 9579), rat anti-integrin alpha 6 (Millipore, MAB1378) and rabbit anti-giantin (Covance, PRB-114C). The following day the slides were washed three times in IF buffer for 20 minutes each and incubated with a secondary antibody (conjugated to Alexa Fluor 488 or

594) diluted in IF buffer +10% goat serum for 40 minutes at room temperature in a humidified chamber. Slides were washed three times in IF buffer for 20 minutes each and then incubated with 1 μM TOPRO3 iodide (Molecular Probes) in PBS for 10 minutes at room temperature in a humidified chamber. Slides were then washed with PBS once for 10 minutes and mounted with Prolong Antifade mounting medium (Molecular Probes). Images were obtained using an Olympus FV-500 confocal microscope with a 20X water objective. Images were processed using the Olympus FLUOVIEW Ver.2.1a Viewer and ImageJ software. For Ki67 and cleaved caspase 3 evaluations, a total of 10 fields with at least 4 acini per field were acquired and then analyzed as indicated.

Acini diameter quantification and statistics

Size analysis was performed using a haemocytometer and ImageJ software for each brightfield image. At least 50 acini from a single field of view were analyzed for acini diameter. The Student's *t*-test was used for statistical analysis.

Immunoblotting

Harvested cells were re-suspended and sonicated in radioimmunoprecipitation assay (RIPA) buffer (50mM Tris-HCl, pH 7.4, 150 mM NaCl, 1% Triton X-100, 0.1% SDS, 0.5% deoxycholic acid) containing protease and phosphatase inhibitors (1mM phenylmethylsulfonyl fluoride (PMSF), 0.4 U/ml aprotinin, 10 μg/ml leupeptin, 10 μg/ml pepstatin, 1 mM β–glycerophosphate, 0.1 mM NaF, 0.1 mM $NaVO_4$). Proteins (30 to 80 μg) were fractionated on 10% Tris-HCl, Criterion Precast Gel (Bio-Rad). Separated proteins were transferred onto polyvinylidene difluoride (PVDF) membranes (Millipore), and probed with the following antibodies: rabbit anti-DAPK3/ ZIPK (abcam, ab51602 and for K42A Cell Signaling, 2928)), rabbit anti-β catenin

(Santa Cruz, H-102), mouse anti-phospho-p70/p85 (Cell Signaling, 9206), rabbit anti-p70/p85 (Cell Signaling, 2708), rabbit anti-phospho-pS6 (Cell Signaling, 2215), mouse anti-S6 (Cell Signaling, 2317), rabbit anti-GAPDH (Sigma-Aldrich, G9545), rabbit anti-phospho-T308 AKT (Cell Signaling, 9275), mouse anti-AKT (Cell Signaling, 2920), rabbit anti-phospho-ERK (Cell Signaling, 4370), rabbit anti-Actin (Sigma-Aldrich, A2066), mouse anti-RAPTOR (Santa Cruz, sc-81537) and rabbit anti-RICTOR (Cell Signaling, 2140). Secondary horseradish peroxidase-conjugated anti-rabbit or anti-mouse antibodies (Sigma-Aldrich) were added and ECL Western Blotting Substrate or SuperSignal West Femto Maximum Sensitivity Substrate (Thermo Scientific) were used to visualize protein bands.

Soft agar assay

MCF10A cells were first infected with $HRas^{V12}$, shNeg, sh1, or sh2 expressing lentivirus and then selected in puromycin (1 μg/ml) until canaries were dead. Following drug selection, 1×10^4 stables cells were seeded in 6-well plates, and the cells were fed with fresh media twice a week. After 3 weeks, plates were stained with crystal violet overnight, washed and colonies were manually counted.

2.3 Results

DAPK3 depletion augments acini morphogenesis

To further investigate additional mechanisms by which DAPK3 exerts tumor suppressive functions, we performed stable shRNA knockdown of DAPK3 in MCF10A cells grown on Matrigel using two independent hairpins. As discussed previously, this model permits interrogation of acini architecture development, which undergoes a series of highly conserved temporally-concerted biochemical and phenotypic events. First, loss of DAPK3 significantly enhances acini diameter by approximately 37$\pm$10 % as compared to negative control shRNA at day 8 (**Figure 1A, B**). Diameter enhancement was observed as early as day 4 and continued to increase over time while the negative control plateaued at later time points. Interestingly, DAPK3 depletion does not enhance anchorage independent growth of MCF10A cells growth in soft agar (**Figure 2**).

Loss of DAPK3 results in enhanced acini proliferation and apoptosis

It has been well established that size and morphogenesis of MCF10A acini is dependent on coordinated proliferation and apoptotic programs. To understand which of these processes was perturbed in DAPK3 knockdown structures, we performed confocal immunofluorescence microscopy on acini structures. DAPK3-depleted structures contained, on average, significantly more Ki67+ cells compared to negative control (**Figure 3**). Interestingly, loss of DAPK3 also augmented cleaved caspase 3-positive acini relative to negative control (**Figure 4**). This was additionally confirmed by ethidium bromide uptake in live MCF10A acini which also indicated a significant increase in cell death in DAPK3 depleted structures (**Figure 5**). Thus, while there was a net increase in acinar size, we hypothesize that as the shDAPK3 structures underwent

hyperproliferation, more cells lost contact with the ECM and as a result underwent apoptosis, a phenomenon which has been observed elsewhere (16). Of note, we did not observe any alterations in acini apical or basolateral polarity as indicated by proper localization of giantin and integrin α6, respectively (**Figure 6 A, B**).

DAPK3 overexpression disrupts normal acini formation

To determine if DAPK3 overexpression impacts acinar morphogenesis, we stably overexpressed DAPK3 fused to GFP in MCF10A cells that were subsequently grown in 3D. Despite a large degree of toxicity observed in the packaging cells, we were able to achieve stable populations of MCF10A cells that survived selection. However, we were not able to achieve high overexpression of DAPK3 most likely due to overexpression toxicities in both target and packaging cells that are commonly observed across several cell types (2,17). Additionally, this expression was lost over time indicating negative selection for sustained high level expression of DAPK3. Given these technical challenges, structures that maintained overexpression (as indicated by GFP fluorescence) displayed a dramatic and significant decrease in structure size compared to empty-GFP vector alone (**Figure 7A, B**). We also attempted to determine if this decrease in size was dependent on DAPK3 kinase activity but we were unable to achieve stable overexpression of a previously characterized kinase deficient point mutant (K42A) fused to GFP (*data not shown*). However, stable overexpression of an unfused K42A mutant exhibited microscopic colony growth in soft agar highly similar to negative control, while a significant decrease was observed in stable cells overexpressing wildtype DAPK3 (**Figure 8**), consistent with growth inhibiting-dependence on kinase activity.

DAPK3 negatively regulates mTOR-S6K-S6 signaling with no effect on ERK or AKT activation

To identify the pathways functionally regulated by DAPK3 we initially compared our structural phenotypes to that reported in the literature. Several groups have shown that enhanced mTOR activity leads to acini with similar abnormalities observed upon loss of DAPK3 (18-20). Indeed, upon loss of DAPK3 in MCF10A cells grown in 2D culture we observed an increase in phosphorylation of S6 (P-S6) and both p70 and p85 S6K1 isoforms (herein referred to as P-S6K) when stimulated with EGF or insulin (**Figure 9**). We additionally observed an increase in P-S6 from MCF10A cells depleted of DAPK3 that were grown in 3D for 6 days (**Figure 10)**. Of note, we did not observe an increase in ERK or AKT signaling (**Figure 10**)

Loss of DAPK3 influences proper acini morphogenesis through mTORC1

To further confirm that this enhanced mTOR signaling was functionally relevant, we treated established negative control and DAPK3-depleted acini with 100 nM rapamycin once starting at day 4. 4 days later we observed that rapamycin had no significant effect on the diameter of the negative control. However, acini stably transduced with both independent DAPK3 hairpins displayed a significant sensitivity to rapamycin treatment (**Figure 11 A**). Additionally, established shDAPK3 acini treated with increasing concentrations (100 nM, 10 μM and 50 μM) of the PI3K inhibitor LY294002 displayed similar increased sensitivity to the drug compared to negative control (**Figure 11B**).

To further delineate how DAPK3 regulates mTOR for proper acini morphogenesis, we stably knocked down DAPK3 and RICTOR or RAPTOR using previously reported hairpins (21). Interestingly, we observed that loss of DAPK3 and RAPTOR blunted the increased acini size

whereas loss of RICTOR did not rescue the phenotype (**Figure 12A**). Additionally, loss of RAPTOR by itself had a profound impact on acini formation whereas knockdown of RICTOR did not.

Clinically observed down regulation of *DAPK3* mRNA

Finally, we wanted to confirm that our cell culture observations mimic that seen in actual patients using the Oncomine database (www.oncomine.org). Indeed, *DAPK3* mRNA is significantly downregulated in ductal breast carcinoma *in situ* (DCIS) and invasive ductal breast versus normal breast and DCIS controls, respectively (**Figure 13 A, B**). *DAPK3* mRNA is also significantly downregulated in pancreatic adenocarcinoma as well as melanoma versus normal controls (**Figure 13 C, D**).

2.4 Discussion

Herein we have shown that loss of DAPK3 leads to increased acini size, enhanced acini proliferation and apoptosis without disrupting apical-basolateral polarity. Conversely, stable overexpression of DAPK3 inhibits acini morphogenesis and is relatively toxic to cells. Loss of DAPK3 augments acini morphogenesis through mTOR-S6 signaling. This regulation appears to be downstream of the mTOR pathway as loss of DAPK3 enhanced S6K-S6 phosphorylation, but not ERK or AKT. Furthermore, this regulation is specific to mTORC1 and not mTORC2 as only loss of RAPTOR (and not RICTOR) partially rescues the augmented acinar morphogenesis observed upon loss of DAPK3. Collectively, our data reveal a novel tumor suppressive mechanism for DAPK3 through its inhibition of mTOR-S6K-S6 signaling (**Figure 12B**)

It is well known that the mTOR pathway plays an important role in cancer cell growth, survival and proliferation (22). As such, activation of the pathway is controlled by several

upstream tumor suppressors including LKB1 and NF1 (23,24). mTOR is the fundamental catalytic component of two distinct complexes, rapamycin-sensitive mTORC1 and rapamycin insentitive-mTORC2, each of which is composed of distinct protein complexes that alter the protein-protein interactions, subcellular localization, activity and substrate specificity of the active complex. Genetic ablation of key scaffolding proteins RAPTOR or RICTOR effectively prevents signaling through mTORC1 and mTORC2, respectively. Our data indicates that the increased acini size observed upon loss of DAPK3 is uniquely sensitive to mTORC1 inhibition. Indeed, mTORC1 has been shown to play a large role regulating many of the processes required for acini morphogenesis and thus these observations are expected.

Interestingly, several other members of the DAPK tumor suppressor family are known to regulate translation and regulate or be regulated by the mTOR pathway. Conflicting reports reveal that DAPK1 disrupts TSC1-TSC2 association thereby enhancing mTOR activation and negatively regulates protein translation through an inhibitory phosphorylation at S235/236 of S6 (25,26). However, *Roux et al.* revealed RSK-dependent phosphorylation at S235/ 236 actually promotes translation through assembly of the translational pre-initiation complex (27). DRAK2 phosphorylates S6K kinase *in vitro* and *in vivo* (28). DAPK3 is phosphorylated by DAPK1 *in vitro* and this DAPK1-DAPK3 kinase cascade has been shown to inhibit transcript-specific translation through phosphorylation of the ribosomal protein L13a and activation of an translational inhibitor complex known as the interferon-gamma activated inhibitor of translation (GAIT) complex (17,29). These observations along with our data implicate the DAPK family as important regulators of translation and mTOR signaling.

Overall, the research presented herein indicates that suppression of mTOR-S6K-S6 signaling by DAPK3 maintains proper acini morphogenesis and that these mechanisms

potentially exist in several human cancers where *DAPK3* mRNA is downregulated. Further studies are necessary to uncover the biochemical mechanism by which DAPK3 inhibits the mTOR pathway. Our data suggests that the kinase activity of DAPK3 is required and thus DAPK3 potentially induces an inhibitory pathway through activation of an mTOR inhibitor or inhibition of an mTOR activator. Interestingly, we did not observe an increase in soft agar micro-colony growth in MCF10A stably expressing the kinase dead mutant relative to empty vector control. This may indicate cell line specific effects as other cell lines have previously shown a dominant negative effect on proliferation with this mutant (2).

2.5 Figures

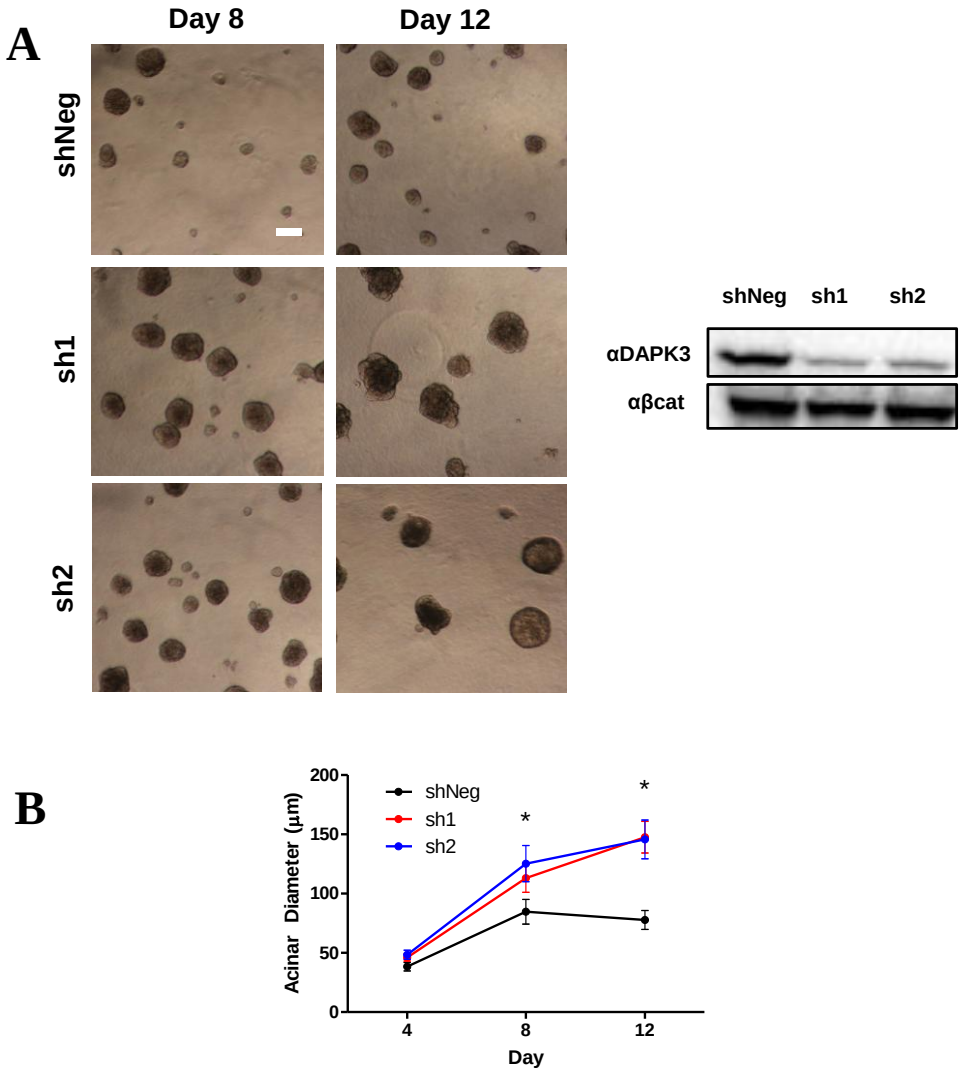

Figure 1. Loss of DAPK3 augments MCF10A acini. (A) MCF10A cells stably expressing shNeg or two independent DAPK3 hairpins (sh1, sh2) were cultured on Matrigel for 12 days. Brightfield images show representative structures at specific time points. (B) Mean diameter of MCF10A acini stably expressing respective hairpins at various time points. Depicted here is a representative of three independent experiments. Error bars indicate 95% confidence intervals. *, $P < 0.005$ relative to control.

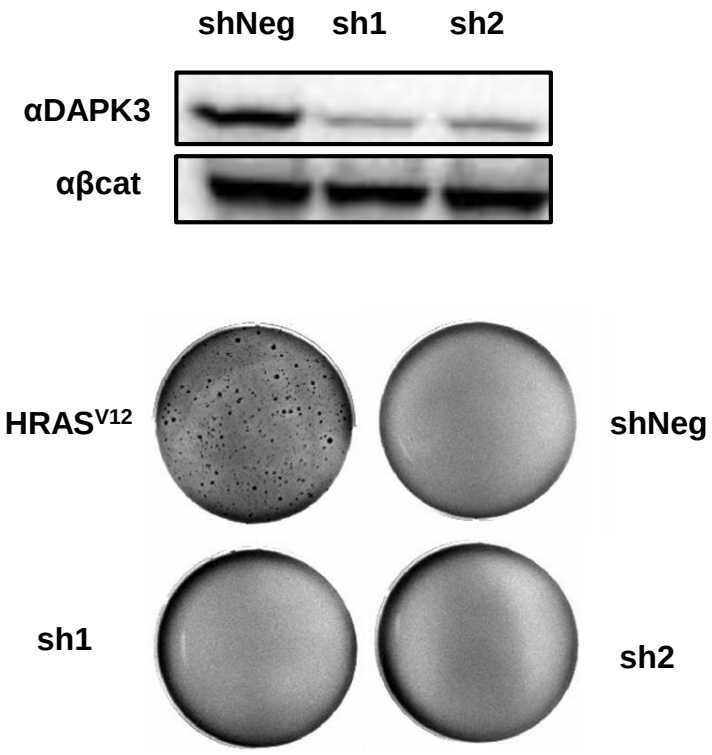

Figure 2. Loss of DAPK3 expression does not promote anchorage independent growth of MCF10A cells. Stable MCF10A cell lines were grown in soft agar for 3 weeks.

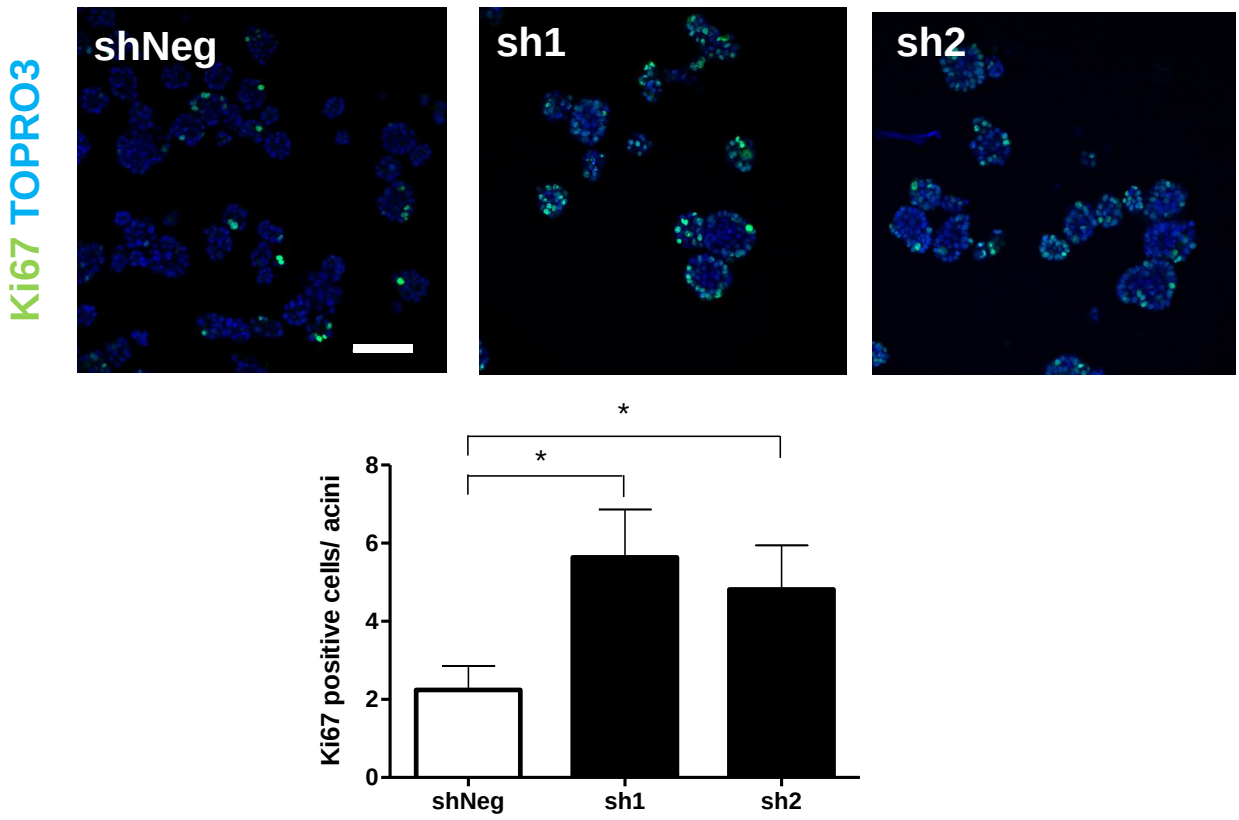

Figure 3. DAPK3 depleted acini exhibit increased proliferation. Fluorescent confocal microscopy analysis of acini stained for Ki67 (green) and DNA (blue). Depicted here is a representative of two independent experiments. Error bars indicate 95% confidence intervals. *, $P < 0.001$.

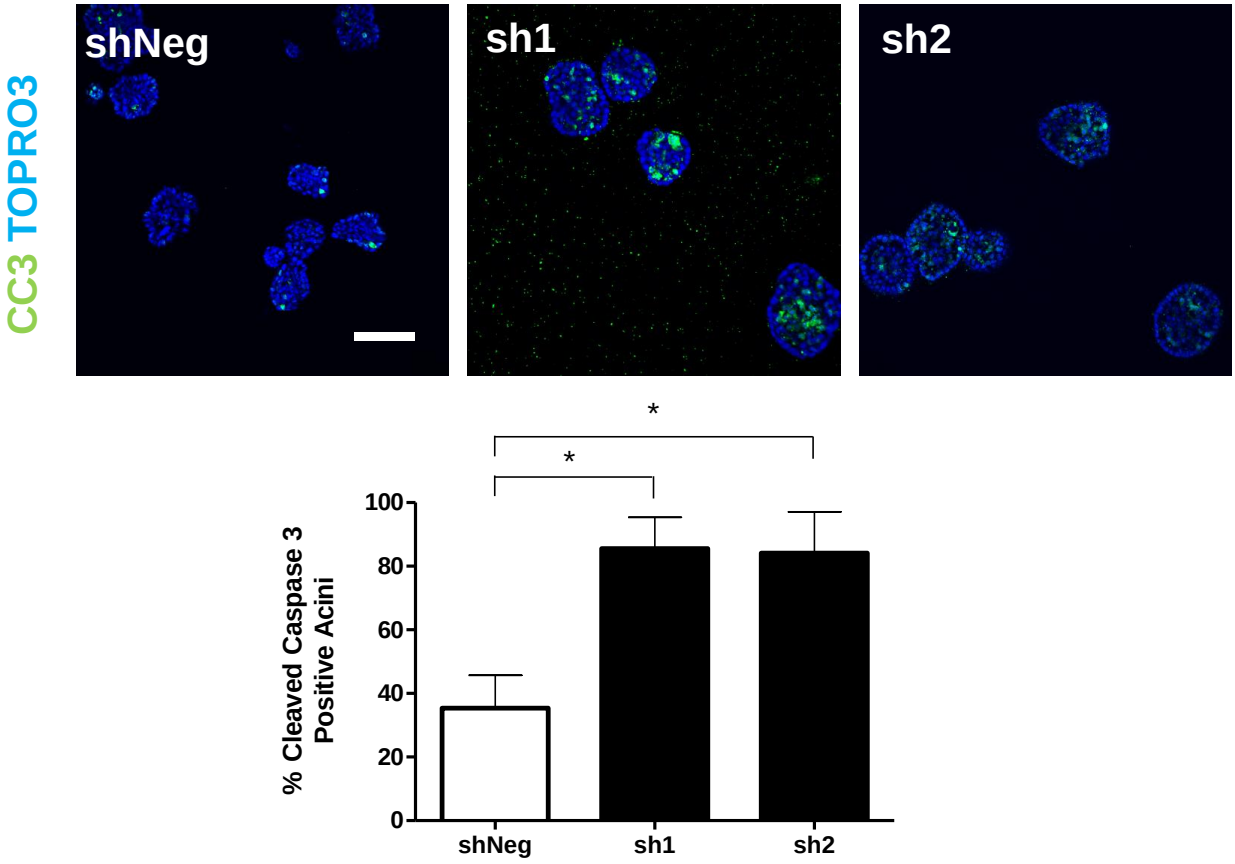

Figure 4. DAPK3 depleted acini exhibit increased apoptosis. Fluorescent confocal microscopy analysis of acini stained for cleaved caspase 3 (CC3, green) and DNA (TOPRO3, blue). Depicted here is a representative of three independent experiments. Error bars indicate 95% confidence intervals. *, $P < 0.0001$ relative to control.

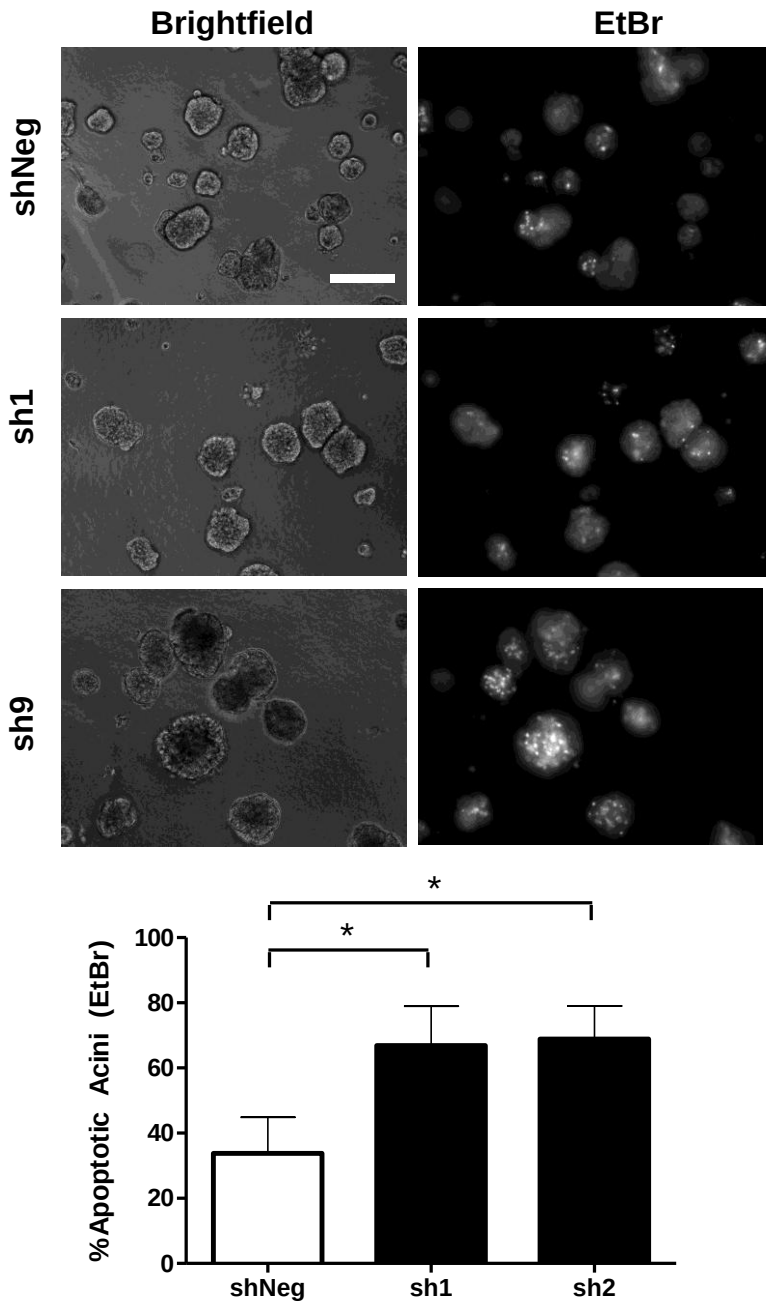

Figure 5. DAPK3 depleted acini display increased ethidium bromide positive cells. Live MCF10A acini stably expressing negative control or shDAPK3 hairpins were incubated with 1 µg/ mL ethidium bromide at day 6 and subsequently analyzed. Shown here is a representative of three independent experiments. Error bars indicate 95% confidence intervals. **, $P < 0.0001$. Scale bar, 100µm.

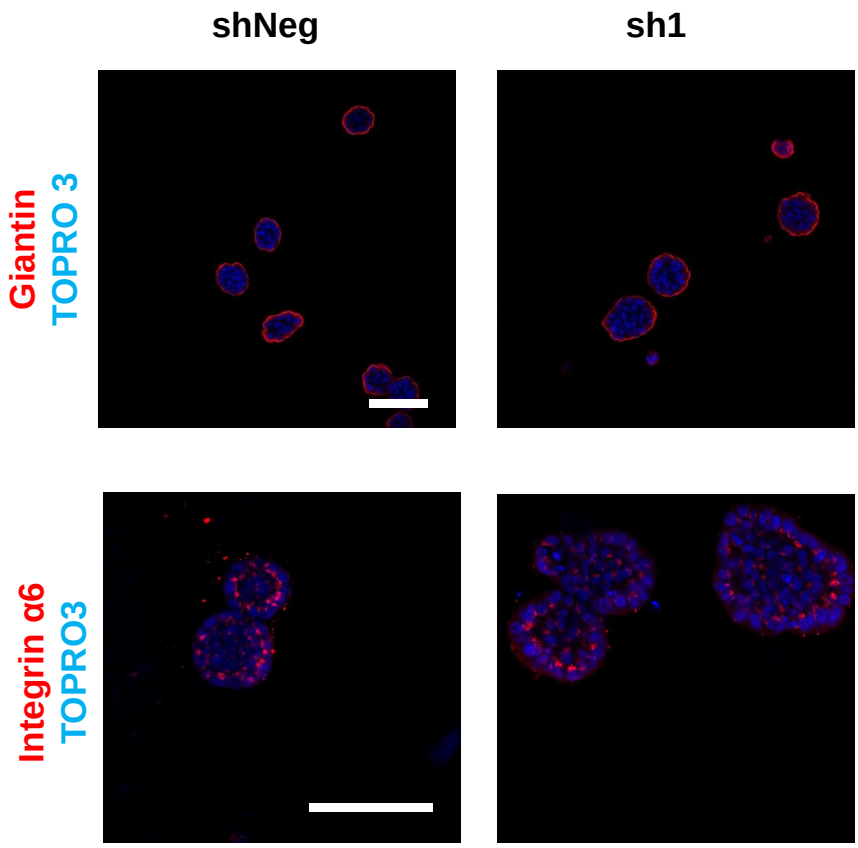

Figure 6. DAPK3 depleted acini show proper localization of apical-basolateral markers. Day 6 structures were analyzed for proper localization of apical marker giantin (red, top panel) and basolateral marker integrin α6 (red, bottom panel) along with DNA stain (TOPRO3, blue). Scale bars, 100µm.

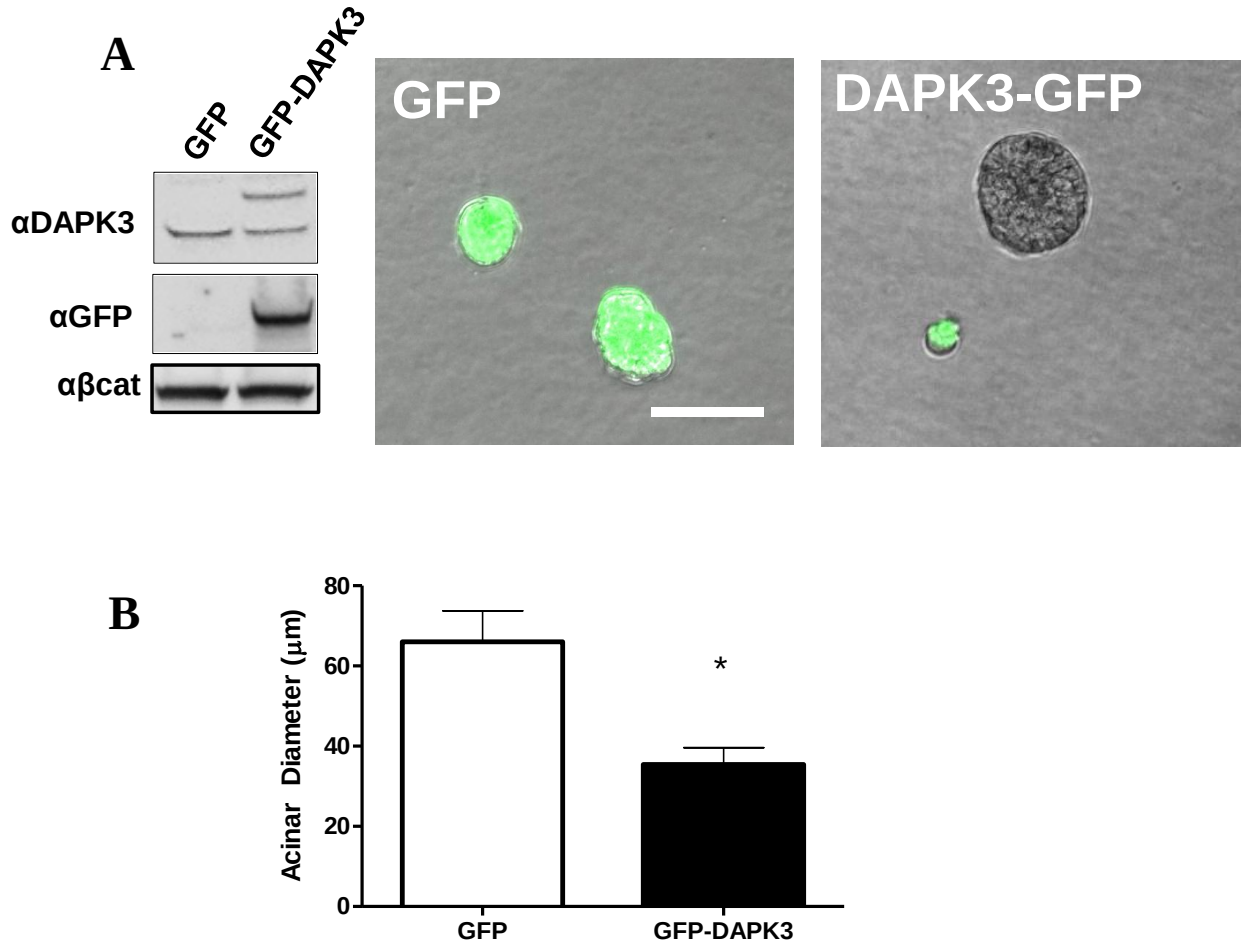

Figure 7. Stable overexpression of DAPK3 inhibits acini growth. (A) Fluorescent microscopy of live acini stably overexpressing GFP or GFP-DAPK3 at day 8. Scale bar, 100μm. (B) Size analysis of day 8 GFP+ acini from GFP or GFP-DAPK3 stable structures. Error bars indicate 95% confidence intervals of three combined independent experiments.*, $P < 0.0001$ relative to control.

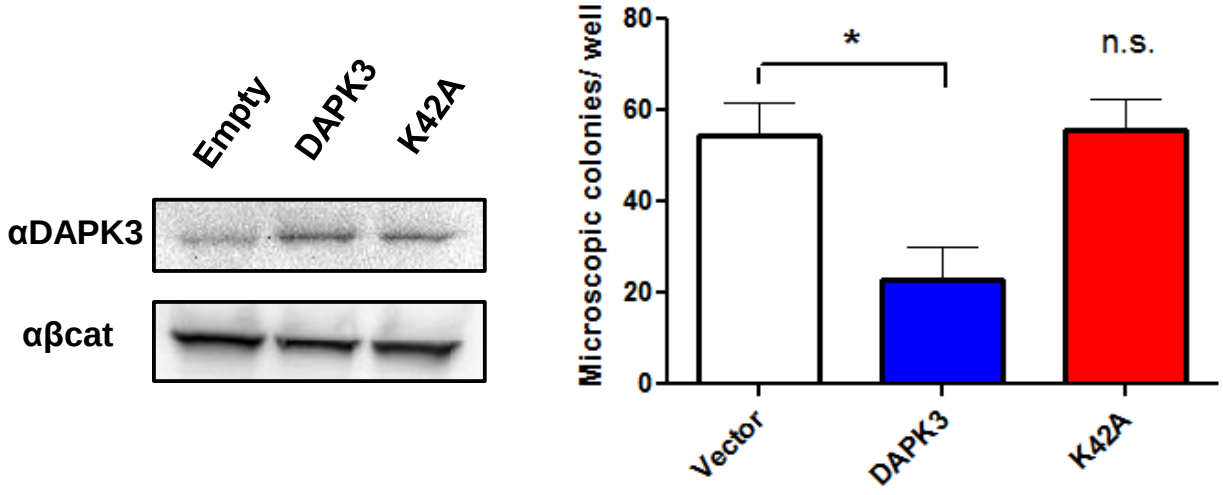

Figure 8. Stable overexpression of a DAPK3 kinase dead point mutant does not alter microscopic colony growth. MCF-10A cell stably overexpression empty vector, DAPK3 or K42A were grown in soft agar for 3 weeks and then total numbers of microscopic colonies were counted. Shown here is a representative of three independent experiments. Error bars indicated 95% confidence intervals.*, P< 0.001.

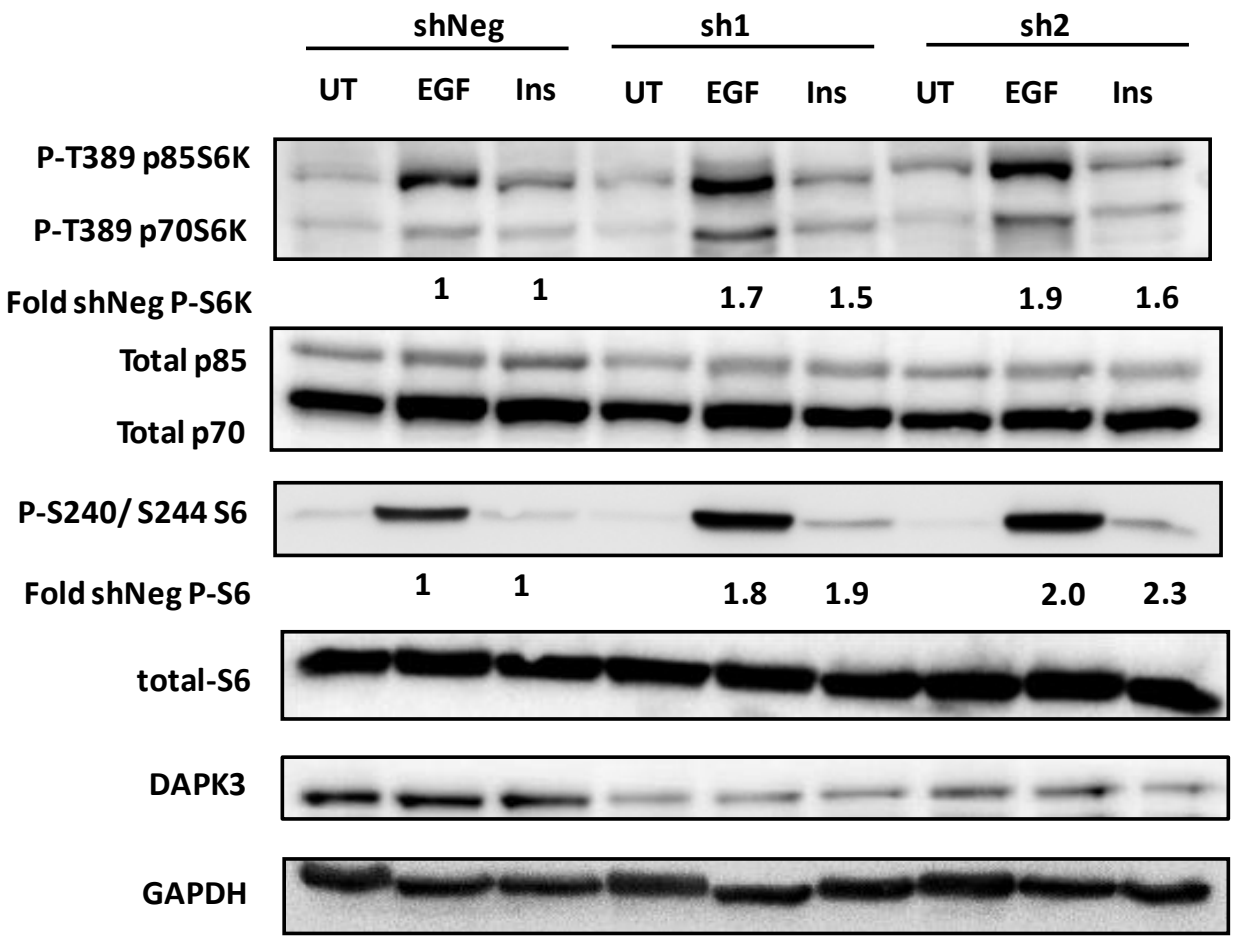

Figure 9. Increased activation of mTOR specific S6K-S6 pathway upon loss of DAPK3 in stable MCF10A cells. Western blot analysis of serum starved MCF10A stable cells grown in 2D and treated with media, EGF (10ng/ mL) or insulin (10 ug/mL) for 24hrs. Shown here is a representative blot of three independent experiments.

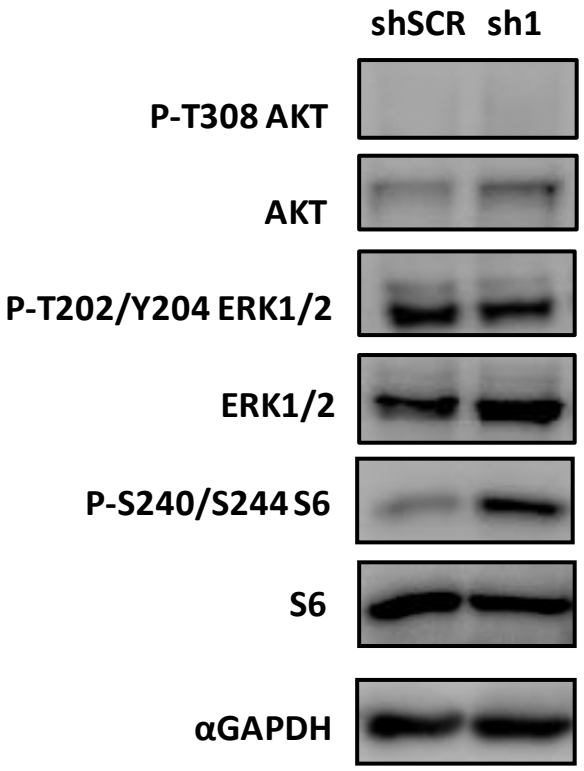

Figure 10. Increased phosphorylation of S6 upon loss of DAPK3 in stable MCF10A acini. Western blot analysis of MCF10A acini grown on Matrigel for 6 days. Shown here is a representative blot of two independent experiments.

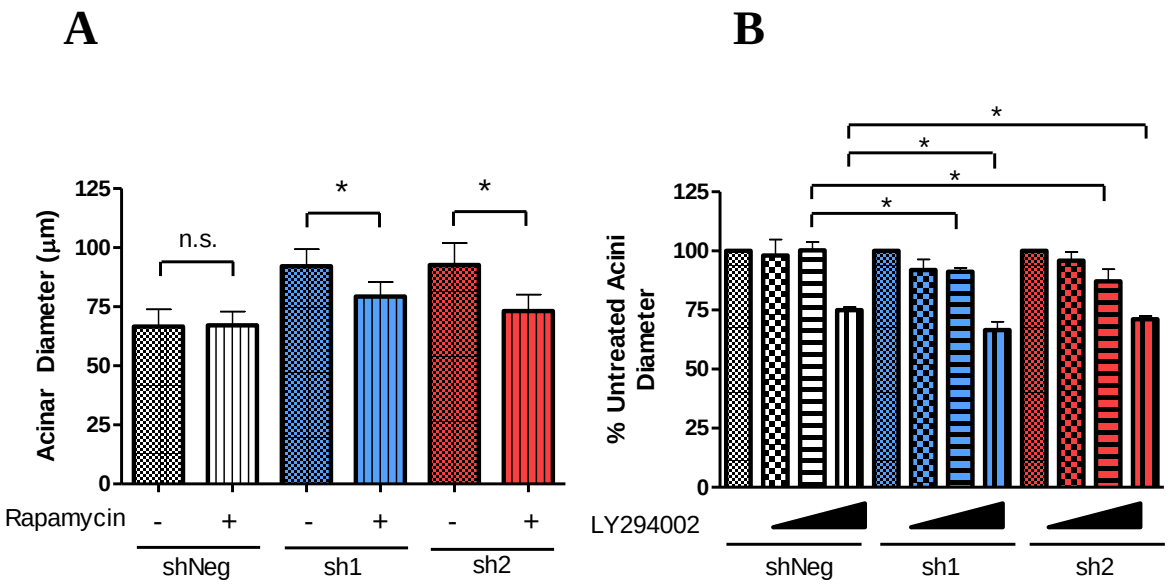

Figure 11. DAPK3 depleted acini are sensitive to rapamycin and LY294002 treatment. (A) Analysis of MCF10A acini grown for 4 days and then treated with 100 nM rapamycin for 4 days. Shown here is a representative of two independent experiments. Error bars indicate 95% confidence intervals. **, P<0.0001. *, P<0.005. (B) Analysis of MCF10A acini grown for 4 days and then treated with varying concentrations of LY294002 (vehicle, 100 nM, 10 µM, or 50 µM) for an additional 4 days. Error bars indicate standard deviations of three combined independent experiments. *, P<0.03.

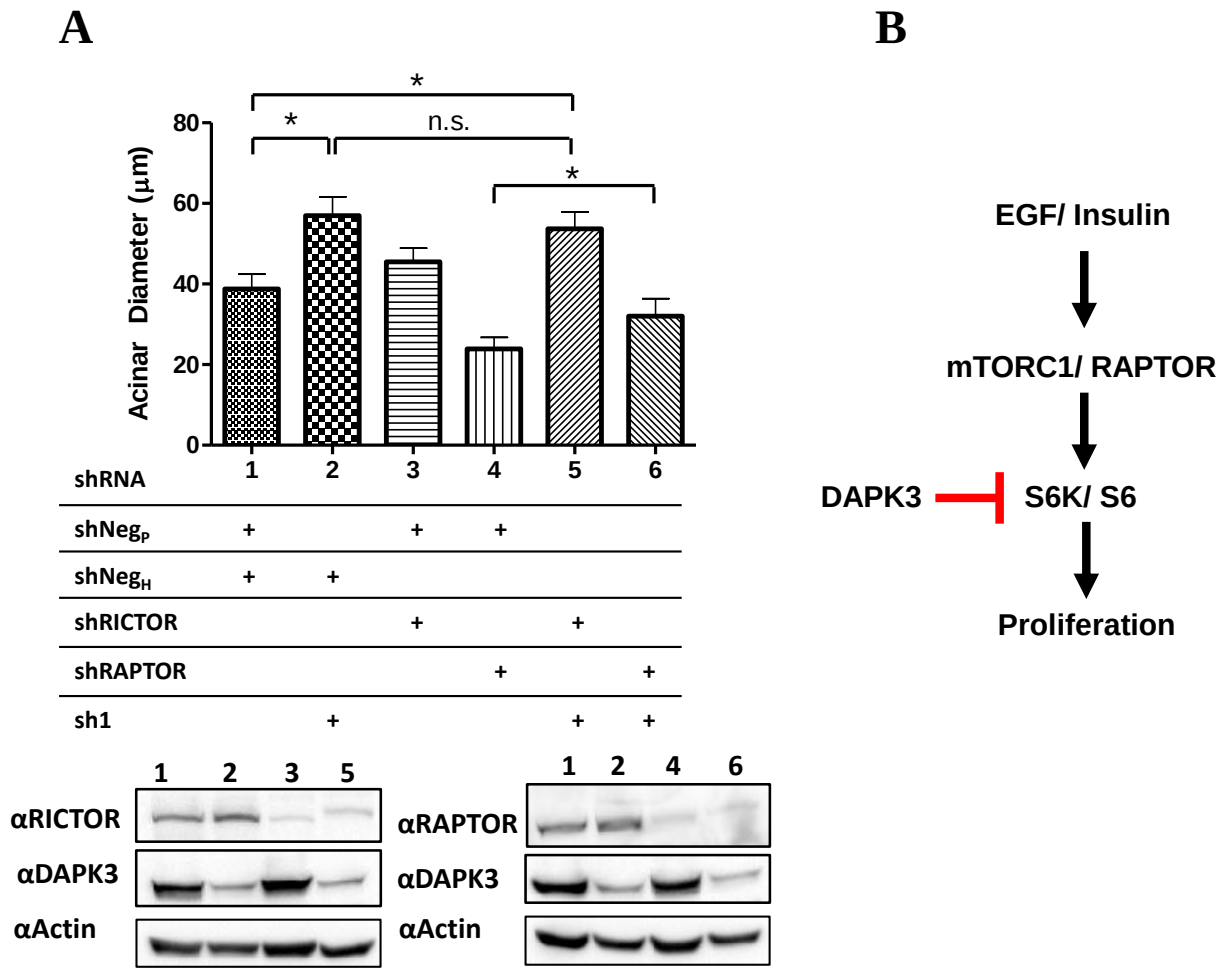

Figure 12. DAPK3 inhibits acini morphogenesis through mTORC1/ RAPTOR. (A) Analysis of day 4 acini from MCF10A cells stably expressing various hairpins. Shown here is a representative of two independent experiments. Error bars indicate 95% confidence intervals. *, P<0.01. (B) Depiction of negative regulation of the mTORC1-S6K-S6 pathway by DAPK3.

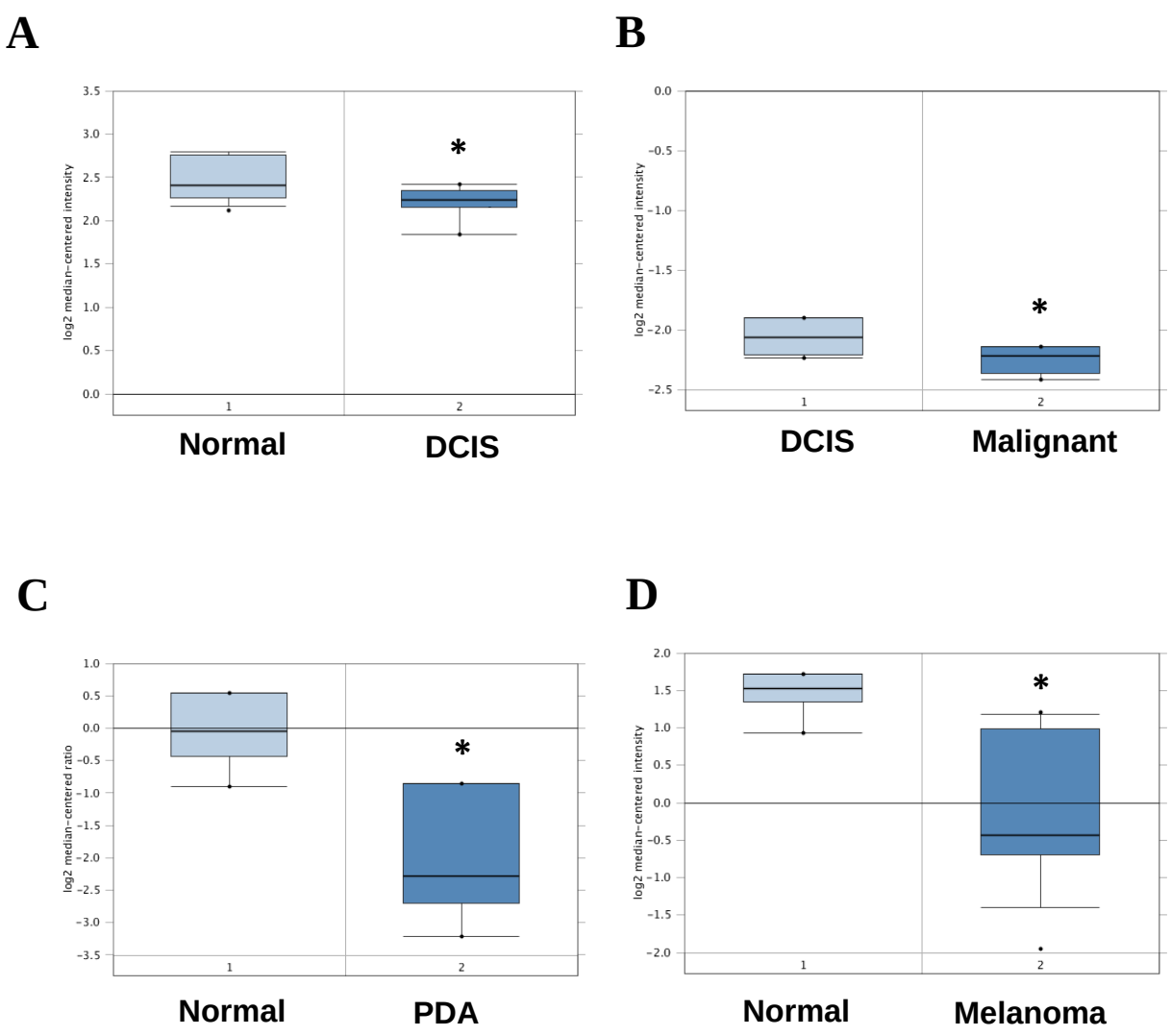

Figure 13. Clinically observed downregulation of *DAPK3* mRNA in breast and various cancers from the Oncomine database (www.oncomine.org). (A) *DAPK3* mRNA is significantly decreased in ductal carcinoma *in situ* (DCIS) relative to normal patient samples. *, P<0.002 (B) *DAPK3* mRNA is significantly decreased in aggressive breast cancer patient samples compared to normal patient samples. *, P<0.04. (C) Significant decrease in *DAPK3* mRNA expression in pancreatic ductal adenocarcinoma (PDA) relative to normal patient samples. *, P<0.01. (D) Significant decrease in *DAPK3* mRNA expression in melanoma relative to normal patient skin samples. *, P<0.001.

2.6 References

1. Usui, T., Okada, M., and Yamawaki, H. (2014) *Apoptosis* **19**, 387-391

2. Brognard, J., Zhang, Y. W., Puto, L. A., and Hunter, T. (2011) *Cancer Res* **71**, 3152-3161

3. Natrajan, R., Mackay, A., Lambros, M. B., Weigelt, B., Wilkerson, P. M., Manie, E., Grigoriadis, A., A'Hern, R., van der Groep, P., Kozarewa, I., Popova, T., Mariani, O., Turajlic, S., Furney, S. J., Marais, R., Rodruigues, D. N., Flora, A. C., Wai, P., Pawar, V., McDade, S., Carroll, J., Stoppa-Lyonnet, D., Green, A. R., Ellis, I. O., Swanton, C., van Diest, P., Delattre, O., Lord, C. J., Foulkes, W. D., Vincent-Salomon, A., Ashworth, A., Henri Stern, M., and Reis-Filho, J. S. (2012) *J Pathol* **227**, 29-41

4. Kawai, T., Matsumoto, M., Takeda, K., Sanjo, H., and Akira, S. (1998) *Mol Cell Biol* **18**, 1642-1651

5. Bi, J., Lau, S. H., Hu, L., Rao, H. L., Liu, H. B., Zhan, W. H., Chen, G., Wen, J. M., Wang, Q., Li, B., and Guan, X. Y. (2009) *Int J Cancer* **124**, 1587-1593

6. Tan, X. L., Moyer, A. M., Fridley, B. L., Schaid, D. J., Niu, N., Batzler, A. J., Jenkins, G. D., Abo, R. P., Li, L., Cunningham, J. M., Sun, Z., Yang, P., and Wang, L. (2011) *Clin Cancer Res* **17**, 5801-5811

7. Togi, S., Ikeda, O., Kamitani, S., Nakasuji, M., Sekine, Y., Muromoto, R., Nanbo, A., Oritani, K., Kawai, T., Akira, S., and Matsuda, T. (2011) *J Biol Chem* **286**, 19170-19177

8. Felten, A., Brinckmann, D., Landsberg, G., and Scheidtmann, K. H. (2013) *Oncogene* **32**, 4981-4988

9. Page, G., Lodige, I., Kogel, D., and Scheidtmann, K. H. (1999) *FEBS Lett* **462**, 187-191

10. Kawai, T., Akira, S., and Reed, J. C. (2003) *Mol Cell Biol* **23**, 6174-6186

11. Boosen, M., Vetterkind, S., Kubicek, J., Scheidtmann, K. H., Illenberger, S., and Preuss, U. (2009) *Mol Biol Cell* **20**, 4010-4020

12. Sato, N., Kawai, T., Sugiyama, K., Muromoto, R., Imoto, S., Sekine, Y., Ishida, M., Akira, S., and Matsuda, T. (2005) *Int Immunol* **17**, 1543-1552

13. Weigelt, B., and Bissell, M. J. (2014) *Adv Drug Deliv Rev*

14. Debnath, J., Muthuswamy, S. K., and Brugge, J. S. (2003) *Methods* **30**, 256-268

15. Moffat, J., Grueneberg, D. A., Yang, X., Kim, S. Y., Kloepfer, A. M., Hinkle, G., Piqani, B., Eisenhaure, T. M., Luo, B., Grenier, J. K., Carpenter, A. E., Foo, S. Y., Stewart, S. A., Stockwell, B. R., Hahn, W. C., Lander, E. S., Sabatini, D. M., and Root, D. E. (2006) *Cell* **124**, 1283-1298

16. Partanen, J. I., Nieminen, A. I., Makela, T. P., and Klefstrom, J. (2007) *Proc Natl Acad Sci U S A* **104**, 14694-14699

17. Shani, G., Marash, L., Gozuacik, D., Bialik, S., Teitelbaum, L., Shohat, G., and Kimchi, A. (2004) *Mol Cell Biol* **24**, 8611-8626

18. Anczukow, O., Rosenberg, A. Z., Akerman, M., Das, S., Zhan, L., Karni, R., Muthuswamy, S. K., and Krainer, A. R. (2012) *Nat Struct Mol Biol* **19**, 220-228

19. Debnath, J., Walker, S. J., and Brugge, J. S. (2003) *J Cell Biol* **163**, 315-326

20. Ghosh, S., Varela, L., Sood, A., Park, B. H., and Lotan, T. L. (2013) *Cancer Res* **73**, 5218-5231

21. Sarbassov, D. D., Guertin, D. A., Ali, S. M., and Sabatini, D. M. (2005) *Science* **307**, 1098-1101

22. Laplante, M., and Sabatini, D. M. (2012) *Cell* **149**, 274-293

23. Johannessen, C. M., Reczek, E. E., James, M. F., Brems, H., Legius, E., and Cichowski, K. (2005) *Proc Natl Acad Sci U S A* **102**, 8573-8578

24. Shaw, R. J., Bardeesy, N., Manning, B. D., Lopez, L., Kosmatka, M., DePinho, R. A., and Cantley, L. C. (2004) *Cancer Cell* **6**, 91-99

25. Stevens, C., Lin, Y., Harrison, B., Burch, L., Ridgway, R. A., Sansom, O., and Hupp, T. (2009) *J Biol Chem* **284**, 334-344

26. Schumacher, A. M., Velentza, A. V., Watterson, D. M., and Dresios, J. (2006) *Biochemistry* **45**, 13614-13621

27. Roux, P. P., Shahbazian, D., Vu, H., Holz, M. K., Cohen, M. S., Taunton, J., Sonenberg, N., and Blenis, J. (2007) *J Biol Chem* **282**, 14056-14064

28. Mao, J., Luo, H., Han, B., Bertrand, R., and Wu, J. (2009) *J Immunol* **182**, 4762-4770

29. Mukhopadhyay, R., Ray, P. S., Arif, A., Brady, A. K., Kinter, M., and Fox, P. L. (2008) *Mol Cell* **32**, 371-382

CHAPTER 3: DAPK3 IS REQUIRED FOR EARLY MOUSE DEVELOPMENT & DISPLAYS DISTINCT EXPRESSION PATTERNS IN EMBRYONIC AND ADULT TISSUES

3.1 Introduction

The serine/ threonine death-associated protein kinase (DAPK) family is a relatively novel kinase family. The DAPK family is known to regulate smooth muscle contraction, cell-cell adhesion, cytoskeleton dynamics, inflammation, and cardiovascular functions as well as tumor suppression through regulation of caspase-dependent and -independent cell death, proliferation and autophagy (1). The DAPK family contains 5 members, including DAPK1 , DRP-1 (DAPK-related protein 1), DAPK3 (also known as zipper interacting protein kinase (ZIPK), DRAK-1 and DRAK-2 (DAPK-related apoptosis-inducing protein kinase-1 and -2), which all share high homology within their kinase domain (1). Compared to the prototypical family member DAPK1, relatively little is known about DAPK3. DAPK3 contains an N-terminal kinase domain that shares 80% amino acid homology with the prototypical DAPK1. It differs from other family members by the presence of a C-terminal leucine zipper motif and the absence of a calmodulin-regulated (CaM) domain and death domain. Similar to other family members, DAPK3 is considered to be a putative tumor suppressor. Overexpression of DAPK3 in mammalian cells results in cell death and cell cycle inhibition while kinase inactivating mutations along with recurrent deleterious somatic mutations are observed in lung and breast cancers, respectively (2–4). Additionally, DAPK3 has been shown to interact with and/ or phosphorylate various proteins *in vitro* including ATF4, AATF, Daxx, Par-4, STAT3, NLK, and AR (2,4–9).

Currently, a fundamental understanding of DAPK3 is limited due to the lack of a knockout mouse. Commonly used model systems such as *Caenorhabditis elegans, Saccharomyces cerevisiae*, and *Drosophila melanogaster* lack clear DAPK3 orthologues, thereby hindering traditional genetic interrogation. Uncovering the physiological contributions of DAPK3 is crucial to understanding the clinical and basic research observations described above. Furthermore, DAPK1 and DAPK3 inhibitors are currently under development for use in smooth muscle related disorders (10,11). Thus, a DAPK3 deficient animal may indicate potentially deleterious phenotypes associated with loss of a functional DAPK3 protein.

Given these gaps in the fundamental understanding of DAPK3 we generated a DAPK3 knockout mouse using a gene trap embryonic stem cell line acquired from the International Gene Trap Consortium. Although mechanistically different than traditional *flx*/ *flx* knockout strategies, gene traps have provided a cost-effective and high throughput means to functionalize the mouse genome (12). Described herein is the generation and characterization of the unexpected early lethality of DAPK3 null mice. Additionally, we identified a distinct and localized pattern of Dapk3 promoter activity within the developing heart and nervous system. We also observed that the Dapk3 promoter is active in the myenteric plexus of the large intestine and breast epithelium of adult mice. Collectively these results identify a fundamental role for DAPK3 in mouse development and identify distinct expression patterns in developing and adult animals.

3.2 Materials & Methods

Generation of DAPK3 KO Mice

The pre-confirmed BayGenomics ES line YTA407, was acquired from the International Gene Trap Consortium and injected into albino C57BL/6 mice using traditional techniques. One initial

founder chimaera was chosen due to high degree chimerism as assessed by coat color and subsequently backcrossed onto a pure albino C57BL/6 background (N6 as determined by speed congenics). Polymerase chain reaction genotyping was performed using the following primers: Forward 5' GTGTGCATATGTGTCTTAGTCACAGCAC, Reverse 5' GGCGATTAAGTTGGGTAACGCCAG, Reverse 5' GACAGTATCGGCCTCAGGAAGATC G.

Southern Blot

For each southern blot, 5 µg of isolated DNA was digested with SphI overnight at 37°C. Digested DNA was run on a 1.0% agarose gel and subsequently transferred to a charged nylon membrane after depurination, denaturation and neutralization. After crosslinking, the transfer membrane was blocked in pre-heated Hyb Plus Buffer (Sigma) and salmon sperm at 68°C for 2 hours with constant agitation. Polymerase chain reaction was used to generate the following southern probes from heterozygous genomic DNA, Internal: Forward, 5' GACTCGATGGCTGAGGACGGTACGAATG, Reverse, 5' CTCAAGAGGCTGAGGCTGGAGGATTAAACA; External: Forward, 5' CACGGAGAATCCGACGGGTTGTTACTCGC, Reverse, 5' GCACATCTGAACTTCAGCCTCCAGTAC. After gel purification, probes were labeled with 50 µCi of 32^{α}P-dCTP (Perkin Elmer) using the Roche Random Prime Labeling Kit and then cleaned on an Ambion Column. Hybridization occurred overnight at 68°C with constant agitation. The following day, membranes were washed and subsequently imaged using a Phospho-screen and Storm 860.

Blastocyst Isolation and Genotyping

E3.5 embryos were harvested from mated super ovulated females (<6 weeks). Whole genome amplification was then performed on individual blastocysts (Sigma WGA4) followed by standard PCR genotyping as described above.

Generation of Embryonic Stem (ES) Cell Lines

E3.5 embryos were harvested from mated super ovulated females (<6 weeks). Isolated blastocysts were then seeded on pre-plated gamma irradiated MEF feeder cells in a 96 well plate. Prior to seeding the blastocysts, standard MEF media was changed to the following primary ES media: KO DMEM (Gibco), 7.5% KO Serum replacement (Invitrogen), 7.5% ES tested FBS (Hyclone), non-essential amino acids (Gibco), L-glutamine (Gibco), 0.1 mM β-mercaptoethanol, 1,000 Units/ mL leukemia inhibitor factor (LIF), 3 µM CHIR99021, 1 µM PD0325901, 10 µM SB431542 and penn/ strep. Plated blastocysts were maintained at 37 C, 5% CO_2. Fresh ES media was supplemented every 2 days. When a large portion of the inner cell mass had grown out of the attached blastocyst the well was trypsinized and plated onto a pre-plated MEF layer in a 96 well plate similar to before. Once ES colonies were clearly apparent the culture was serially passaged up to a T25 at which point multiple freeze downs were made.

Quantitative PCR (qPCR)

The TaqMan Assay was used to quantify *Dapk3* mRNA isolated (RNAeasy) from genotype confirmed ES lines. FAM conjugated probes were manufactured by Life Technologies/ Applied Biosystems that were complimentary and spanned exons 8-9 of the endogenous mouse Dapk3 locus (Mm00492083_g1). A VIC conjugated mouse actin probe was used as a control.

Immunoblotting

Harvested cells were re-suspended and sonicated in radioimmunoprecipitation assay (RIPA) buffer (50mM Tris-HCl, pH 7.4, 150 mM NaCl, 1% Triton X-100, 0.1% SDS, 0.5% deoxycholic acid) containing protease and phosphatase inhibitors (1mM phenylmethylsulfonyl fluoride (PMSF), 0.4 U/ml aprotinin, 10 μg/ml leupeptin, 10 μg/ml pepstatin, 1 mM β–glycerophosphate, 0.1 mM NaF, 0.1 mM $NaVO_4$). Proteins (30 to 80 μg) were fractionated on 10% Tris-HCl, Criterion Precast Gel (Bio-Rad). Separated proteins were transferred onto polyvinylidene difluoride (PVDF) membranes (Millipore), and probed with the following antibodies: rabbit anti-DAPK3/ ZIPK (Cell Signaling, 2928), rabbit anti-β catenin (Santa Cruz, H-102), rabbit anti-Actin (Sigma-Aldrich, A2066) and rabbit IGG fraction against *β*-galactosidase (MP, 08559761).

Tissue prep, fixation and β-galactosidase activity

Embryos were fixed in 0.2 % glutaraldehyde for 20 minutes at 4°C and then washed twice for 10 minute in wash buffer (0.1M phosphate buffer pH7.3, 2 mM $MgCl_2$, 5 mM EGTA, 0.01% sodium deoxycholate and 0.02% NP40). Washed embryos were then stained overnight at 37°C in the following staining solution: wash buffer, 5 mM potassium ferrocyanide, 5 mM potassium ferricyanide and 1 mg/ mL Xgal. The following day embryos were fixed in 10% paraformaldehyde for 30 minutes and then washed 3 times in PBS for 10 minutes each. Whole mount photography was performed after embryos were serially incubated in 50%, 75% and 90% glycerol. For intestinal fixation and β-gal activity, the same protocol was generally followed as described above.

Immunofluorescence

Mammary glands from 8 week old female littermates were dissected and fixed in 4% paraformaldehyde for 1 hour at 4°C. Glands were then washed twice for 5 minutes in PBS at 4°C. Subsequently, glands were immersed in 15% sucrose for 4 hours at 4°C and then 30% sucrose overnight at 4°C. The following day glands were embedded in OCT and stored at -80°C overnight. 10 µm sections were placed on Superfrost/ Plus charged slides and stored at -80°C overnight. For labeling, slides were thawed at room temperature for 10 minutes and then washed for 5 minutes in PBS to remove OCT residue. Slides were then blocked with 10% donkey serum, 1% bovine serum albumin, 0.2% non-fat dry milk and 0.3% Triton X-100 in PBS for 1.5 hours at room temperature. Slides were then incubated with respective primary antibodies in blocking buffer overnight at 4°C in a humidified chamber. The following primary antibodies were used: rabbit anti-β-galactosidase (MP, 559761) and mouse anti-E-cadherin (BDbiosciences, 610182). Slides were washed three times for 5 minutes with PBS and then incubated with fluorophore conjugated secondary antibodies (Alexa Fluor 488 or 594) diluted in blocking buffer for 1 hour at room temperature in the dark. Slides were then washed three times for 5 minutes in PBS and then mounted in DAPI-containing Vecta Shield and imaged using a Nikon Eclipse T*i* microscope at the same exposure settings and subsequently processed using ImageJ software.

3.3 Results

Generation of DAPK3 null mice

In an attempt to understand the overall *in vivo* contribution of DAPK3, we created a constitutive DAPK3 knockout mouse using a pre-confirmed gene trap ES line from the

International Gene Trap Consortium. The gene trap (Gt) is composed of a 5' splice acceptor site followed by a β galactosidase- neomycin fusion (*βgeo*) and a *polyA* tail (**Figure 1 A**). Initially we confirmed that the locus and the entire gene trap were intact and incorporated as a single insertion through Southern Blot analysis using both external probes and internal probes on a single clonal population of YTA407 ES cells (**Figure 1 B**). These ES cells were then used to generate a mouse using traditional blastocyst injection and animal husbandry techniques that were successfully genotyped as seen in the representative genotyping polymerase chain reaction (PCR) (**Figure 1 B, lower panel**).

Characterization of early embryonic lethality of DAPK3 null mice

Overall, heterozygous animals appear to develop and grow normally with no overt phenotypes under standard laboratory conditions (**Figure 1 C**). However, we were unable to find homozygous gene trap animals on a mixed 129Ola or backcrossed C57BL/6 (N5) background (**Table I**). We were also unable to locate homozygous gene trap embryos at E12.5, 10.5, and 8.5 despite near Mendelian ratios for wild type and heterozygous embryos, indicating early homozygous lethality (**Table I**).

We also observed the presence of several sites of fetal resorption on uteri extracted from heterozygous crosses versus heterozygous and wild type crosses (**Figure 2 A**). We were able to isolate and genotype homozygous gene trap blastocysts at E3.5 (**Figure 2 B**) indicating that lethality was potentially occurring post-implantation. Furthermore, there was no difference in distribution of homozygous embryos across blastocyst, morula and pre-morula (**Figure 2 C**).

In order to confirm that the gene trap was functional, we used both quantitative PCR (qPCR) and immunoblotting analysis. qPCR performed on mRNA extracted from established and genotype-confirmed primary embryonic stem cells indicated a gene-dose dependent decrease in the expression of *Dapk3* mRNA. Specifically, a heterozygous ES lines expressed approximately 50% *Dapk3* mRNA and several homozygous gene trap lines expressed very little *Dapk3* mRNA relative to a wild type control (**Figure 3 A**).

Next to further confirm a functional gene trap, we attempted to visualize differences in DAPK3 protein expression from established primary ES lines. After several discussions with technical staffs at various commercial antibody manufacturers we were unable to locate antibodies that were able to detect endogenous levels of the mouse 53 kDa DAPK3 protein (**Figure 3 B**). A representative inaccurate antibody is provided that recognized a single protein shown to repeatedly migrate lower than 50 kDa. Despite these technical setbacks we were able to utilize a β-galactosidase specific antibody that displayed a reactive band that migrated at the size calculated to match a protein produced from the fusion of the first 2 exons of DAPK3 and the remaining β-galactosidase-neomycin cassette produced by the gene trap (**Figure 3 B**).

Embryonic and adult expression patterns of the mouse Dapk3 promoter

Taking advantage of the functional βgal expressed under the endogenous Dapk3 promoter we characterized the expression patterns of *Dapk3* during the development of heterozygous mice. We observed distinct and strong βgal activity in the developing heart of E8.5 and E10.5 embryos (**Figure 4A, B**). Additionally, E10.5 heterozygous embryos displayed localized activity within the developing notochord (**Figure 4B**). As expected, no β-gal activity was observed in developing wildtype littermates (*data not shown*). We were also able to

visualize localized activity in the developing arms, legs and notochord of E13.5 fetuses (**Figure 4 C**).

We next attempted to visualize Dapk3 promoter activity through β-gal activity and immunofluorescence techniques in the large intestine and breast of adult heterozygous mice. Strong and distinct β-gal activity was observed in the myenteric plexus (gastrointestinal nervous system) of the large intestine (**Figure 5 A**) with no β-gal activity observed in wildtype littermate controls (*data not shown).* Additionally, immunofluorescence using a β-gal specific antibody indicated that the Dapk3 promoter is active in epithelial cells of the mouse mammary gland (**Figure 5 B**).

3.4 Discussion

Our work has identified that DAPK3 is necessary for early mouse development and that the Dapk3 promoter displays distinct organ and cellular promoter expression patterns. Our analysis indicates that DAPK3 deficient blastocysts are able to implant but subsequent development is problematic. These results were unanticipated given that DAPK1 null mice develop normally as indicated by their overall health in common laboratory settings (13). This dichotomy raises a number of questions regarding signaling redundancies between DAPK and DAPK3 and suggests important DAPK-independent developmental functions for DAPK3. Clearly, future investigation is required and our work supports the development of conditional DAPK3 knockout mice.

Our work also suggests that mouse DAPK3 exhibits localized expression in the developing heart and nervous system. These expression patterns and our developmental observations are of potential relevance to human development as human DAPK3 resides on

19p13.3, a region shared by 7 other genes that when deleted results in face and heart structure abnormalities, along with intellectual disability and development delay(14).

3.5 Figures

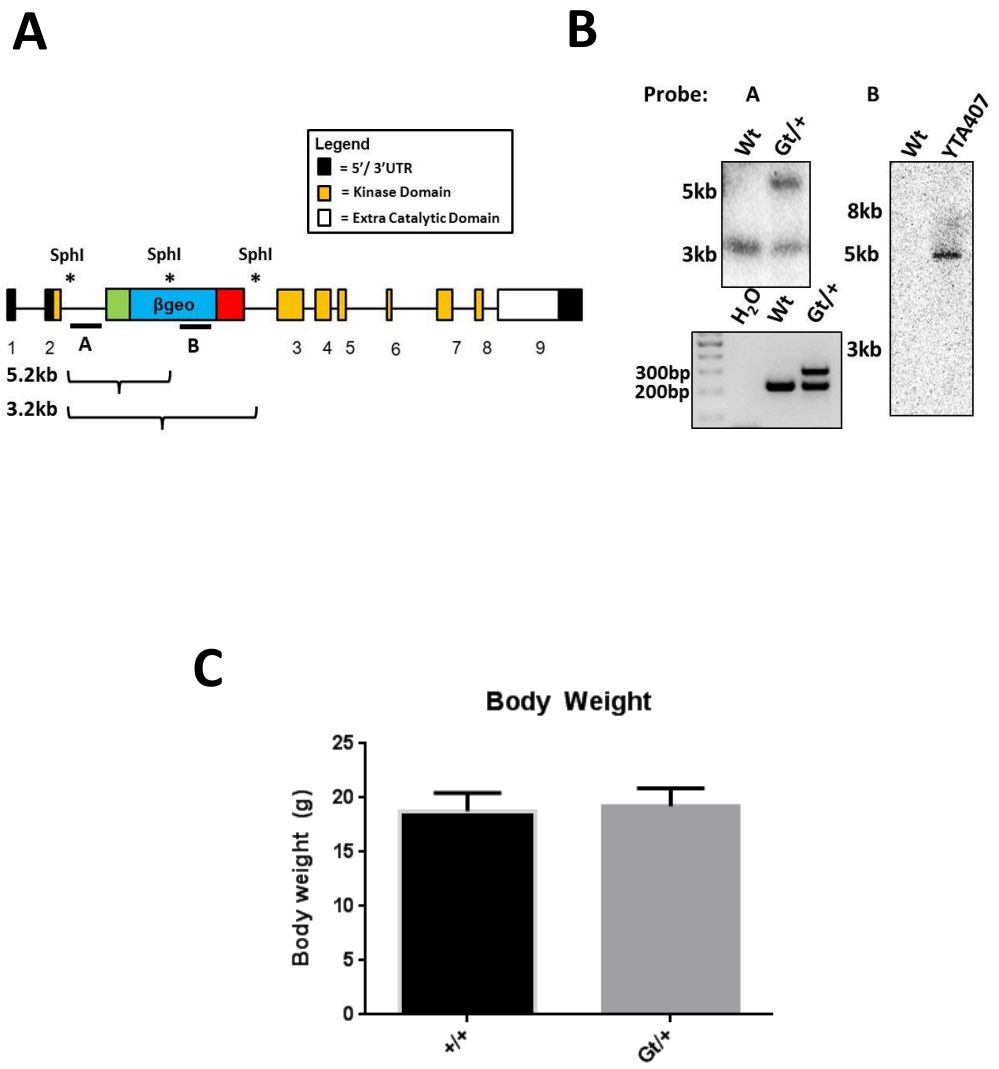

Figure 1. Generation and characterization of DAPK3 knockout mice. (A) Schematic representation of the Dapk3$^{Gt(YTA407)Byg}$ locus. (B) Southern blot of a correct positional and single integration with the endogenous *dapk3* locus from the YTA407 ES line. A representative PCR genotyping from adult mice is also included. (C) Gross body weight of wildtype versus heterozygous adult mice.

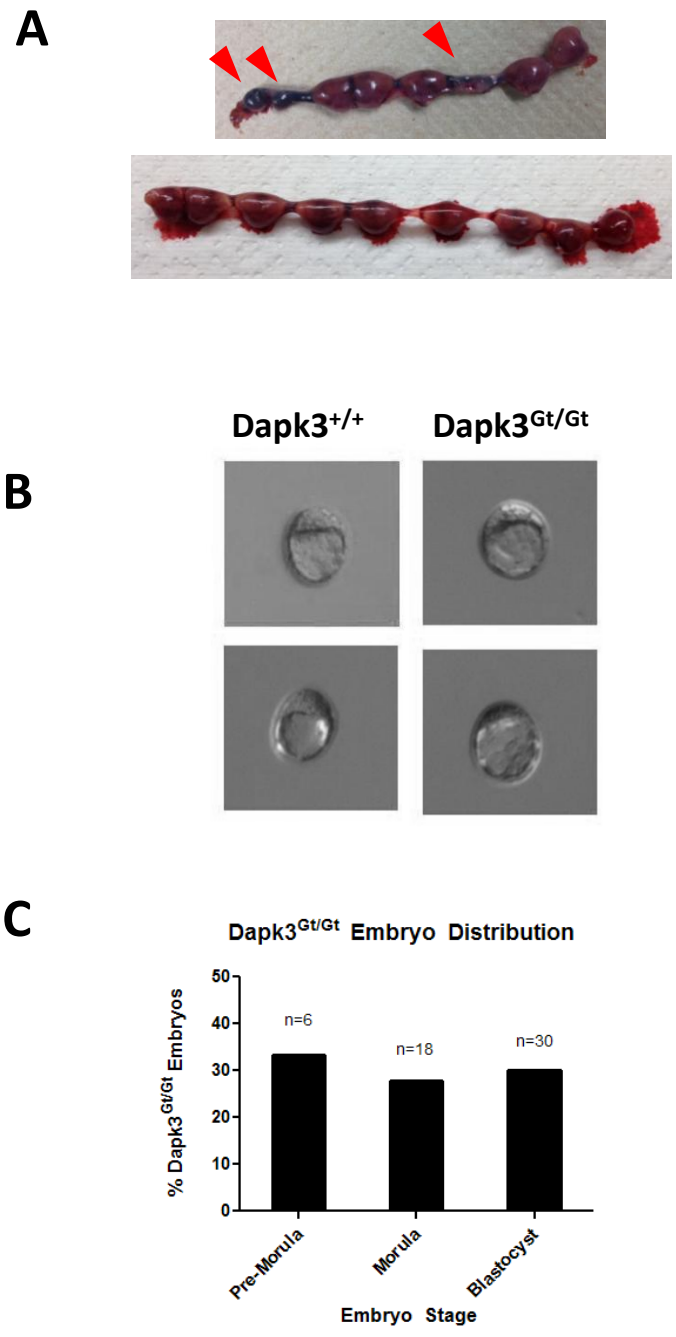

Figure 2. (A) The appearance of increased resorbed E10.5 fetuses (red arrows) in uteri extracted from heterozygous crosses (top) versus wildtype-heterzoygous crosses (below). (B) Brightfield images of genotype confirmed blastocysts isolated from heterozygous crosses. (C) Distribution of early stage homozygous gene trap embryos.

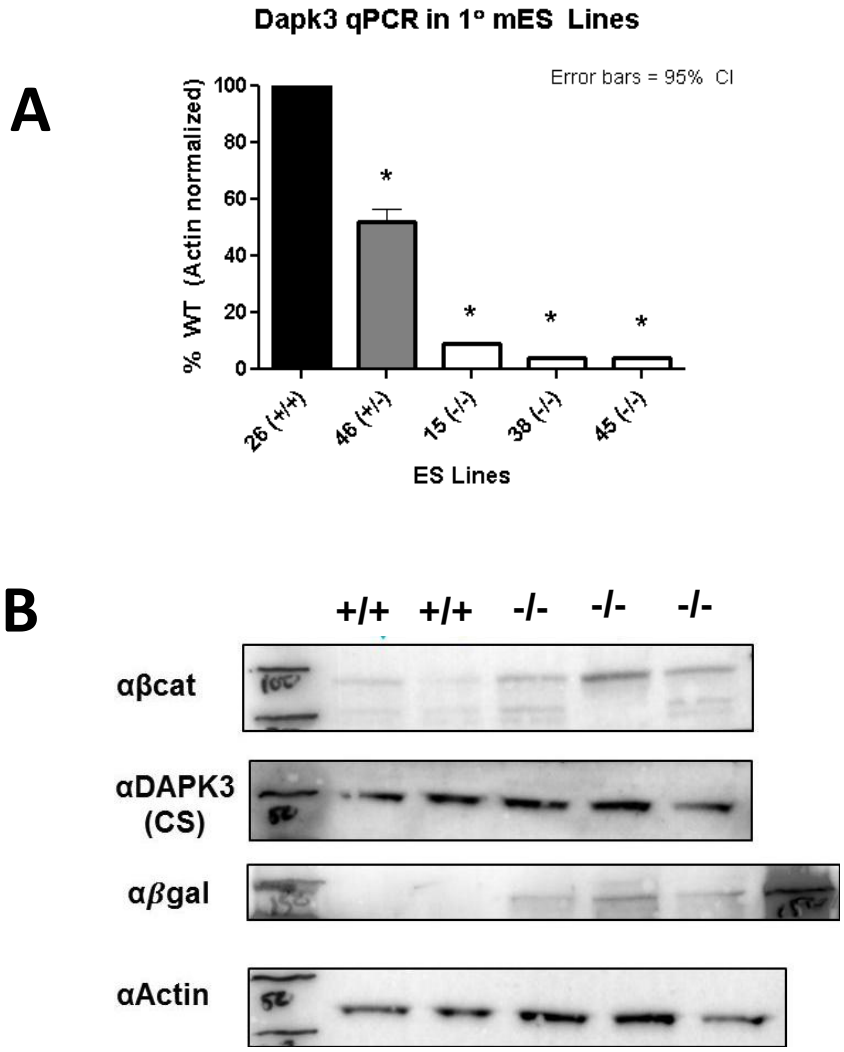

Figure 3. (A) qPCR analysis of *Dapk3* mRNA extracted from genotype confirmed primary ES cells. (B) Western blot analysis of expression of DAPK3-βgeo protein product in wildtype and homozygous gene trap primary ES lines. (C) Embryonic developmental stage distribution of genotype confirmed homozygous gene trap embryos.

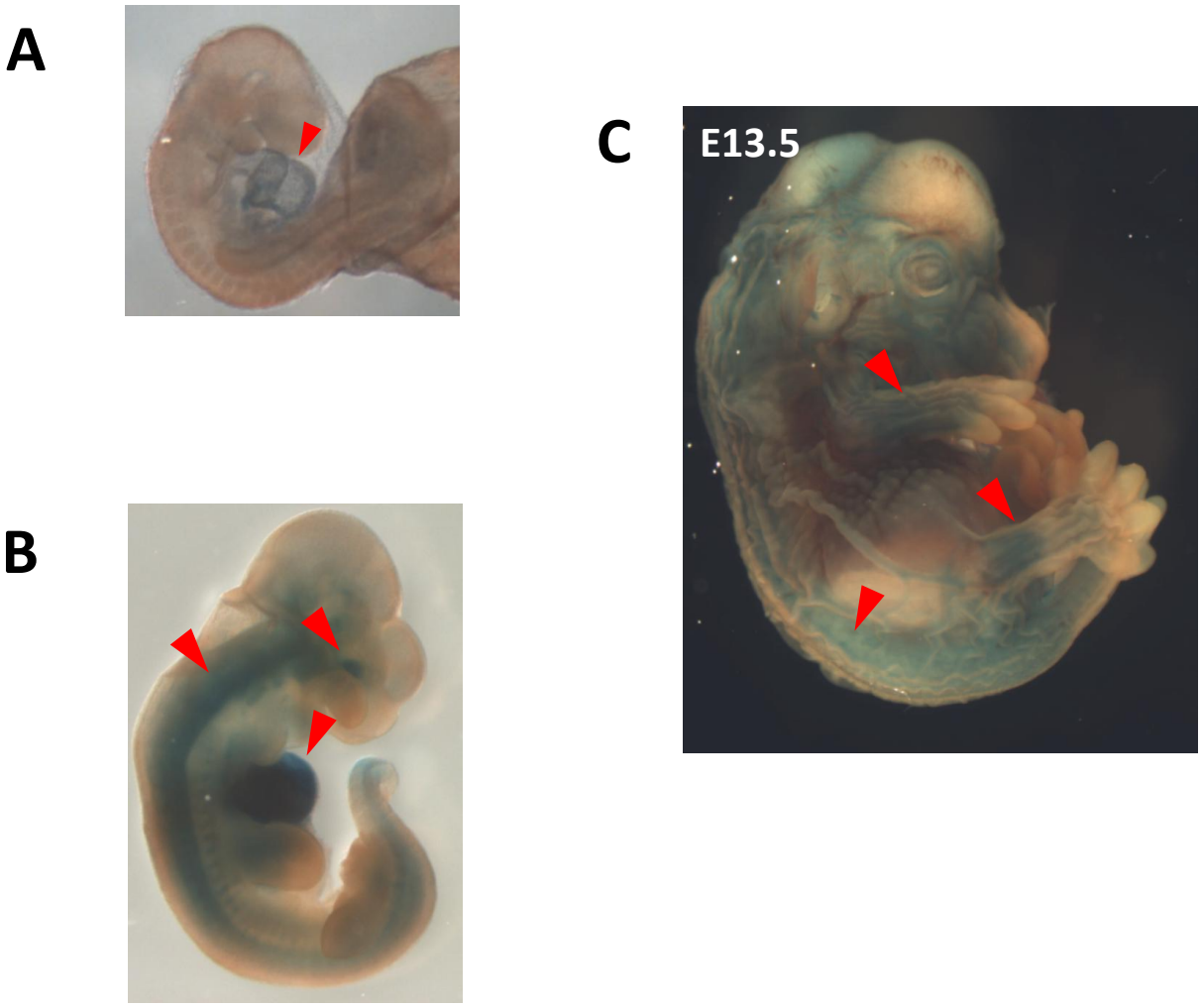

Figure 4. (A) Distinct and localized βgal activity in the developing heart of genotype confirmed heterozygous E8.5 embryo (red arrows). Similar specific localization of βgal activity in the developing heart and notochord (red arrows) from genotype confirmed heterozygous E10.5 embryos. (C) Activity also observed in the developing arms, legs and notochord of E13.5 fetuses.

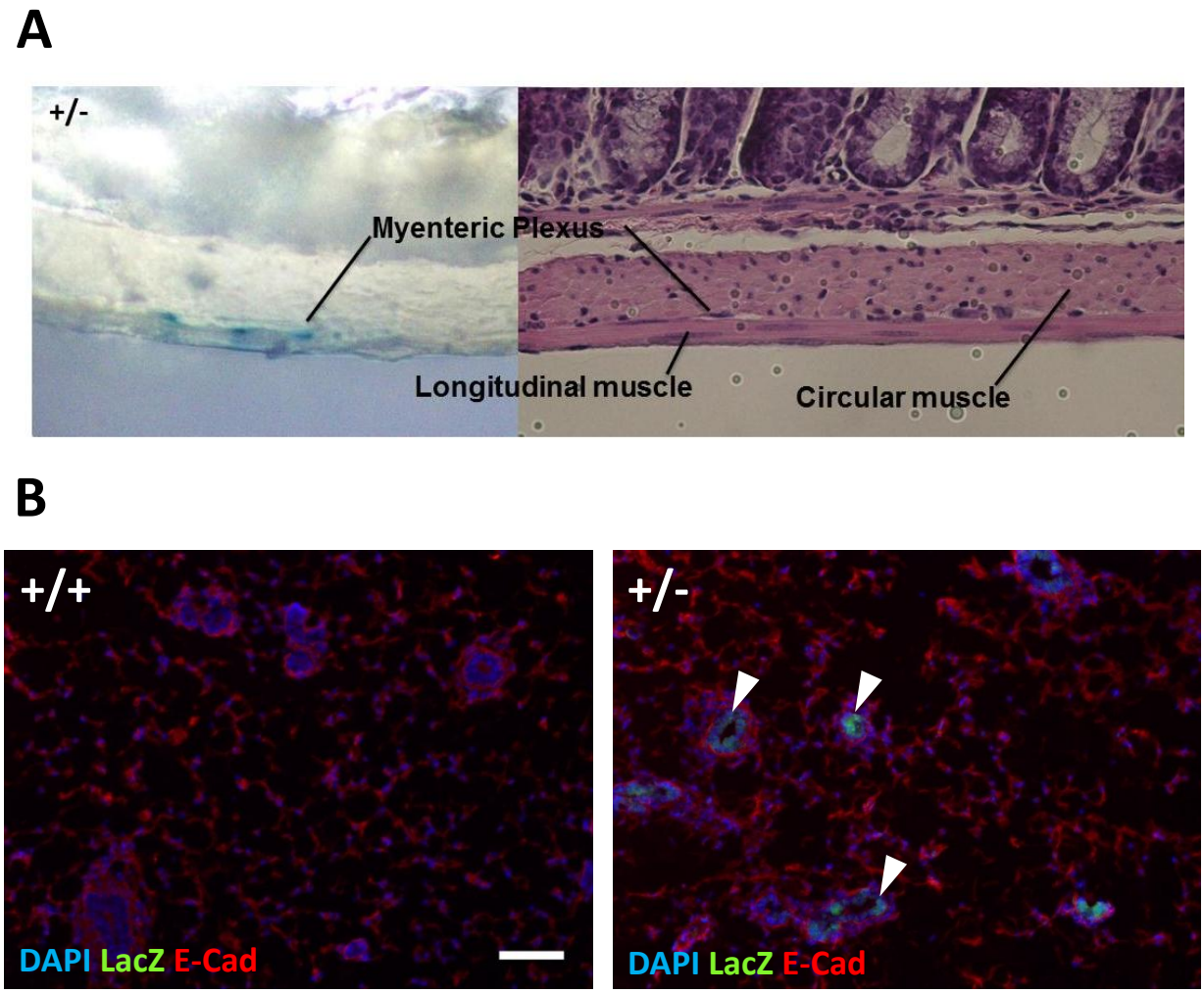

Figure 5. (A) Distinct β-gal activity in the myentereic plexus of the large intestine from 10 week old heterozygous animals. Shown here is an H&E fusion for topographical comparison. (B) The *dapk3* promoter is active in the epithelia of mouse mammary glands as visualized using immunofluorescence.

3.6 Table

Table I. Ratios of various genotypes in embryos and adult mice.

Genotype	E8.5	E10.5	E12.5	129Ola	C57BL/6
+/+	4	2	4	39	8
+/Gt	4	5	6	68	13
Gt/Gt	0	0	0	0	0

3.7 References

1. Bialik S, Kimchi A. The death-associated protein kinases: structure, function, and beyond. Annu Rev Biochem. 2006;75:189–210.

2. Kawai T, Matsumoto M, Takeda K, Sanjo H. ZIP Kinase , a Novel Serine / Threonine Kinase Which Mediates Apoptosis ZIP Kinase , a Novel Serine / Threonine Kinase Which Mediates Apoptosis. 1998;18.

3. Brognard J, Zhang Y-W, Puto L a, Hunter T. Cancer-associated loss-of-function mutations implicate DAPK3 as a tumor-suppressing kinase. Cancer Res. 2011;71:3152–61.

4. Kawai T, Akira S, Reed JC. ZIP Kinase Triggers Apoptosis from Nuclear PML Oncogenic Domains ZIP Kinase Triggers Apoptosis from Nuclear PML Oncogenic Domains. 2003;23.

5. Page G, Lödige I, Kögel D, Scheidtmann KH. AATF, a novel transcription factor that interacts with Dlk/ZIP kinase and interferes with apoptosis. FEBS Lett. 1999;462:187–91.

6. Boosen M, Vetterkind S, Kubicek J, Scheidtmann K, Illenberger S, Preuss U. Par-4 Is an Essential Downstream Target of DAP-like Kinase (Dlk) in Dlk / Par-4 – mediated Apoptosis. 2009;20:4010–20.

7. Sato N, Kawai T, Sugiyama K, Muromoto R, Imoto S, Sekine Y, et al. Physical and functional interactions between STAT3 and ZIP kinase. 2005;17:1543–52.

8. Togi S, Ikeda O, Kamitani S, Nakasuji M, Sekine Y, Muromoto R, et al. Zipper-interacting protein kinase (ZIPK) modulates canonical Wnt/beta-catenin signaling through interaction with Nemo-like kinase and T-cell factor 4 (NLK/TCF4). J Biol Chem. 2011;286:19170–7.

9. Leister P, Felten a, Chasan a I, Scheidtmann KH. ZIP kinase plays a crucial role in androgen receptor-mediated transcription. Oncogene. 2008;27:3292–300.

10. Carlson D a, Franke AS, Weitzel DH, Speer BL, Hughes PF, Hagerty L, et al. Fluorescence linked enzyme chemoproteomic strategy for discovery of a potent and selective DAPK1 and ZIPK inhibitor. ACS Chem Biol. 2013;8:2715–23.

11. Haystead T a J. ZIP kinase, a key regulator of myosin protein phosphatase 1. Cell Signal. 2005;17:1313–22.

12. Skarnes W, Melchner H, Wurst W, Hicks G, Nord A, Cox T, Young S, Ruiz P, Soriano P, Tessier-Lavigne M, Conklin B, Stanford W RJ. A public gene trap resource for mouse functional genomics. Nat Genet. 2004;36:543–4.

13. Raveh T, Droguett G, Horwitz MS, DePinho R a, Kimchi a. DAP kinase activates a p19ARF/p53-mediated apoptotic checkpoint to suppress oncogenic transformation. Nat Cell Biol. 2001;3:1–7.

14. Risheg H, Pasion R, Sacharow S, Proud V, Immken L, Schwartz S, et al. Clinical comparison of overlapping deletions of 19p13.3. Am J Med Genet A. 2013;161A:1110–6.

CHAPTER 4: CONCLUSIONS & FUTURE DIRECTIONS

4.1 Conclusions

Collectively, the data described herein has revealed a novel mechanism by which DAPK3 exerts its potential tumor suppressive functions and additionally identifies an unexpected role in mouse development. Specifically, we have identified that DAPK3 negatively regulates mTOR signaling which has functional implications for breast tumorigenesis. Furthermore, complete loss of DAPK3 leads to early lethality (E 4.5-6.5) in mouse embryos. The Dapk3 promoter is active in the developing heart and nervous system as well as the gastrointestinal myenteric nervous system and breast epithelium of adult animals. Our studies suggest that loss of DAPK3 expression in the breast epithelium can facilitate breast cancer development as reduced *DAPK3* expression is observed in DCIS and aggressive breast cancers relative to normal and DCIS, respectively. Overall, both the MCF10A 3D morphogenesis phenotypes and mouse developmental defect (s) argue against the clinical use of DAPK3 inhibitors that are currently under development and support future studies.

4.2 Future Directions

Despite these important discoveries there remains much to be known about DAPK3 and other members of the DAPK family. Future DAPK3 research should involve a detailed biochemical evaluation of mTOR-S6K-S6 inhibition, identification of functionally relevant substrates, identification of translationally repressed target mRNAs, and subsequent development of more exquisite and appropriate genetically engineered mouse models for breast cancer inquiries. A general discussion of these future studies is discussed in detail below.

Based on the data presented above, DAPK3 negatively regulates S6K-S6 signaling in a potentially kinase-dependent manner. First, kinase-dependency should be confirmed. As discussed, initial attempts involved stably overexpressing a kinase dead mutant (K42A). However, these failed potentially due to combined instability of the point mutant and an N-terminal GFP fusion. Subsequent attempts to ameliorate this set back could involve using different fluorescence proteins (mCherry, YFP) and different DAPK3 kinase deficient mutants in various N- and C-terminal orientations. Additional studies are also warranted within different cancer cell lines to determine the ubiquity of DAPK3 repression of mTOR signaling. This includes a breast cancer-focused panel of benign and malignant breast cancer cell lines along with different breast cancer subtypes (luminal A/B, triple negative, and Her2) and also additional malignant cell lines derived from non-breast tumors. The differential growth-factor or nutrient deprivation response of various cell lines (lacking or overexpressing DAPK3) should also be evaluated within the mTOR pathway. While my studies have determined that DAPK3 regulates mTOR-S6K-S6 signaling potentially downstream of ERK/ AKT mediated activation, additional studies should confirm 4E-BP1 regulation. This will help to determine if these is a general mechanism or if it is specific to S6K-S6 regulation.

Beyond general pathway dissection, further biochemical studies are warranted to identify the DAPK3 phosphorylation substrate(s) (herein referred to as protein X) and how this negatively regulates the mTOR pathway. While our data indicates potential DAPK3 mediated inhibition downstream of mTOR, this should be confirmed through evaluation of upstream components. Initial cursory investigations should include surveying known inhibitory phosphorylation sites within the mTOR pathway that can potentially be directly or indirectly induced by DAPK3. This could include TSC2 activating phosphorylations by AMPK (T1227

and S1345) (1) or GSK3β (S1337 and S1341) (2). Downstream of TSC1/2, RheB GTPase activity should be evaluated. Additionally, TSC1-TSC2 interaction and differential phosphorylation of S6K should be evaluated given that several other DAPK family members are known regulate S6K/ S6. These approachable studies will be able to determine if commonly regulated nodes within the mTOR pathway are impacted by DAPK3 but screens of some sort will be required to identify less obvious regulators.

To date, the molecular mechanisms of DAPK3 have only been surveyed by protein interactions assays that involve the ectopic expression of DAPK3. Additionally, novel phosphorylation substrates have been identified through primary interaction assays as well. Alternative approaches to detail the DAPK3-mTOR-S6K-S6 pathway using high throughput screens with genetically encoded optical readouts might be inherently flawed due to the translational-sensitivity of the optical system output. Specifically, identifying a normalization control that does not respond to alterations in translation would be difficult.

One potential method to define the molecular mechanism by which DAPK3 regulates the mTOR pathway would be to utilize two dimensional (2D) differential in-gel electrophoresis (DIGE) proteomic profiling of immobilized metal affinity chromatography (IMAC) enriched phosphoproteins. This type of phosphoproteomic approach was recently used to identify novel ERK-MAPK kinase substrates (3) and these services are offered through proteomics scores such as Siteman Cancer Center-Proteomics Core headed by Dr. Reid Townsend located on the Washington University Medical Campus. DIGE allows for differential labeling of several protein populations from different sources to be run in the same gel thereby preventing the inherent variability in cross comparisons of 2D-PAGE gels.

This technique could be applied to knockdown and overexpression experiments to simultaneously identify substrates based on respective converse outputs from each assay. To reduce background labeling and enrich low abundant phosphoproteins, whole cell lysates will be run over commercially available IMAC columns. Subsequent elutions will be labeled with spectrally distinct Cy3, and Cy5 dyes. Knockdown and over expression of DAPK3 should reveal converse phosphorylation events on DAPK3. Individual phosphoprotein populations will be fluorescently imaged within the gel and pseudo-colored digital images will be overlaid to quantitatively measure changes in phosphoprotein status between experiments. Selected gel features will be selected using DeCyder software, robotically excised, digested and subjected to liquid chromatography and tandem mass spectroscopy analysis for simultaneous substrate and phosphorylation site identification. Alternative methods include mass spectroscopy-based semi-quantitative liquid chromatography mass spectrometry. Herein, lysates would be collected from similar cellular conditions, subjected to trypsin digestion, enriched for phosphoproteins using IMAC, and subjected to HPLC tandem mass spectrometry. Changes in the relative abundance of specific m/z spikes when compared between treatments will be used to semi-quantitatively indicate potential differential phosphoprotein status as well as substrate identification.

For technical ease, phosphoprotein populations should be extracted from 2D MCF10A EGF-stimulation assays similar to those discussed in the western blots above. EGF induces robust activation of the mTOR system potentially increasing the sensitivity of phosphoproteomic approaches. After primary identification of putative DAPK3 phosphorylation substrates, subsequent *in vitro* phosphorylation assays with DAPK3 and protein substrates should be performed along with respective point mutant controls (DAPK3 K42A-kinase dead, DAPK3-phosphorylation site mutated protein X). Subsequently, protein X-point mutants should be

overexpressed (S/T/Y->Q or S/T/Y->A) during manipulation of DAPK3 expression to confirm respective effects on mTOR activation as regulated by DAPK3. After mTOR regulation is confirmed, if possible, monoclonal antibodies directed against the phospho-protein X should be used to confirm DAPK3-dependent phosphorylation *in vitro* and *in vivo.* Following these studies, appropriate targets should be functionally confirmed in the 3D MCF10A morphogenesis assay.

It will also be important to further understand the translational program repressed by DAPK3. Specifically, which mRNA transcripts are translationally repressed by DAPK3. This might lead to identification of novel oncogenes and further detail the inhibitory mechanism of DAPK3. To identify which transcripts are translationally upregulated by depletion of DAPK3, polysome ribosome profiling followed by gene expression analysis will be performed. Increased transcripts present within polysome fractions will indicate increased transcript-specific translation. Total mRNA will be collected from 2D MCF10A treated as stated previously and appropriate polysome fractions will be collected and submitted for gene expression analysis. This approach is supported by the already reported role of DAPK3 repression of transcript-specific translational in response to interferon-gamma (4).

It will also be crucial to investigate the functional similarity between human and mouse DAPK3 by developing and utilizing more exquisite genetically engineered DAPK3 mouse models. As discussed previously, it has been posited that human DAPK3 and murine DAPK3 (rat and mouse) differ in localization and sub-cellular functional capabilities (5). Interestingly the authors did not show immunofluorescence localization or nuclear-cytoplasmic fractionation data for mouse DAPK3 so the exact subcellular localization remains unknown. Our data suggests that DAPK3 is expressed in the mammary epithelium and clinical evidence suggests its downregulation can facilitate breast cancer development and progression. Regardless of the

localization of ectopically expressed DAPK3, endogenous DAPK3 might display a completely different localization pattern that cannot be evaluated due to lack of appropriate antibodies. These arguments should not hinder the development of additional mouse models given the data presented within this dissertation.

To technically approach these questions within the context of mouse models of breast cancer, one would first need to overcome the early lethality of homozygous null DAPK3 mice using a conditional genetic system. This could be done using two systems: transplantation or a transgenic-conditional system. Both approaches would first require the generation of a floxed Dapk3 mouse such that when Cre-recombinase is conditionally expressed subsequent DAPK3 expression is appropriately ablated. For transplantation mammary glands post-Cre recombination will have to be transplanted into wildtype donors. In order to distinguish and monitor the transplanted mammary gland development the conditional mouse and breast tissue will also have to express a marker (GFP, LacZ) after Cre-recombination. The second approach would involve crossing the conditional DAPK3 mouse with that of a transgenic mouse that expresses Cre within the breast under the control of a mammary gland specific promoter such as mouse mammary tumor virus (MMTV) or whey acidic protein (WAP) promoters. Downsides of each approach involve troublesome viable transplantation for the former and lack of organ-specific expression for MMTV/ WAP promoters (6). Results from these studies paired with orthotopic xenografts in which DAPK3 is depleted will shed light on the extent of DAPK3's tumor suppressive properties in accurate physiological contexts. Additionally, these conditional models can be crossed with other organ/ cancer-specific mouse models to evaluate the functional contribution of DAPK3 alterations to other diseases and cancers.

4.3 References

1. Inoki K, Zhu T, Guan K-L. TSC2 mediates cellular energy response to control cell growth and survival. Cell. 2003;115:577–90.

2. Inoki K, Ouyang H, Zhu T, Lindvall C, Wang Y, Zhang X, et al. TSC2 integrates Wnt and energy signals via a coordinated phosphorylation by AMPK and GSK3 to regulate cell growth. Cell. 2006;126:955–68.

3. Kosako H, Yamaguchi N, Aranami C, Ushiyama M, Kose S, Imamoto N, et al. Phosphoproteomics reveals new ERK MAP kinase targets and links ERK to nucleoporin-mediated nuclear transport. Nat Struct Mol Biol. Nature Publishing Group; 2009;16:1026–35.

4. Mukhopadhyay R, Ray PS, Arif A, Brady AK, Kinter M, Fox PL. DAPK-ZIPK-L13a axis constitutes a negative-feedback module regulating inflammatory gene expression. Mol Cell. Elsevier Inc.; 2008;32:371–82.

5. Shoval Y, Pietrokovski S, Kimchi A. ZIPK: a unique case of murine-specific divergence of a conserved vertebrate gene. PLoS Genet. 2007;3:1884–93.

6. Vargo-Gogola T, Rosen JM. Modelling breast cancer: one size does not fit all. Nat Rev Cancer. 2007;7:659–72.

APPENDIX A: ILLUMINATING CANCER SYSTEMS WITH GENETICALLY-ENGINEERED MOUSE MODELS AND COUPLED LUCIFERASE REPORTERS IN VIVO

A.1 Published Manuscript

Kocher, B. & Piwnica-Worms, D. Illuminating Cancer Systems with Genetically-Engineered Mouse Models and Coupled Luciferase Reporters *In Vivo*. *Cancer Discovery* (peer reviewed-review). 2013 Jun;3(6)616-29.

Statement of Significance

- Deciphering the complex molecular interactions between cancer somatic lesions and host microenvironment are crucial to understanding cancer cell proliferation, migration, invasion, and immune evasion, and may guide new anti-cancer therapies.
- Of equal importance as digitized genomics, the next essential challenge is to functionalize the cancer genome and to correctly capture these molecular mechanisms in their proper biological context within cancer systems.
- Molecular imaging with genetically-encoded imaging reporters, especially bioluminescence, provides a dynamic and noninvasive analysis platform to resolve the cooperative genetic elements of cancer systems at various temporal and spatial scales.
- Bioluminescence reporters expressed in live cells and mouse models of cancer have provided powerful tools to monitor cancer-associated genetic circuits, signaling pathways, and drug-targeted protein function *in vivo*.

Abstract

Bioluminescent imaging (BLI) is a powerful non-invasive tool that has dramatically accelerated the *in vivo* interrogation of cancer systems and longitudinal analysis of mouse models of cancer over the past decade. Various luciferase enzymes have been genetically engineered into mouse models (GEMMs) of cancer which permit investigation of cellular and molecular events associated with oncogenic transcription, post-transcriptional processing, protein-protein interactions, transformation and oncogene addiction in live cells and animals. Luciferase-coupled GEMMs ultimately serve as a non-invasive, repetitive, longitudinal, and physiological means by which cancer systems and therapeutic responses can be investigated accurately within the autochthonous context of a living animal.

Introduction

Transitioning into the Proper Context

Genomic lesions within incipient cancer cells in collaboration with alterations in the microenvironment contribute to neoplastic progression (1-3). Tumor cells can modulate the surrounding microenvironment to promote the progression of cancer through intrinsic oncogenic pathways. Furthermore, key genetic lesions have a profound impact on cancer cell migration, invasion and regulation of the immune system through tumor-extrinsic manipulation of the microenvironment (4, 5). The importance of the host microenvironment in neoplastic progression, independent of tumor manipulation, is also underscored by studies demonstrating that fibroblasts, among many other stromal and immune cell types, stimulate growth of pre-neoplastic and neoplastic cells along with promoting drug resistance (6-8). Given these observations, understanding the complex interactions between genomic lesions and tumor microenvironment in mouse models is crucial to uncovering new anti-cancer therapies. Thus, implementation of molecular imaging within basic research and pre-clinical mouse models of cancer has become an essential tool for interrogating these hallmarks of cancer and monitoring tumor progression within the proper physiologic context.

Currently, the most commonly used types of mouse models of cancer can be grouped into primary tumor cells, tumor cell lines and their associated tumor engraftments, or genetically-engineered mouse models (GEMMs) of spontaneous cancer. Xenograft models entail subcutaneous or orthotopic transplantation of human cell lines or primary tumors into an immunodeficient mouse while mouse allografts similarly employ orthotopic or subcutaneous

host implantation. Although traditional cell line xenografts and mouse allografts have yielded limited clinical correlations (9-11), the robust ability of human 'xenopatient' models (12) and newly adapted "human-in-mouse" (HIM) cancer models for accurately modeling patient disease and predicting patient response have been encouraging (11, 12, 13). However, due to the inherent nature of xenograft and HIM models, immune compromised mice are required, and thus the contribution of the immune system and the autochthonous tumor stroma cannot be fully interrogated. Additionally, these tumors are implanted as a population of late-stage tumorigenic cells and do not accurately recapitulate all steps of tumorigenesis. In contrast, GEMMs permit investigation of the proper tumor microenvironment, model tumor development from the initial genetic alteration *in situ* to subsequent neoplastic progression to metastasis, and enable tissue-relevant drug pharmacodynamics (13). Constitutive or conditional GEMMs of cancer (transgenic, knock-out or knock-in) as well as chimeric or non-germline GEMMs have proven to be of significant interest for cancer biology research as well as accurate predictive models of human cancers for pre-clinical drug development (14-16).

Molecular Imaging with Genetically-Encoded Reporters

Regardless of the mouse model, molecular imaging techniques (nuclear, fluorescence, and bioluminescence) at both macroscopic and microscopic scales make it possible to explore the consequences of the interactions between tumor cells and microenvironment during tumor progression *in vivo*, in real time. This expanding set of molecular probes, detection technologies, and imaging strategies, collectively termed molecular imaging, now provides researchers and clinicians alike, new opportunities to visualize gene expression, biochemical reactions, signal transduction, protein–protein interactions, regulatory pathways, cell trafficking, and drug action noninvasively and repetitively in their normal physiological context within living organisms *in*

vivo (17-21). In particular, integration of genetically-encoded imaging reporters into live cells and, more importantly, whole animal mouse models of cancer has provided powerful tools to monitor cancer-associated molecular, biochemical, and cellular pathways *in vivo* (22). Traditional means of interrogating these oncogenic-associated biological processes and characterizing new anti-cancer therapeutics have relied on invasive techniques that are often laborious and only provide a static window of analysis. Microscopic fluorescence imaging with green fluorescent protein (GFP) provided pioneering studies of biological activities and cellular processes at high resolution (23). Concurrently, molecular probes, contrast agents, exploitation of fundamental tissue characteristics, and development of multi-spectral fluorescent and bioluminescent (luciferase) proteins and highly sensitive instrumentation, have revolutionized non-invasive and longitudinal imaging of cancer biology at the whole organism level.

These various imaging modalities and strategies acquire macroscopic information *in vivo* through two basic strategies: injected agents or genetically-encoded reporters. Injected agents have contributed significantly to pre-clinical cancer research and also have great potential for translation, but require significant optimization and characterization depending on the experimental model, biological target, background noise, instrumentation, route of administration, and, for human use, are impacted by similar regulatory hurdles as therapeutic agents (21, 22). An inherent constraint to the development of conventional injectable agents is that the details of synthesizing, labeling and validating a new and different ligand for every new receptor or protein of interest impose long cycle times on development. However, genetically-encoded reporters offer more modular tools for preclinical research, which once cloned into appropriate vectors and biologically confirmed, can be quickly applied to a broad array of applications with minimal modification (22, 24). While genetically-encoded imaging reporters

are under development for use in humans, the potential for immunogenicity and transduction inefficiencies raise unique challenges (25). However, genetically-encoded imaging reporters represent a technically and biologically robust means of monitoring the dynamics of tumor biology with relatively high temporal resolution and various levels of spatial resolution when coupled with GEMMs.

Imaging of biological processes using genetically-encoded reporters relies on the ability of the reporter gene to produce a measureable signal that can be detected and quantified by extrinsic instrumentation. Reporter expression and thus signal output is controlled by a regulatory element such as constitutive or conditional DNA-promoter system, or subsequent peptide fusion that regulates posttranslational modulation of the reporter. Most commonly used genetically-encoded imaging reporters produce signal through optical imaging strategies, but magnetic resonance imaging (MRI) and radiopharmaceutical (PET/SPECT) approaches have been explored. Optical imaging of genetically-encoded reporters can provide image contrast through, 1) reporter-mediated enzymatic activation of an optically silent substrate (e.g., light-producing luciferase-based oxidation of D-luciferin in the presence of Mg^{2+}, ATP, and O_2) (22, 26), 2) photo-excitation signal production (e.g., fluorescent proteins) (23), or 3) reporter-mediated enzymatic release/trapping of optically-tuned leaving groups (e.g., β-glucuronidase-mediated hydrolysis of glucuronide groups coupled to NIR imaging dyes (27)). Nuclear imaging of genetically-encoded reporters can utilize, 1) enzyme-mediated modification of a labeled substrate causing intracellular accumulation or proximal cell association (e.g., HSV1-TK-mediated phosphorylation of radiolabelled nucleosides for PET imaging) (28, 29), or 2) direct import of a labeled tracer (e.g., sodium iodide transporters/ radioiodines for PET/SPECT) (22, 30). An early innovation for MRI was use of a galactopyranose blocking group coupled to a

gadolinium-based relaxivity agent that rendered the MRI contrast agent sensitive to expression of the reporter gene β-galactosidase (31).

Genetically-encoded reporters with optical outputs, specifically fluorescence or bioluminescence, are most commonly used for cancer research in mouse models due to overall modest cost, sensitivity and lack of technical restrictions and required regulatory barriers often encountered with other approaches. Whole animal fluorescence imaging *in vivo* suffers from low signal-to-noise as a result of background auto-fluorescence, modeling-dependent photon quantification, photo-bleaching, low tissue penetration and low resolution (26). In addition, fluorescent proteins are known to generate reactive oxygen species (ROS) that can induce significant cellular stress under selected conditions (23). However, computed image analysis along with laser-induced fluorescence has increased the sensitivity of non-invasive fluorescence imaging *in vivo (32)*. Also, compared to other genetically-encoded reporters, fluorescent proteins are independent of substrate delivery and pharmacokinetics, are amenable to high resolution microscopic analysis, and several new far red-shifted fluorescent proteins have been developed that enhance the penetration of photons *in vivo* (21).

Bioluminescence imaging has emerged as an invaluable optical imaging tool and has become widely adapted to molecular imaging of cancer models *in vivo*. The major advantages of luciferase reporter systems *in vivo* include essentially zero background signal, high signal-to-noise imaging, relative ease of signal acquisition, modest cost, user-friendly instrumentation and direct measure of live cell mass (ATP-dependent activity). Moreover, luciferase enzymes have a shorter half-life (~3-5 hrs for native North American *P. Pyralis* firefly luciferase and *Renilla* luciferase versus 12-26 hrs for native GFP variants) and are rapidly folded and functional post-translationally, thereby providing a more robust readout of kinetic processes such as

transcriptional activation, protein degradation, reversible protein-protein interactions and other rapid biological processes (22, 33, 34). Also, red-emitting firefly and click beetle luciferases with relatively higher photon outputs have advanced luciferase imaging beyond the original long wavelength luciferase variants, providing further advantages over *Renilla/ Gaussia* luciferases and related mutants that emit at blue or blue-green wavelengths, which, while perhaps useful, remain suboptimal for imaging *in vivo*. However, luciferase enzymes in general are dependent on substrate pharmacokinetics, and furthermore, the *Renilla/ Gaussia* substrate (coelenterazine) is transported by P-glycoprotein and auto-luminesces due to auto-oxidation from serum albumin (35, 36), which can confound analysis *in vivo*. Additionally, due to overall low photon output, luciferase reporters traditionally have been limited to macroscopic imaging analysis. However, recent advances in low-light microscopy technologies have permitted the interrogation of live cells and live bioluminescent tissues *ex vivo* at high magnifications (37-39), a notable advance that extends the capacity of BLI.

Similar to studies in cultured cells, genetically-encoded bioluminescent reporters in mice offer the ability to non-invasively monitor transcriptional regulation, post-transcriptional and post-translational events, as well as transformation and neoplastic progression. When coupled with an oncogenic protein or signaling pathway of interest, these properties of BLI allow various features of cancer to be interrogated such as chemoresistance, inflammation, angiogenesis, DNA maintenance, apoptosis, therapeutic response and oncogene addiction. Additionally, BLI reporter mice can simultaneously and directly assess tumor burden through constitutive or conditional expression of luciferase. With the sensitivity of BLI reporter mice, one can also non-invasively survey and monitor small, non-palpable tumors as well as metastases in a relatively fast and efficient manner. While a considerable amount of early effort was directed toward fluorescent

GEMMs of cancer, only more recently have mouse models been advanced with the versatility of BLI. Thus, the development and utility of BLI in GEMMs of cancer is the focus of this review and the reader is referred elsewhere for overviews of molecular imaging in non-GEMM models (19-22, 40). More specifically, this review highlights GEMMs of cancer reported in the last half-decade that utilize genomically-encoded bioluminescence reporters for investigating tumor biology and associated signaling pathways inherent to the cancer system or pathway of interest, summarizes notable models, and suggests future directions for BLI-coupled GEMMs of cancer. In addition to the models highlighted in detail below, an extensive referenced list of cancer-related luciferase-coupled GEMMs according to mode of luciferase regulation (Table I) and cancer type (Table II) are included for the general reader.

Regulation of Luciferase in GEMMs of Cancer

Transcriptional

Transcriptionally-regulated luciferase enzymes provide a robust tool to monitor tissue-specific tumor burden or interrogate biological processes in tumors *in vivo*. Transcriptional systems are simple in design and consist of a composite or endogenous promoter sequence upstream of luciferase and introduced into the mouse genome either through transgenic or targeted knock-in approaches. Conventionally, genetic regulatory elements derived from cytomegalovirus (CMV) or simian vacuolating virus 40 (SV40) provide robust protein or reporter expression in the cell or tissue harboring the construct. However, at the whole animal level, to track spontaneous tumor progression, researchers have utilized promoters or *cis* acting regulatory regions from endogenous or viral genes activated specifically in neoplastic cells. For example, prostate growth and development is largely governed by androgen signaling, thus offering an avenue to specifically image prostate cells in physiological or pathological states. With this in mind, a plethora of transgenic luciferase mice have been developed utilizing composite promoters from human kallikrein 2, probasin, prostate-specific antigen and various forms of concatenated minimal androgen response elements (Table I). Other transgenic models also use endogenous androgen-responsive promoters derived from rat probasin and human prostate specific antigen (41, 42). Baseline signal with varying intensities is confined to the prostate with minimal promoter activity outside of the prostate for most models, allowing non-invasive prostate-specific BLI. Prostate bioluminescent signal from these promoters correlates with normal prostate development and decreases upon castration or androgen ablation. However,

in only one transgenic model (Tg(*PSA->Luc)*) did the reporter mouse demonstrate an increase in prostate bioluminescence when crossed to a previously characterized TRAMP model that expresses oncogenic SV40 small and large T antigen in the prostate via a minimal rat probasin promoter (42). Two other similar prostate transcriptional luciferase reporter models failed to show a consistent increase in prostate signal when crossed to TRAMP models despite histologically confirmed tumor progression (43, 44). It was suggested that the inability of these reporter models to show a tumorigenic increase in prostate bioluminescence, as seen in Tg(*PSA->Luc; rPB-Tag)* mice, was due to the androgen independence of these aggressive, neuroendocrine carcinomas that are characteristically observed on a FVB background (45). However, this observation is unsatisfying given the fact that if the tumors were truly AR-independent, the relatively high prostate-specific signal ($>10^6$ photons) would be, by default, representative of tumor mass only and would have been expected to increase along with the tumor, which was not observed despite tumor progression (43, 44). These discrepancies point out the potential pitfalls of using transgenic strategies with regulated promoter-based reporters for readout of tumor burden which can be confounded by gene locus effects, gene silencing, or tumor evolution, independent of promoter- or gene-dependent luciferase expression. This discordance can be investigated by correlating bioluminescence with tumor burden as measured by an alternative means (caliper measurements, MRI, etc.). Conversely, bioluminescent promoter systems in transgenic GEMMs of cancer that are intended to interrogate gene-associated oncogenic processes can ultimately become a measure of tumor burden alone, completely separate from the original gene-associated biological intent. Thus, care should be taken when developing a reporter mouse using luciferase (or any reporter gene) to monitor tumor hallmarks when coupled to a gene of interest. Transcriptional bioluminescent reporters knocked into an

endogenous locus or immediately downstream of a start codon also provide a means to monitor tumor biology and development *in vivo* with decreased signal variability compared to that often observed between transgenic founder lines. Although technically more difficult, knock-in strategies maintain the entire promoter regulatory region adjacent to the luciferase gene and thus, in principle, provide a more accurate measure of gene transcription within the native context of the genome. This is exemplified in a $p21^{Waf1/CIP}$ knock-in luciferase model ($p21^{FLuc}$) in which firefly luciferase was genetically introduced into the endogenous p21 locus downstream of the native promoter (Fig. 1A) (37). p21 is a critical regulator of cell cycle progression, is a direct transcriptional target of p53 among many other signaling pathways and is frequently altered in human cancers (46). As expected, p53-dependent activation of the *p21* promoter in response to external beam irradiation (IR) could be non-invasively and repetitively monitored over time in $p21^{FLuc}$ mice (37) using surgically implanted micro-osmotic pumps that constantly delivered D-luciferin substrate (47) (Fig1. B). Previous attempts to non-invasively monitor p21 levels *in vivo* utilized transgenic transcriptional luciferase or lacZ reporter mice that were regulated by short fragments of the *p21* promoter (<5 kb) and only produced robust signal when strains harbored multiple copies of the reporter (up to 23) (48, 49). In the knock-in reporter strain, baseline bioluminescence levels three logs higher than the luciferase transgenic strain allowed *Tinkum et al*. (37) to identify specific organs that contained high levels of p21 independent of p53 status. Additionally, select organs showed dramatic regional differences in p21-luciferase activity that was identified using high-resolution bioluminescence microscopy to localize live sub-organ structures and specific cell populations with high-level expression of p21 (Fig. 1C), providing new insight into future lines of investigation.

Similar to organ-specific imaging in the aforementioned prostate transgenic models, sub-cellular whole animal imaging of tumor burden can be accomplished using transcriptional reporter mice as well. *Scotto et al.* (50) introduced a mCherry-Luciferase fusion into the endogenous *CD19* locus. This enabled non-invasive longitudinal imaging and microscopic analysis *ex vivo* of the B-cell lineage under normal and pathologic conditions when crossed to a λ-MYC transgenic mouse model of spontaneous B-cell lymphoma (50). Knock-in strategies appear to offer more refined imaging of whole organs or distinct cell lineages in terms of sensitivity and specificity when it comes to analysis of GEMMs of cancer at the macroscopic scale.

However, a caveat is that knock-in strategies can potentially disrupt expression of the endogenous locus by usurping its promoter function or preventing expression of the targeted locus, thereby disrupting the process under investigation. In this regard, several groups have adapted viral internal ribosome entry sites (IRES) to couple translation of luciferase enzymes to the transcriptional activation of an upstream gene in a bicistronic fashion while maintaining expression of the targeted gene. One group utilized this strategy by knocking-in an IRES-EGFP-luciferase fusion downstream of the endogenous vascular endothelial growth factor receptor 3 stop codon ($Vegfr3^{EGFPluc}$) (Fig. 2A) (51). VEGFR3 is a potent regulator of angiogenesis, lymphangiogenesis and metastasis and is emerging as an alternative target in combination with other VEGF anticancer therapeutics (52-54). The authors used this reporter mouse to quantify the association between inflammation and lymphangiogenesis during wound healing and in response to a contact hypersensitivity inflammation model. Microscopic analysis of the coupled EGFP reporter allowed the authors to show that $Vegfr3^{EGFPluc}$ luciferase intensity correlated with increased lymphatic network density. Additionally, tumor-activated lymphangiogenesis was

observed in DMBA/TPA-skin papillomas and at lymph nodes distant from subcutaneous injection of B16-V5 melanoma cells (Fig. 2B-C). Importantly, the sensitivity and longitudinal capability of luciferase imaging permitted identification of tumor-activated lymphangiogenesis at distant lymph nodes that preceded tumor metastasis (Fig. 2C).

Post-Transcriptional

The luciferase enzyme can also be coupled to post-transcriptional mechanisms that monitor mRNA modifications associated with oncogenic signaling. This can be accomplished by coupling or fusing a luciferase enzyme to a coding sequence such that modification or interaction of the mRNA or protein results in modulation of luciferase signal. This strategy was applied to investigate the effect of the tumor microenvironment on tumor unfolded protein response (UPR) and endoplasmic reticulum (ER) stress in live animals by visualizing alternative splicing (55). The heterogeneous tumor microenvironment imposes ER stress upon the tumor through hypoxia, acidic pH and low nutrients (56). These constraints, along with deregulated translation and proteotoxicity place evolutionary pressure on developing cancer cells, which can respond by augmenting several key steps of the UPR pathway for survival. Thus, UPR is an emerging target for anti-cancer therapies (56). Upon loss of ER homeostasis, activation of inositol-requiring 1α (IRE1α), one of the three UPR pathways, results in unconventional splicing of a 26 bp intron from IRE1α-X-box binding protein 1 (XBP-1), thereby incorporating an extended open reading frame that increases protein stability and augments XBP-1 transcriptional activation of essential UPR response genes (57, 58). *Spiotto et al.* (55) created a transgenic mouse that harbors a *CMV->XBP1-Luc* transgene which is regulated in a manner similar to that of the endogenous XBP1 and thus, luciferase expression is a direct readout of this splicing event (55). Under normal physiological conditions, the reporter mouse maintained background photonic levels, but

appropriately displayed tumor-specific signal once crossed to breast cancer models such as, Tg(*MMTV-TAg)* and Tg(*MMTV-Her2)*, that localized with ER stress markers upon microscopic analysis of tumors. Importantly, the authors observed no correlation between tumor size and bioluminescent signal suggesting XBP1-Luc was a measure of the tumor-intrinsic ER stress and not overall tumor load. Tumors arising within the same mouse possessed variable signal intensities, which portrayed the heterogeneic nature of tumor metabolism as further indicated by differential glucose uptake and hypoxia, and the contribution of the unique tumor microenvironments within the same mouse. These observations serve as an example of the sensitivity of BLI compared to other optical imaging modalities that were employed in a similar transgenic Tg(*XBP1-GFP)* mouse, which had very low signal that at the time only allowed endpoint analysis of XBP1 activation in a few extracted organs (59).

Post-Translational

Cancer-associated post-translational modifications and the subsequent effects on protein processing and protein-protein interactions are amenable to luciferase reporter mice and BLI in general. Previous designs and biologically affirmed reporters have transitioned from cell culture to provide the framework for whole animal preclinical evaluation of anti-cancer drugs in the proper physiological context. Interrogation of inhibitors of the hypoxia inducible transcription factor 1α (HIF-1α) have been aided by the development and application of various transgenic mouse models that fused the oxygen-dependent degradation domain of HIF-1α to firefly luciferase (Tg(*ODD-Luc)* and Tg(*Hypoxic RE->ODD-Luc)*) (60-62). Under normoxic conditions, endogenous HIF-1α protein is retained at low levels due to hydroxylation, polyubiquitination and subsequent proteasomal degradation and correspondingly, luciferase background signal levels are low in these luciferase reporter mice during normoxia (63). During

hypoxia or hydroxylase inhibition, HIF-1α is stabilized and appropriately, bioluminescence intensity of these reporter mice increases as a result, thereby indirectly monitoring HIF-1α-dependent responses to acute or chronic hypoxia. When crossed to spontaneous Tg(*MMTV-neu);Beclin1*$^{+/fl}$ or carcinogen susceptible *RasH2* cancer models, increased bioluminescence was detected in hypoxic tumors, highlighting the ability to monitor both tumor growth and tumor hypoxia non-invasively with this reporter mouse (60, 62). Additionally, inclusion of *cis* acting hypoxia response elements before a minimal *CMV* promoter in the Tg(*HRE->ODD-Luc)* mice inherently provided interrogation of the transcriptional phase of the HIF-1α positive feedback loop, which attempts to recapitulate HIF-1α-dependent transcriptional activation of its own mRNA (62).

The analysis of druggable oncogenic protein-protein interactions can also be interrogated non-invasively using luciferase reporter mice. This notion is exemplified in a proof-of-principle mouse model utilizing the Gal4-VP16 "two hybrid" interaction system in which nuclear interaction of the DNA binding domain of the yeast transcription factor Gal4 with the transactivation domain from herpes simplex virus VP16 protein can functionally lead to the transcriptional activation of a *Gal4* responsive reporter gene (64). If each component is individually fused to a set of proteins known to interact, visualization of their proximity and interaction can be indirectly assessed through *Gal4*-responsive reporter activation. *Pichler et al. (64)* generated a transgenic mouse harboring a luciferase reporter regulated by *Gal4* response elements which could indirectly monitor protein-protein interactions by hydrodynamic somatic gene transfer of constructs expressing Gal4 fused to p53 and VP16 fused to the SV40 large T antigen. Using this reporter mouse, abrogation of p53-TAg interaction due to loss of p53 was readily observed in mice upon shRNA-mediated knockdown of p53 *in vivo*. Adapting this

modular system to other models of protein interactions could aid in the preclinical evaluation of modulators of oncogenic protein-protein interactions longitudinally in whole animals (65).

Conditional Transformation

Exquisite genetic techniques have enabled researchers to initiate and follow transformation, progression, invasion, metastasis, therapeutic response and oncogene dependence in spontaneous or conditional GEMMs of cancer. Luciferase reporter mice can be genetically coupled to these molecular and biological events, thus permitting longitudinal and non-invasive imaging of a relatively small cohort of mice that can provide statistically meaningful results since each animal serves as its own control. In one example, inactivation of the retinoblastoma (RB) tumor suppressor pathway in response to platelet-derived growth factor (PDGF)-induced oligodendrogliomas was indirectly monitored through activation of a *E2F1* promoter driving luciferase in an engineered transgenic reporter mouse (66, 67). Direct monitoring of genetic deletion of tumor suppressors or activation of oncogenes is also possible through the use of several floxed firefly luciferase transgenic mice in which Cre-mediated excision of an upstream floxed-stop cassette allows downstream luciferase expression. Previously, *Lyons et al.* generated a transgenic strain in which the beta actin promoter-driven luciferase expression is regulated by removal of a floxed GFP-polyA transgene (68). Crossing the reporter strain with a floxed $Kras2^{v12}$ followed by adeno-Cre inhalation induced lung adenocarcinomas that could be simultaneously monitored using BLI for over 100 days. Using the same reporter mouse crossed to a conditional prostate-specific Cre-expressing strain, $Tg(PB\text{-}Cre4);Pten^{fl/fl}$, another group was able to monitor for over 400 days spontaneous prostate adenocarcinoma initiation, progression, response to castration and subsequent development of castration-resistant prostate cancers (CRPC) reliably in a small cohort of animals (69). The emergence of CRPC was not observed

and potentially may never be observed through coupled-reporter gene imaging in the androgen-dependent transcriptional prostate carcinoma reporter models discussed earlier. This highlights the utility of Cre/loxP approaches, which can mark tumor cell lineage prior to biologic-specific functions, thereby improving upon the complexities of transcriptional reporters, such as the prostate cancer reporter mice discussed above. The authors observed that the non-recombined β-actin promoter-driven reporter was leaky and read-through could be observed in muscle tissue using reverse transcriptase PCR of tissue mRNA. This was potentially due to the strength of this promoter in regions of high actin expression and/or from the variability associated with the loci or extent of genomic integration of the reporter. Also, the authors observed pronounced luciferase signal at intraperitoneal sites of repeated luciferin injection, which could be remedied through tail vein injection of the luciferase substrate. *Svensson et al.* also utilized a conditional *Rosa-Luc* knock-in reporter mouse to monitor prostate carcinoma progression on the less aggressive C57BL/6 background (70), using the same strategy as *Liao et al.* (*Tg(PB-Cre4);Pten$^{fl/fl}$)* (71). Despite the now well-characterized differences in prostate development due to the genetic backgrounds of the mouse used (e.g., C57BL/6 versus aggressive FVB/N), *Svensson et al.* noted a dramatic reduction in luciferase signal variability over time compared to *Liao et al.* These differences potentially stem from the *Rosa26* locus and/ or the fact that the *Rosa-Luc* mouse was strategically backcrossed onto an albino C57BL/6 background, thereby greatly reducing signal attenuation due to coat color. Additionally, analysis of *Tg(PB-Cre4);Pten$^{fl/fl}$* prostate tumors indicated the BLI was a more accurate readout of prostate tumor burden because *ex vivo* analysis revealed massive fluid retention in the anterior prostate that could be misinterpreted as tumor mass when analyzed via MRI.

Cre/LoxP-luciferase reporter mice have also been used for following stochastic neoplastic genetic lesions and marking distinct cell lineages when coupled to other fluorescent or LacZ reporter strains. *Liu et al.* implemented this strategy to identify organ susceptibility and monitor subsequent tumor progression in a sophisticated whole animal *Notch1* loss-of-heterozygosity (LOH) model crossed to a floxed stop cassette-*Rosa26-click beetle red luciferase* (*Rosa->CBR*) knock-in reporter mouse (Fig. 3) (72). The authors generated a mouse harboring a knock-in non-functioning *Notch1-Cre* fusion on one allele along with a conditional Notch1 knockout cassette on the second allele (*Notch1*^{fl}), which was further crossed with either the conditional *Rosa->CBR* mouse or other conditional *Rosa->LacZ* and *Rosa->EYFP* reporter mice strains (Fig. 3A). Following the first round of embryogenic Notch1 expression, any second endogenous ligand-dependent activation of Notch signaling in *Notch1-Cre;Notch1*^{fl} mice results in cleavage and subsequent nuclear translocation of the Notch-intracellular-domain (NCID)-Cre fusion, which in turn results in excision of the remaining floxed *Notch1* allele throughout all active Notch1-signaling cells (Fig. 3A). Thus, stochastic LOH and the subsequent development of highly vascularized tumors could be indirectly monitored at the macroscopic (*Rosa->CBR)* and at the cell lineage level (*Rosa->LacZ/EYFP*) by Cre-mediated excision of the co-engineered lox-stop-lox cassette inserted upstream of the *Rosa* locus on each allele in these reporter mice (Fig. 3B, C). The *Rosa->CBR* mouse has since been crossed with the Rosa->*LacZ* mouse to create a conditional *Rosa->CBR/ LacZ* dual-modality reporter mouse that has been extensively backcrossed onto the albino C57BL/6 background (*Piwnica-Worms, D. et al. unpublished*). This dual reporter mouse has the potential to provide a robust and powerful readout of Cre-activation and carcinogenesis through the high, red-emitting photonic output of CBR and the microscopic utility of LacZ staining.

Tet-Regulated Systems

Conditional cancer mouse models using genetically-coupled luciferase reporters can also utilize tetracycline (or the more stable analogue, doxycycline)-regulated expression systems or tamoxifen-inducible systems for spatial and temporal induction and reversion of oncogene biology in mice. However, tetracylcine (tet)-systems are more commonly used due to toxicities associated with tamoxifen and the Cre-estrogen receptor fusion observed in tamoxifen-inducible mice (73, 74). In the tet-on system, expression is dependent on binding of a reverse tetracycline-regulated transactivator (rtTA) to the tetracycline-response promoter elements in the tet-operator (tet-o) engineered upstream of the coding sequence of interest in the presence of tetracycline (75). The tet-off system uses a different tetracycline-regulated transactivator protein (tTA) which cannot bind *tet-o* in the presence of tetracycline, effectively silencing expression only when tetracycline is present (75-77). Regardless of the system, expression of the tetracycline transactivator (and hence the gene of interest) can be regulated through promoters specific to a tissue or cell type of interest. Ultimately, these systems have been instrumental in determining the extent of oncogene dependence in spontaneous mouse tumor models within the proper context *in vivo*. Additionally, conditional repression of an oncogene mimics therapeutic inhibition in a targeted molecular pathway and coupled luciferase reporters allow longitudinal imaging confirmation of this 'therapeutic inhibition'. In one example, *Du et al.* generated a conditional tet-o-polyoma middle T antigen (PyMT)-IRES-luciferase reporter mouse, Tg(*tet-o-PyMT-IRES-Luc*), to investigate the cell-specific effect of oncogene induction on the development and progression of pancreatic cancer using two previously reported conditional Tet-system mice Tg(*Rip7-rtTA and Pdx1-tTA*) (78). Within 1 day of doxycycline removal, non-invasive BLI imaging allowed confirmation of subsequent oncogene withdrawal in Tg(*Rip7-*

rtTA; tet-o-PyMT-IRES-Luc) mice. Interestingly, this had no effect on the established hyperplastic β cell islets, indicating oncogene independence, which was also conversely confirmed using the *Pdx1-tTA mice.* Additionally, 10% of Tg(*Pdx1-tTA; tet-o-PyMT-IRES-Luc)* mice developed aggressive acinar cell carcinomas as a result of activation of the *Pdx1* promoter in early pancreatic progenitor cells. Regression of these tumors when deprived of PyMT, confirmed as soon as 1 day after doxycycline addition by BLI, indicated a requirement or dependence on PyMT for sustained tumor maintenance. Another group generated a tet-off luciferase reporter mouse to delineate the requirement of MYCN in medulloblastoma (79). One of the two lines crossed to generate this bigenic mouse contained the cerebellum-specific glutamate transporter1 (*Glt1*) promoter driving expression of tTA and the other a *tet-o*-driven bidirectional MYCN and firefly luciferase expression cassette. Using a characterized amount of photon flux as a measure of tumor burden, the authors repressed MYCN expression in a subset of mice by feeding them doxycycline-containing chow. Within one week, they observed a dramatic drop in bioluminescence and tumor regression, confirming the requirement for sustained MYCN expression in these tumors and suggesting its potential for targeted therapy in medulloblastomas. Thus, bioluminescent reporter mice coupled to integrated conditional tet-regulated systems are invaluable tools to quickly and efficiently monitor oncogene expression in manageable cohorts of mice and validate potential therapeutic targets, which guide and inform more invasive and laborious secondary tumor analyses.

Lessons Learned and Future Considerations

As with all experiments, meticulous planning and a dose of foresight are paramount to the success of engineering a genetically-encoded luciferase mouse. There are several

considerations and nuances that can dramatically reduce time and labor and expand upon the potential of a reporter mouse in terms of signal sensitivity, biological accuracy and overall utility. As the genetic background of the mouse strain can dramatically affect the biology of the cancer, for example, as seen in the differential sensitivity of C57BL/6 and FVB strains to prostate cancer models as well as other models (80), so will genetic background inherently modulate the signal strength and interpretation of coupled luciferase reporters. When possible, an albino mouse strain should be used to minimize signal attenuation. This will allow for enhanced sensitivity for gross analysis of luciferase expression, and will strongly benefit low luciferase-expressing tissues in scenarios such as low endogenous expression, metastasis or tumor regression. Commercial albino C57BL/6 embryonic stem cells are now available that have high germline rates, and are technically amenable to genomic manipulation for targeted or transgenic reporter approaches, thereby minimizing onerous backcrossing. When specifically attempting to monitor live tumor cells, a relevant genetically-encoded reporter should be specific to live cell mass alone and will likely be most accurate when using Cre/loxP-based or knock-in strategies as discussed previously. Although technically much simpler, transgenic transcriptional reporters can be overridden by tumor evolution or genomic loci effects as seen in the androgen-sensitivity GEMMs of prostate cancer discussed above. Low light microscopy, which is capable of imaging live luminescent tissues, is becoming accessible to the general researcher and is approaching the high levels of magnification and resolution necessary for subcellular inspection. Nonetheless, analysis e*x vivo* of live tissues and organs synergizes with the whole animal imaging capabilities of luciferase reporter mice and also can be performed using luciferase antibodies or secondary coupled reporters such as fluorescent proteins as used to observe lymphatic vessels in $Vegfr3^{EGFPluc}$ mice (51).

Conclusions

Genetically-encoded luciferase reporter mice have made a profound impact on imaging tumorigenesis, cancer progression, response to therapies and the contributions of the tumor microenvironment when crossed with GEMMs of cancer. Compared to other imaging modalities, bioluminescence provides an efficient, relatively low cost, non-invasive and longitudinal means to investigate genetic alterations in the autochthonous tumor environment and its ultimate effect on tumor biology. Combining the advantages of genetically-encoded luciferase reporters with the development of new and clinically accurate GEMMs of cancer paints a bright horizon for our understanding of molecular cancer biology and the development of novel and durable anti-cancer therapies.

Acknowledgements

The authors would like to thank colleagues of the BRIGHT Institute for their discussions and input.

Grant Support

This review was supported in part by a center grant from the NIH to the Molecular Imaging Center at Washington University (P50 CA094056) and a NIH training fellowship for stipend support to Brandon Kocher (T32 CA113275).

A.2 References

1. Bissell M, Radisky D. Putting tumours in context. Nat Rev Cancer. 2001;1:46-54.

2. Hanahan D, Coussens LM. Accessories to the crime: functions of cells recruited to the tumor microenvironment. Cancer Cell. 2012;21:309-22.

3. Hanahan D, Weinberg RA. Hallmarks of cancer: the next generation. Cell. 2011;144:646-74.

4. Mantovani A, Allavena P, Sica A, Balkwill F. Cancer-related inflammation. Nature. 2008;454:436-44.

5. Friedl P, Alexander S. Cancer invasion and the microenvironment: plasticity and reciprocity. Cell. 2011;147:992-1009.

6. Krtolica A, Parrinello S, Lockett S, Desprez PY, Campisi J. Senescent fibroblasts promote epithelial cell growth and tumorigenesis: a link between cancer and aging. Proc Natl Acad Sci U S A. 2001;98:12072-7.

7. Pazolli E, Stewart SA. Senescence: the good the bad and the dysfunctional. Curr Opin Genet Dev. 2008;18:42-7.

8. Wang W, Li Q, Yamada T, Matsumoto K, Matsumoto I, Oda M, et al. Crosstalk to stromal fibroblasts induces resistance of lung cancer to epidermal growth factor receptor tyrosine kinase inhibitors. Clin Cancer Res. 2009;15:6630-8.

9. Johnson JI, Decker S, Zaharevitz D, Rubinstein LV, Venditti JM, Schepartz S, et al. Relationships between drug activity in NCI preclinical in vitro and in vivo models and early clinical trials. Br J Cancer. 2001;84:1424-31.

10. Voskoglou-Nomikos T, Pater JL, Seymour L. Clinical predictive value of the in vitro cell line, human xenograft, and mouse allograft preclinical cancer models. Clin Cancer Res. 2003;9:4227-39.

11. Sausville EA, Burger AM. Contributions of human tumor xenografts to anticancer drug development. Cancer Res. 2006;66:3351-4.

12. Bertotti A, Migliardi G, Galimi F, Sassi F, Torti D, Isella C, et al. A molecularly annotated platform of patient-derived xenografts ("xenopatients") identifies HER2 as an effective therapeutic target in cetuximab-resistant colorectal cancer. Cancer discovery. 2011;1:508-23.

13. Olive KP, Tuveson DA. The use of targeted mouse models for preclinical testing of novel cancer therapeutics. Clin Cancer Res. 2006;12:5277-87.

14. Sharpless N, Depinho R. The mighty mouse: genetically engineered mouse models in cancer drug development. Nat Rev Drug Discov. 2006;5:741-54.

15. Heyer J, Kwong LN, Lowe SW, Chin L. Non-germline genetically engineered mouse models for translational cancer research. Nat Rev Cancer. 2010;10:470-80.

16. Cheon DJ, Orsulic S. Mouse models of cancer. Annual review of pathology. 2011;6:95-119.

17. Villalobos V, Naik S, Piwnica-Worms D. Current state of imaging protein-protein interactions in vivo with genetically encoded reporters. Annu Rev Biomed Eng. 2007;9:321-49.

18. Singer R, Lawrence D, Ovryn B, Condeelis J. Imaging of gene expression in living cells and tissues. J Biomed Opt. 2005;10:051406.

19. Weissleder R, Pittet MJ. Imaging in the era of molecular oncology. Nature. 2008;452:580-9.

20. Dothager R, Flentie K, Moss B, Pan M, Kesarwala A, Piwnica-Worms D. Advances in bioluminescence imaging of live animal models. Curr Opin Biotechnol. 2009;20:45-53.

21. Condeelis J, Weissleder R. In vivo imaging in cancer. Cold Spring Harbor perspectives in biology. 2010;2:a003848.

22. Gross S, Piwnica-Worms D. Spying on cancer: molecular imaging in vivo with genetically encoded reporters. Cancer Cell. 2005;7:5-15.

23. Giepmans BN, Adams SR, Ellisman MH, Tsien RY. The fluorescent toolbox for assessing protein location and function. Science. 2006;312:217-24.

24. Bhang HE, Pomper MG. Cancer imaging: Gene transcription-based imaging and therapeutic systems. Int J Biochem Cell Biol. 2012;44:684-9.

25. Tobias A, Ahmed A, Moon K, Lesniak M. The art of gene therapy for glioma: a review of the challenging road to the bedside. Journal of neurology, neurosurgery, and psychiatry. 2013;84:213-22.

26. Contag CH, Bachmann MH. Advances in *in vivo* bioluminescence imaging of gene expression. Annu Rev Biomed Eng. 2002;4:235-60.

27. Cheng T, Roffler S, Tzou S, Chuang K, Su Y, Chuang C, et al. An activity-based near-infrared glucuronide trapping probe for imaging β-glucuronidase expression in deep tissues. J Am Chem Soc. 2012;134:3103-10.

28. Luker G, Sharma V, Pica C, Dahlheimer J, Li W, Ochesky J, et al. Noninvasive imaging of protein-protein interactions in living animals. Proc Natl Acad Sci USA. 2002;99:6961-6.

29. Tjuvajev J, Finn R, Watanabe K, Joshi R, Oku T, Kennedy J, et al. Noninvasive imaging of herpes virus thymidine kinase gene transfer and expression: a potential method for monitoring clinical gene therapy. Cancer Res. 1996;56:4087-95.

30. Blasberg R, Piwnica-Worms D. Imaging: strategies, controversies, and opportunities. Clin Cancer Res. 2012;18:631-7.

31. Louie A, Huber M, Ahrens E, Rothbacher U, Moats R, Jacobs R, et al. In vivo visualization of gene expression using magnetic resonance imaging. Nat Biotechnol. 2000;18:321-5.

32. Wack S, Hajri A, Heisel F, Sowinska M, Berger C, Whelan M, et al. Feasibility, sensitivity, and reliability of laser-induced fluorescence imaging of green fluorescent protein-expressing tumors in vivo. Mol Ther. 2003;7:765-73.

33. Corish P, Tyler-Smith C. Attenuation of green fluorescent protein half-life in mammalian cells. Protein Eng. 1999;12:1035-40.

34. Thompson JF, Hayes LS, Lloyd DB. Modulation of firefly luciferase stability and impact on studies of gene regulation. Gene. 1991;103:171-7.

35. Zhao H, Doyle T, Wong R, Cao Y, Stevenson D, Piwnica-Worms D, et al. Characterization of coelenterazine analogs for measurements of Renilla luciferase activity in live cells and living animals. Mol Imaging. 2004;3:43-54.

36. Pichler A, Prior J, Piwnica-Worms D. Imaging reversal of multidrug resistance in living mice with bioluminescence: *MDR1* P-glycoprotein transports coelenterazine. Proc Natl Acad Sci USA. 2004;101:1702-7.

37. Tinkum KL, Marpegan L, White LS, Sun J, Herzog ED, Piwnica-Worms D, et al. Bioluminescence imaging captures the expression and dynamics of endogenous p21 promoter activity in living mice and intact cells. Mol Cell Biol. 2011;31:3759-72.

38. Ilagan MX, Lim S, Fulbright M, Piwnica-Worms D, Kopan R. Real-time imaging of notch activation with a luciferase complementation-based reporter. Sci Signal. 2011;4:rs7.

39. Spiller DG, Wood CD, Rand DA, White MR. Measurement of single-cell dynamics. Nature. 2010;465:736-45.

40. Higgins LJ, Pomper MG. The evolution of imaging in cancer: current state and future challenges. Semin Oncol. 2011;38:3-15.

41. Ellwood-Yen K, Wongvipat J, Sawyers C. Transgenic mouse model for rapid pharmacodynamic evaluation of antiandrogens. Cancer Res. 2006;66:10513-6.

42. Lyons SK, Lim E, Clermont AO, Dusich J, Zhu L, Campbell KD, et al. Noninvasive bioluminescence imaging of normal and spontaneously transformed prostate tissue in mice. Cancer Res. 2006;66:4701-7.

43. Seethammagari MR, Xie X, Greenberg NM, Spencer DM. EZC-prostate models offer high sensitivity and specificity for noninvasive imaging of prostate cancer progression and androgen receptor action. Cancer Res. 2006;66:6199-209.

44. Hsieh CL, Xie Z, Yu J, Martin WD, Datta MW, Wu GJ, et al. Non-invasive bioluminescent detection of prostate cancer growth and metastasis in a bigenic transgenic mouse model. Prostate. 2007;67:685-91.

45. Chiaverotti T, Couto SS, Donjacour A, Mao JH, Nagase H, Cardiff RD, et al. Dissociation of epithelial and neuroendocrine carcinoma lineages in the transgenic adenocarcinoma of mouse prostate model of prostate cancer. Am J Pathol. 2008;172:236-46.

46. Abbas T, Dutta A. p21 in cancer: intricate networks and multiple activities. Nat Rev Cancer. 2009;9:400-14.

47. Gross S, Abraham U, Prior JL, Herzog ED, Piwnica-Worms D. Continuous delivery of D-luciferin by implanted micro-osmotic pumps enables true real-time bioluminescence imaging of luciferase activity in vivo. Mol Imaging. 2007;6:121-30.

48. Ohtani N, Imamura Y, Yamakoshi K, Hirota F, Nakayama R, Kubo Y, et al. Visualizing the dynamics of p21(Waf1/Cip1) cyclin-dependent kinase inhibitor expression in living animals. Proc Natl Acad Sci U S A. 2007;104:15034-9.

49. Vasey DB, Wolf CR, MacArtney T, Brown K, Whitelaw CB. p21-LacZ reporter mice reflect p53-dependent toxic insult. Toxicol Appl Pharmacol. 2008;227:440-50.

50. Scotto L, Kruithof-de Julio M, Paoluzzi L, Kalac M, Marchi E, Buitrago JB, et al. Development and characterization of a novel CD19CherryLuciferase (CD19CL) transgenic mouse for the preclinical study of B-cell lymphomas. Clin Cancer Res. 2012;18:3803-11.

51. Martinez-Corral I, Olmeda D, Dieguez-Hurtado R, Tammela T, Alitalo K, Ortega S. In vivo imaging of lymphatic vessels in development, wound healing, inflammation, and tumor metastasis. Proc Natl Acad Sci U S A. 2012;109:6223-8.

52. Tammela T, Zarkada G, Wallgard E, Murtomaki A, Suchting S, Wirzenius M, et al. Blocking VEGFR-3 suppresses angiogenic sprouting and vascular network formation. Nature. 2008;454:656-60.

53. Padera TP, Kuo AH, Hoshida T, Liao S, Lobo J, Kozak KR, et al. Differential response of primary tumor versus lymphatic metastasis to VEGFR-2 and VEGFR-3 kinase inhibitors cediranib and vandetanib. Mol Cancer Ther. 2008;7:2272-9.

54. Heckman CA, Holopainen T, Wirzenius M, Keskitalo S, Jeltsch M, Yla-Herttuala S, et al. The tyrosine kinase inhibitor cediranib blocks ligand-induced vascular endothelial growth factor receptor-3 activity and lymphangiogenesis. Cancer Res. 2008;68:4754-62.

55. Spiotto MT, Banh A, Papandreou I, Cao H, Galvez MG, Gurtner GC, et al. Imaging the unfolded protein response in primary tumors reveals microenvironments with metabolic variations that predict tumor growth. Cancer Res. 2010;70:78-88.

56. Moenner M, Pluquet O, Bouchecareilh M, Chevet E. Integrated endoplasmic reticulum stress responses in cancer. Cancer Res. 2007;67:10631-4.

57. Calfon M, Zeng H, Urano F, Till JH, Hubbard SR, Harding HP, et al. IRE1 couples endoplasmic reticulum load to secretory capacity by processing the XBP-1 mRNA. Nature. 2002;415:92-6.

58. Yoshida H, Matsui T, Yamamoto A, Okada T, Mori K. XBP1 mRNA is induced by ATF6 and spliced by IRE1 in response to ER stress to produce a highly active transcription factor. Cell. 2001;107:881-91.

59. Iwawaki T, Akai R, Kohno K, Miura M. A transgenic mouse model for monitoring endoplasmic reticulum stress. Nat Med. 2004;10:98-102.

60. Goldman SJ, Chen E, Taylor R, Zhang S, Petrosky W, Reiss M, et al. Use of the ODD-luciferase transgene for the non-invasive imaging of spontaneous tumors in mice. PLoS ONE. 2011.

61. Safran M, Kim WY, O'Connell F, Flippin L, Gunzler V, Horner JW, et al. Mouse model for noninvasive imaging of HIF prolyl hydroxylase activity: assessment of an oral agent that stimulates erythropoietin production. Proc Natl Acad Sci U S A. 2006;103:105-10.

62. Kadonosono T, Kuchimaru T, Yamada S, Takahashi Y, Murakami A, Tani T, et al. Detection of the onset of ischemia and carcinogenesis by hypoxia-inducible transcription factor-based in vivo bioluminescence imaging. PLoS ONE. 2011;6:e26640.

63. Weidemann A, Johnson RS. Biology of HIF-1alpha. Cell Death Differ. 2008;15:621-7.

64. Pichler A, Prior JL, Luker GD, Piwnica-Worms D. Generation of a highly inducible Gal4-->Fluc universal reporter mouse for in vivo bioluminescence imaging. Proc Natl Acad Sci U S A. 2008;105:15932-7.

65. Pan MH, Lin J, Prior JL, Piwnica-Worms D. Monitoring molecular-specific pharmacodynamics of rapamycin in vivo with inducible Gal4->Fluc transgenic reporter mice. Mol Cancer Ther. 2010;9:2752-60.

66. Burkhart DL, Sage J. Cellular mechanisms of tumour suppression by the retinoblastoma gene. Nat Rev Cancer. 2008;8:671-82.

67. Uhrbom L, Nerio E, Holland EC. Dissecting tumor maintenance requirements using bioluminescence imaging of cell proliferation in a mouse glioma model. Nat Med. 2004;10:1257-60.

68. Lyons SK, Meuwissen R, Krimpenfort P, Berns A. The generation of a conditional reporter that enables bioluminescence imaging of Cre/loxP-dependent tumorigenesis in mice. Cancer Res. 2003;63:7042-6.

69. Liao C-P, Zhong C, Saribekyan G, Bading J, Park R, Conti P, et al. Mouse models of prostate adenocarcinoma with the capacity to monitor spontaneous carcinogenesis by bioluminescence or fluorescence. Cancer Res. 2007;67:7525-33.

70. Svensson RU, Haverkamp JM, Thedens DR, Cohen MB, Ratliff TL, Henry MD. Slow disease progression in a C57BL/6 pten-deficient mouse model of prostate cancer. Am J Pathol. 2011;179:502-12.

71. Liao CP, Zhong C, Saribekyan G, Bading J, Park R, Conti PS, et al. Mouse models of prostate adenocarcinoma with the capacity to monitor spontaneous carcinogenesis by bioluminescence or fluorescence. Cancer Res. 2007;67:7525-33.

72. Liu Z, Turkoz A, Jackson EN, Corbo JC, Engelbach JA, Garbow JR, et al. Notch1 loss of heterozygosity causes vascular tumors and lethal hemorrhage in mice. J Clin Invest. 2011;121:800-8.

73. Mehasseb MK, Bell SC, Habiba MA. The effects of tamoxifen and estradiol on myometrial differentiation and organization during early uterine development in the CD1 mouse. Reproduction. 2009;138:341-50.

74. Higashi AY, Ikawa T, Muramatsu M, Economides AN, Niwa A, Okuda T, et al. Direct hematological toxicity and illegitimate chromosomal recombination caused by the systemic activation of CreERT2. J Immunol. 2009;182:5633-40.

75. Kistner A, Gossen M, Zimmermann F, Jerecic J, Ullmer C, Lubbert H, et al. Doxycycline-mediated quantitative and tissue-specific control of gene expression in transgenic mice. Proc Natl Acad Sci U S A. 1996;93:10933-8.

76. Furth PA, St Onge L, Boger H, Gruss P, Gossen M, Kistner A, et al. Temporal control of gene expression in transgenic mice by a tetracycline-responsive promoter. Proc Natl Acad Sci U S A. 1994;91:9302-6.

77. Gossen M, Bujard H. Tight control of gene expression in mammalian cells by tetracycline-responsive promoters. Proc Natl Acad Sci U S A. 1992;89:5547-51.

78. Du YC, Klimstra DS, Varmus H. Activation of PyMT in beta cells induces irreversible hyperplasia, but oncogene-dependent acinar cell carcinomas when activated in pancreatic progenitors. PLoS ONE. 2009;4:e6932.

79. Swartling FJ, Grimmer MR, Hackett CS, Northcott PA, Fan QW, Goldenberg DD, et al. Pleiotropic role for MYCN in medulloblastoma. Genes Dev. 2010;24:1059-72.

80. Hunter KW. Mouse models of cancer: does the strain matter? Nat Rev Cancer. 2012;12:144-9.

81. Ishikawa TO, Jain NK, Taketo MM, Herschman HR. Imaging cyclooxygenase-2 (Cox-2) gene expression in living animals with a luciferase knock-in reporter gene. Mol Imaging Biol. 2006;8:171-87.

82. Dussmann P, Pagel JI, Vogel S, Magnusson T, Zimmermann R, Wagner E, et al. Live in vivo imaging of Egr-1 promoter activity during neonatal development, liver regeneration and wound healing. BMC Dev Biol. 2011;11:28.

83. Gu L, Tsark WM, Brown DA, Blanchard S, Synold TW, Kane SE. A new model for studying tissue-specific mdr1a gene expression in vivo by live imaging. Proc Natl Acad Sci U S A. 2009;106:5394-9.

84. Li F, Cheng Q, Ling X, Stablewski A, Tang L, Foster BA, et al. Generation of a novel transgenic mouse model for bioluminescent monitoring of survivin gene activity in vivo at various pathophysiological processes: survivin expression overlaps with stem cell markers. Am J Pathol. 2010;176:1629-38.

85. Jia W, Wang S, Horner JW, Wang N, Wang H, Gunther EJ, et al. A BAC transgenic reporter recapitulates in vivo regulation of human telomerase reverse transcriptase in development and tumorigenesis. FASEB J. 2011;25:979-89.

86. Wang Y, Iyer M, Annala A, Wu L, Carey M, Gambhir S. Noninvasive indirect imaging of vascular endothelial growth factor gene expression using bioluminescence imaging in living transgenic mice. Physiol Genomics. 2006;24:173-80.

87. Faley SL, Takahashi K, Crooke CE, Beckham JT, Tomemori T, Shappell SB, et al. Bioluminescence imaging of vascular endothelial growth factor promoter activity in murine mammary tumorigenesis. Mol Imaging. 2007;6:331-9.

88. Zhang N, Fang Z, Contag PR, Purchio AF, West DB. Tracking angiogenesis induced by skin wounding and contact hypersensitivity using a Vegfr2-luciferase transgenic mouse. Blood. 2004;103:617-26.

89. Carlsen H, Moskaug JO, Fromm SH, Blomhoff R. In vivo imaging of NF-kappa B activity. J Immunol. 2002;168:1441-6.

90. Lin AH, Luo J, Mondshein LH, ten Dijke P, Vivien D, Contag CH, et al. Global analysis of Smad2/3-dependent TGF-beta signaling in living mice reveals prominent tissue-specific responses to injury. J Immunol. 2005;175:547-54.

91. Vooijs M, Jonkers J, Lyons S, Berns A. Noninvasive imaging of spontaneous retinoblastoma pathway dependent tumors in mice. Cancer Res. 2002;62:1862-7.

92. Becher OJ, Hambardzumyan D, Fomchenko EI, Momota H, Mainwaring L, Bleau AM, et al. Gli activity correlates with tumor grade in platelet-derived growth factor-induced gliomas. Cancer Res. 2008;68:2241-9.

93. Pihlajamaa P, Zhang FP, Saarinen L, Mikkonen L, Hautaniemi S, Janne OA. The phytoestrogen genistein is a tissue-specific androgen receptor modulator. Endocrinology. 2011;152:4395-405.

94. Lu X, Guo H, Molter J, Miao H, Gerber L, Hu Y, et al. Alpha-fetoprotein-thymidine kinase-luciferase knockin mice: a novel model for dual modality longitudinal imaging of tumorigenesis in liver. J Hepatol. 2011;55:96-102.

95. Park JH, Kim KI, Lee YJ, Lee TS, Kim KM, Nahm SS, et al. Non-invasive monitoring of hepatocellular carcinoma in transgenic mouse with bioluminescent imaging. Cancer Lett. 2011;310:53-60.

96. Marchini C, Gabrielli F, Iezzi M, Zenobi S, Montani M, Pietrella L, et al. The human splice variant Delta16HER2 induces rapid tumor onset in a reporter transgenic mouse. PLoS ONE. 2011;6:e18727.

97. Zumsteg A, Strittmatter K, Klewe-Nebenius D, Antoniadis H, Christofori G. A bioluminescent mouse model of pancreatic {beta}-cell carcinogenesis. Carcinogenesis. 2010;31:1465-74.

98. Ciana P, Raviscioni M, Mussi P, Vegeto E, Que I, Parker M, et al. In vivo imaging of transcriptionally active estrogen receptors. Nat Med. 2003;9:82-6.

99. Safran M, Kim WY, Kung AL, Horner JW, DePinho RA, Kaelin WG, Jr. Mouse reporter strain for noninvasive bioluminescent imaging of cells that have undergone Cre-mediated recombination. Mol Imaging. 2003;2:297-302.

100. Buschow C, Charo J, Anders K, Loddenkemper C, Jukica A, Alsamah W, et al. In vivo imaging of an inducible oncogenic tumor antigen visualizes tumor progression and predicts CTL tolerance. J Immunol. 2010;184:2930-8.

101. Liu J, Esmailpour T, Shang X, Gulsen G, Liu A, Huang T. TBX3 over-expression causes mammary gland hyperplasia and increases mammary stem-like cells in an inducible transgenic mouse model. BMC Dev Biol. 2011;11:65.

102. Gunther EJ, Moody SE, Belka GK, Hahn KT, Innocent N, Dugan KD, et al. Impact of p53 loss on reversal and recurrence of conditional Wnt-induced tumorigenesis. Genes Dev. 2003;17:488-501.

103. Jabbar SF, Abrams L, Glick A, Lambert PF. Persistence of high-grade cervical dysplasia and cervical cancer requires the continuous expression of the human papillomavirus type 16 E7 oncogene. Cancer Res. 2009;69:4407-14.

A.3 Figures

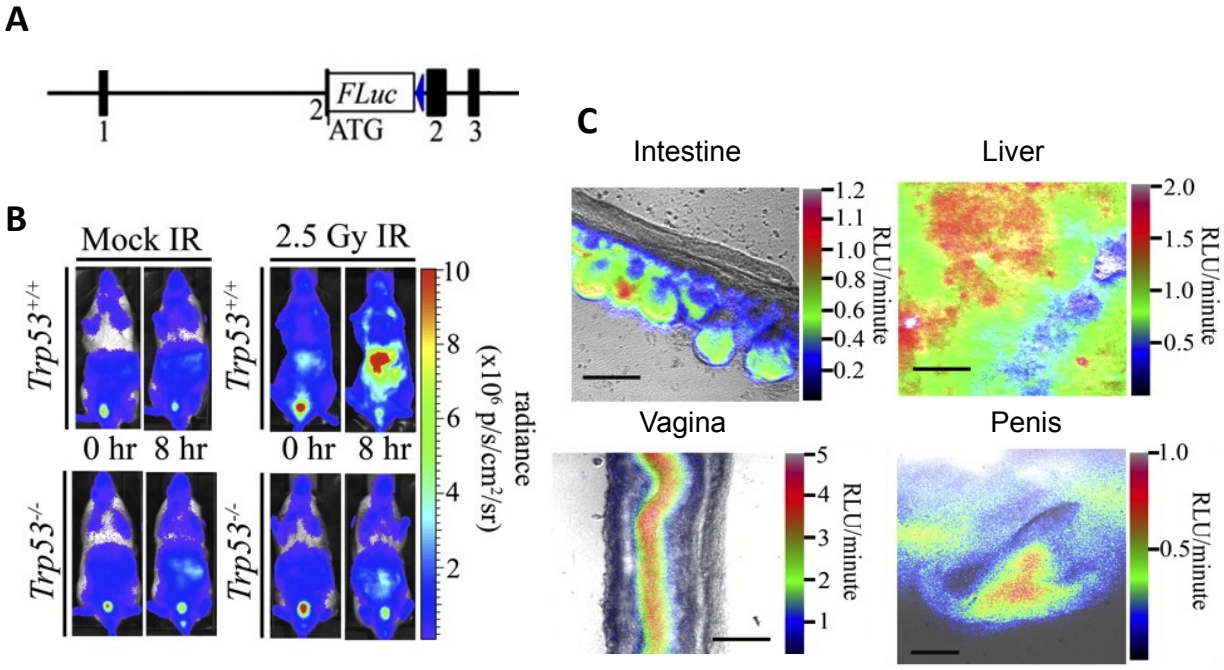

Figure 1. Whole animal imaging of p21 promoter activity. (**A**) Schematic representation of *p21*^{FLuc} reporter mice with luciferase knocked into the endogenous p21 locus. (**B**) Non-invasive, whole animal imaging of p53-dependent p21 promoter activity in response to radiation in *p21*$^{+/FLuc}$*Trp53*$^{+/+}$ and *p21*$^{+/FLuc}$*Trp53*$^{fl/fl}$ mice. (**C**) Low-light, bioluminescence microscopy of p21 promoter activity in various *p21*$^{+/FLuc}$ live tissues, including the villi from the small intestine, throughout the liver, in the epithelial cell layer below the keratinized penile spines, as well as the epithelial cell layer of the vagina. Bars, 200 μm; 50 μm for the penis. Images were modified and reprinted with permission from Molecular and Cellular Biology.

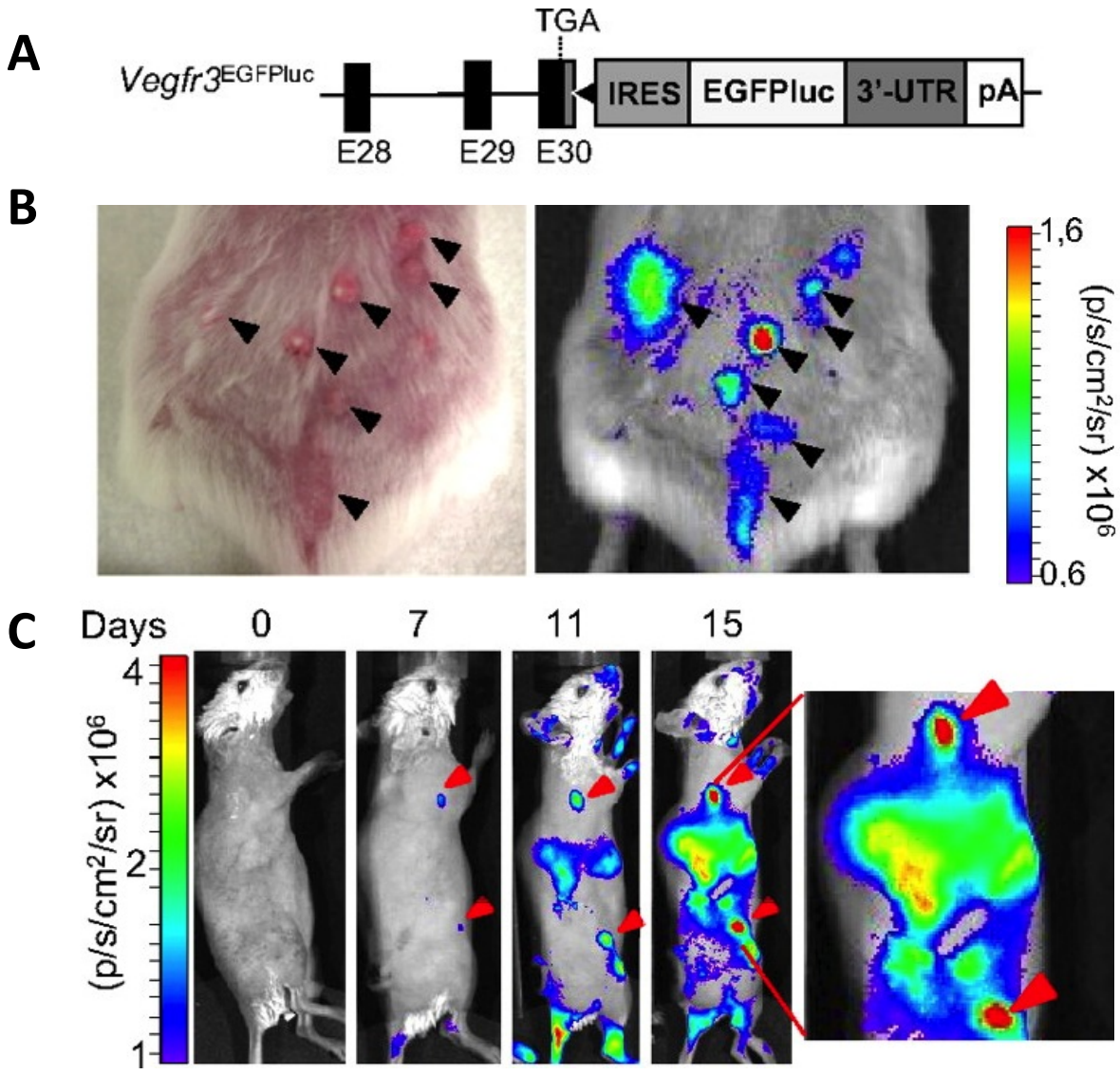

Figure 2. Imaging inflammation and tumor-associated lymphangiogenesis. (**A**) Schematic representation of the *Vegfr3*^{EGFPluc} reporter knocked in downstream of the endogenous *Vegfr3* locus, which utilizes an internal ribosome entry site (IRES) for monitoring Vegfr3 expression. (**B**) DMBA/TPA-induced skin papillomas in *Vegfr3*$^{EGFPluc/+}$ reporter mice displayed localized lymphangiogenesis as indicated by the black arrows. (**C**) Whole body imaging of tumor-activated lymphangiogenesis over time in a B16-V5 melanoma xenograft model at distant lymph nodes (red arrows) prior to metastasis of the primary tumor xenograft in female *Vegfr3*$^{EGFPluc/+}$ reporter mice. Images modified and reprinted with permission from Proceedings of the National Academy of Sciences.

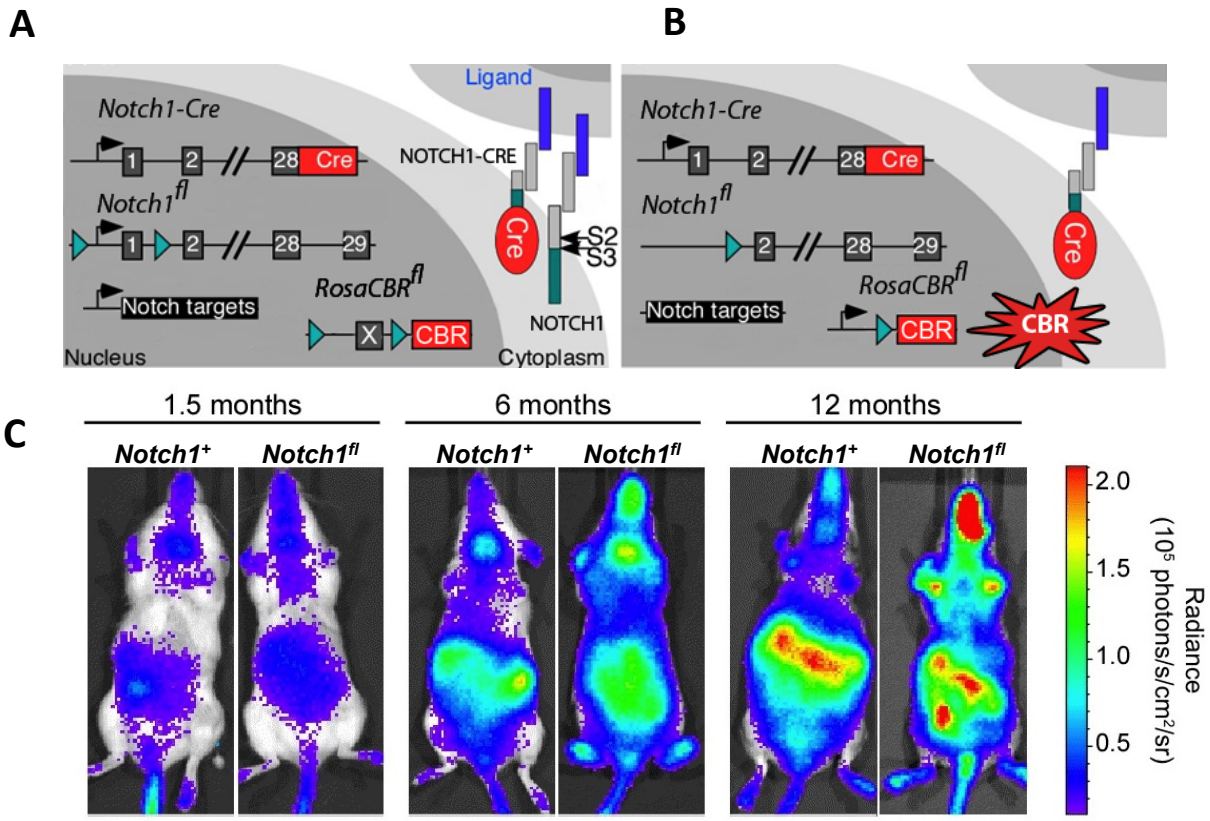

Figure 3. Imaging whole animal *Notch1* loss-of-heterozygosity (LOH) and surveying subsequent tumor development. (**A**) Schematic representation of *Notch1-Cre;Notch*^{fl}*; Rosa->CBR* cells prior to Notch1 ligand activation. (**B**) Upon activation, cleavage of NOTCH1 (between S2 and S3) permits translocation of the Notch-intracellular-domain (NCID)-Cre fusion into the nucleus where it excises both the remaining wildtype *Notch1*^{fl} allele, and the floxed stop cassette preceding *CBR*. Through these series of Cre-mediated excisions, lineage tracking of *Notch1* LOH can be longitudinally imaged via the genetically-coupled floxed *Rosa->CBR* reporter. (**C**) Whole animal imaging of the development and progression of *Notch1* LOH-induced angiosarcomas of the liver as imaged in *Notch1*$^{+}$ or *Notch1*^{fl} mice crossed to *Notch1-Cre;Rosa->CBR* reporter mice. Images modified and reprinted with permission from Journal of Clinical Investigation.

Table I. Cancer-Associated Processes Observable in Genetically-Encoded Luciferase Reporter Mice.

Mode of Regulation	Cancer Biology Target	Genetic Strategy	Ref.
Transcriptional			
	Cell cycle	KI(*p21 promoter->Luc*)	(37)
	B-cell specific imaging	KI(*CD19 promoter->Luc*)	(50)
	Various	KI(*Cox-2 promoter->Luc*)	(81)
	Various	Tg(*Egr1 promoter-> Luc*)	(82)
	Chemoresistance	KI(*Mdr1a promoter->Luc*)	(83)
	Lymphangiogenesis	KI(*IRES-EGFP-Luc* downstream of *Vegfr3*)	(51)
	Apoptosis	Tg(*Birc5 promoter-> Luc*)	(84)
	Telomerase regulation	Tg(*hTERT BAC->Rluc*)	(85)
	Angiogenesis	Tg(*Vegf promoter->TSTA-Luc*)	(86)
	Angiogenesis	Tg(*Vegfa promoter->EGFP-Luc*)	(87)
	Angiogenesis	Tg(*Vegfr2 promoter->Luc*)	(88)
	Various	Tg(*NF-κB RE-> Luc*)	(89)
	Various	Tg(*Smad 2/3 RE-> Luc*)	(90)
	Cre mediated Rb inactivation in pituatary gland.	Tg(*Pomc promoter-> Luc*)	(91)
	PDGF induced inactivation of Rb pathway	Tg(*E2f1 promoter->Luc)*	(67)
	PDGF-induced activation of Gli1/2	Tg(*Gli1/2 responsive promoter->Luc*)	(92)
	Prostate specific imaging	Tg(*Pbsn promoter + androgen response elements->Luc*)	(41)
	Systemic response to anti-androgen therapy	Tg(*Slp-androgen response elements -TK->Luc*)	(93)
	Afp activation in DEN induced HCC	KI(*Afp promoter->TK-IRES-Luc*)	(94)
	Afp activation in DEN induced HCC	Tg(*Afp promoter -> Luc*)	(95)
	Androgen deprivation in normal prostate, TAg, and JOCK models	Tg(*syn. Pbsn promoter-> Luc*)	(43)
	Androgen deprivation in normal prostate, TAg, and JOCK models	Tg(*syn. Psa promoter -> Luc*)	(43)
	Androgen deprivation in normal prostate and TAg model	Tg(*Psa promoter-> Luc*)	(42)
	Androgen deprivation in normal prostate and TAg model	Tg(*Psa promoter-> Luc*)	(44)
	Δ16Her2 induced mammary gland dysplasia	Tg(*MMTV-Δ16Her2-IRES-Luc*)	(96)
	SV40 ER induced pancreatic cancer monitoring	Tg(*Rip1 promoter->SV40 ER-IRES-Luc*)	(97)
	Estrogen receptor activation	Tg(*Estrogen RE->Luc*)	(98)
Post-Transcriptional			
	ER Stress	Tg(*CMV->XBP1-STOP-SA-Luc*)	(55)
Post-Translational			
	Hypoxia	Tg(*Hypoxic RE->ODD-Luc*)	(62)
	Hypoxia	KI(*Rosa26 promoter->ODD-Luc*)	(61)
	Hypoxia, Neu/ Beclin1$^{+/fl}$ induced mammary gland dysplasia	Tg(*MMTV->neu; ODD-Luc*); *Beclin1*$^{fl/+}$	(60)
Protein-Protein Interactions			
	Modular nuclear protein-protein interactions	Tg(*Gal4 promoter-> Luc*)	(64)

Transformation			
Cre-Activation			
	Cre Recombination	Tg(*Pomc promoter->Cre; Pomc promoter->Luc*)	(91)
	Cre Recombination	Tg(*β-actin promoter->flx-GFP-pA-flx-Luc-pA*)	(68), (71)
	Cre Recombination	KI(*Rosa26 promoter ->flx-STOP-flx-Luc*)	(99), (70)
	Cre Recombination	Tg(*CAG promoter->flx-STOP-pA-flx-TAg-Luc*)	(100)
	Cre Recombination	KI(*Notch1 promoter ->Notch1-Cre;->Notch1flx; Rosa26 promoter->flx-STOP-flx-CBR*)	(72)
Tet-Regulated			
	Coupled to MYCN expression	Tg(*Glt1 promoter->tTA; tet-o-Mycn-Luc)*	(79)
	TBX3 induced mammary gland dysplasia	Tg(*MMTV->rtTA; tet-o-myc-Tbx3-IRES-Luc)*	(101)
	Wnt1 induced mammary adenocarcinoma	Tg(*MMTV->rtTA; tet-o-Wnt1-IRES-Luc*)	(102)
	PyMT induced pancreatic cancer monitoring	Tg(*Pdx1-rtTA; tet-o-PyMT-IRES-Luc*)	(78)
	PyMT induced pancreatic cancer monitoring	Tg(*Rip7 promoter->tTA; tet-o-PyMT-IRES-Luc*)	(78)
	HPV16 *E7* induced cervical cancer	Tg(*Krt5 promoter->rtTA; tet-o-Luc- E7)*	(103)

Legend:

Tg = transgenic mouse; KI= knock-in mouse; -> indicates promoter driving gene expression; RE = response elements multiple; TK= thymidine kinase; gene loci are separated by a semicolon (;).

Table II. Luciferase-Coupled Reporter Mice Utilized in GEMMs of Cancer.

Cancer Type	Reporter Regulation	Target Gene/ Process Investigated	Reporter Strategy	Ref.
Brain				
	Transcriptional	Rb inactivation and tumor development in pituitary gland	Tg(*Pomc promoter-> Luc*)	(91)
	Transcriptional	PDGF inactivation of Rb pathway	Tg(*E2f1 promoter->Luc*0	(67)
	Transcriptional	PDGF activation of Gli1/2 and gliomagenesis	Tg(*Gli1/2 responsive promoter-> Luc*)	(92)
	Translational	MYCN driven medulloblastoma	Tg(*Glt1 promoter->tTA; tet-o-Mycn-Luc*)	(79)
Prostate				
	Transcriptional	Androgen deprivation in normal prostate, TAg, and JOCK models	Tg(*Pbsn promoter-> Luc*)	(43)
	Transcriptional	Androgen deprivation in normal prostate, TAg, and JOCK models	Tg(*Psa promoter -> Luc*)	(43)
	Transcriptional	Androgen deprivation in normal prostate	Tg(*Pbsn promoter + androgen response elements->Luc*)	(41)
	Transcriptional	Androgen deprivation in normal prostate and TAg model	Tg(*Psa promoter-> Luc*)	(42)
	Transcriptional	Androgen deprivation in normal prostate and TAg model	Tg(*Psa promoter-> Luc*)	(44)
	Cre Recombination	Conditional Pten loss	Tg(*β-actin promoter->flx-GFP-pA-flx Luc-pA)*	(71)
	Cre Recombination	Conditional Pten loss	KI(*Rosa26 promoter->flx-STOP-flx-Luc*)	(70)
	Transcriptional	Systemic response to anti-androgen therapy	Tg(*Slp-androgen response elements -TK->Luc*)	(93)
Liver				
	Transcriptional	Afp activation in DEN induced HCC	KI(*Afp promoter->TK-IRES-Luc*)	(94)
	Transcriptional	Afp activation in DEN induced HCC	Tg(*Afp promoter -> Luc*)	(95)
Breast				
	Tet-on	TBX3 induced mammary gland dysplasia	Tg(*MMTV->rtTA/; tet-o-myc-TBX3-IRES-Luc*)	(101)
	Transcriptional	Δ16Her2 induced mammary gland dysplasia	Tg(*MMTV->Δ16Her2-IRES-Luc*)	(96)
	Transcriptional	Neu, Beclin+/- induced mammary gland dysplasia	KI(*Rosa26 promoter ->ODD-Luc*)	(60)
	Tet-on	Wnt1 induced mammary adenocarcinoma	Tg(*MMTV->rtTA; tet-o-Wnt1-IRES-Luc*)	(102)
Pancreas				
	Tet-on	PyMT induced pancreatic cancer monitoring	Tg(*Pdx1-rtTA; tet-o-PyMT-IRES-Luc*)	(78)
	Tet-off	PyMT induced pancreatic cancer monitoring	Tg(*Rip7 promoter->tTA; tet-o-PyMT-IRES-Luc*)	(78)
	Transcriptional	SV40 ER induced pancreatic cancer monitoring	Tg(*Rip7 promoter->SV40 ER-IRES-Luc*)	(97)
Lung				
	Transcriptional	$Kras^{v12}$ induced lung tumorigenesis	Tg(*β-actin promoter->flx-GFP-pA-flx-Luc-pA*)	(68)
Lymphoma				
	Transcriptional	B-cell lymphoma	KI(*CD19 promoter->Luc*)	(50)

Cervical				
	Tet-off	HPV16 *E7* induced cervical cancer	Tg(*Krt5 promoter->tTA; tet-o-Luc- E7)*	(103)
Spontaneous				
	Transcriptional	Ubiquitous TAg induced tumorigenesis	Tg(*CAG promoter->flx-STOP-pA-flx-TAg-Luc*)	(100)
	Cre Recombination	Whole animal stochastic Notch1 loss of heterozygosity	KI(*Notch1 promoter ->Notch1-Cre;->Notch1flx; Rosa26 promoter->flx-STOP-flx-CBR*)	(72)

Legend:

Tg = transgenic mouse; KI= knock-in mouse; -> indicates promoter driving gene expression; RE = response elements multiple; TK= thymidine kinase; gene loci are separated by a semicolon (;).

Appendix B: DEVELOPMENT OF TUMOR-MICROENVIRONMENT ACTIVATED ANTI-CANCER SALMONELLA

B.1 Contribution to authorship

As second author on the following published manuscript, I performed *in vitro* and *in vivo* anti-tumor experiments and analyzed relevant data in addition to writing the complete introduction, discussion and respective results and methods sections. Specifically, I personally cloned P1786-Stx2 anti-tumor vector and performed the *in vitro* toxicity experiments where in HeLa cells were incubated with conditioned media extracted from HeLa cells co-cultured with various genetically engineered *Salmonella* strains (Figure 5). I also prepared the tumor cells, and bacteria for the *in vivo* bioluminescence imaging of the anti-tumor efficacy of P1787-Stx2 in addition to extracting and preparing the tumor for IHC as well as all data analysis (Figure 6).

B.2 Published manuscript

Flentie, K., Kocher, B., Gammon, S., Novack, D., McKinney, J. & Piwnica-Worms, D. A Bioluminescent Transposon Reporter-Trap Identifies Tumor-Specific Microenvironment-Induced Promoters in *Salmonella* for Conditional Bacterial-Based Tumor Therapy. *Cancer Discovery*. 2012 Jul; 2(7):624-37.

Abstract

Salmonella specifically localize to malignant tumors *in vivo*, a trait potentially exploitable as a delivery system for cancer therapeutics. To characterize mechanisms and genetic responses of *Salmonella* during interaction with living neoplastic cells, we custom designed a promoterless transposon reporter containing bacterial luciferase. Analysis of a library containing 7,400 independent *Salmonella* transposon insertion mutants in co-culture with melanoma or colon carcinoma cells identified five bacterial genes specifically activated by cancer cells: *adiY*, *yohJ*, *STM1787*, *STM1791*, and *STM1793*. Experiments linked acidic pH, a common characteristic of the tumor microenvironment, to a strong, specific and reversible stimulus for activation of these *Salmonella* genes *in vitro* and *in vivo*. Indeed, a *Salmonella* reporter strain encoding a luciferase transgene regulated by the *STM1787* promoter, which contains a *tusp* motif, showed tumor-induced bioluminescence *in vivo*. Furthermore, *Salmonella* expressing Shiga toxin from the *STM1787* promoter provided potent and selective anti-tumor activity *in vitro* and *in vivo*, demonstrating the potential for a conditional bacterial-based tumor-specific therapeutic.

Statement of significance

Salmonella, which often encounter acidic environments during classical host infection, may co-opt evolutionarily conserved pathways for tumor colonization in response to the acidic tumor microenvironment. We identified specific promoter sequences that provide a platform for targeted *Salmonella*-based tumor therapy *in vivo*.

Introduction

The evolving and highly heterogeneous landscape of tumor genetics and the tumor microenvironment pose a significant challenge for treating advanced solid tumors (1). Many characteristics of the tumor microenvironment, such as hypoxia, acidic pH, and a disorganized vascular architecture, limit delivery and efficacy of therapeutics and radiation treatments (2). Additionally, tumors undergoing targeted molecular therapy often relapse due to the utilization of autonomous parallel-redundant signaling pathways (3). Beyond the primary tumor, identifying disseminated disease that has metastasized to various organ sites is challenging, and systemically treating cancer often produces off-target toxicities. The ultimate anti-tumor therapy is one that overcomes these physiologic obstacles while simultaneously targeting tumors and avoiding normal tissue toxicity.

The remarkable ability of commensal and pathogenic bacterial strains to localize and preferentially grow within tumors has been well documented (4). The immune-privileged, hypoxic and nutrient-rich 'tumor soil' facilitates colonization by facultative anaerobic bacteria (5). These observations have spurred research into the diagnostic and therapeutic potential of genetically engineered and attenuated therapeutic strains of bacteria such as *Salmonella, Listeria* and *Clostridium* (5). *Salmonella* is one of the most studied of therapeutic bacteria, and upon systemic administration, is able to colonize xenograft tumors at rates 1,000 times greater than that of other organs, thereby abrogating tumor growth (6, 7). A firm understanding of the genetic programs involved in normal pathogenesis, characterization of spatiotemporal kinetics and dynamics during intra-tumoral colonization *in vivo*, genetic tractability, as well as the oncolytic

capacity of *Salmonella* typhimurium have made *Salmonella* strains ideal candidates for anti-cancer bacterial development (8).

S. typhimurium by itself can illicit an anti-tumoral response through several potentially separate but synergistic mechanisms. First, as a pathogenic and cytotoxic bacterium, *S.* typhimurium can induce apoptosis of cancer cells (9). Second, pathogen-associated molecular patterns (PAMPs) of *S.* typhimurium, such as lipopolysaccharide (LPS) and flagellin, are capable of activating innate immunity by initiating pro-inflammatory TLR-MyD88/ TRIF-NF-κB signaling cascades (10). Third, intracellular *Salmonella* flagellin can also enhance an anti-tumor adaptive immune response caused by the associative recognition with cancer cell antigen. The resulting signaling cascades ultimately augment antigen presentation by dendritic cells (DC), thereby promoting T cell clonal expansion and differentiation, which leads to an associative recognition of the cancer cell with the PAMPs of *Salmonella* (11, 12). Finally, despite the initial tumor regression, these tumors may eventually relapse, which has spurred the development of *Salmonella* as a delivery vehicle for anti-cancer co-therapies (13). Indeed, *Salmonella* have been used as tumor-specific vectors for gene transfer of RNAi or suicide genes, as well as targeted expression of apoptosis-inducing biologics, such as TRAIL, FASL and the bacterial toxin, Cytolysin A, all of which display pronounced anti-tumor affects *in vivo* (5).

However, few studies have investigated the specific genetic responses of *Salmonella* to tumor cells and bacterial mechanisms regulating these atypical "host" interactions. To address these quires, we engineered a bioluminescent transposon reporter-trap to screen a *S.* typhimurium library for genes specifically regulated by co-culture with malignant cells *in vitro*. Five genes were identified by the screen and their promoter sequences were found to be specifically activated by the acidic microenvironment associated with cancer cells *in vitro* and tumors *in*

vivo. Finally, we utilized the most pH-sensitive promoter sequence to demonstrate the utility of tumor-regulated *Salmonella* promoters to conditionally regulate the expression of a toxic tumor transgene *in vitro* and *in vivo*.

Results

A high-throughput screen to identify tumor cell-induced gene activation events in *Salmonella*.

To conduct a large-scale, unbiased screen for genes up-regulated by contact with malignant cells, we used a Tn5-based promoterless transposon as the backbone of a *luxAB* reporter construct. We chose to use the bacterial luciferase enzyme genes (*luxAB)* only, in contrast to the full bacterial luciferase operon (*luxCDABE*), because the size of the transposon containing the full operon prohibited efficient chromosomal integration, while using only the *luxAB* genes allowed for efficient genomic insertion of the transposon. The transposon was designed to restrict reporter gene expression to only those chromosomal integration sites downstream of an active promoter. A kanamycin resistance cassette with a constitutive promoter was also included to select for integration into the chromosome (**Figure 1A**). After construction, the purified transposon was electroporated into *S.* typhimurium strain SB300A1 (14) for random chromosomal integration, producing a 7,400 clone bacterial library.

Initially, the entire *Salmonella* library was subjected to a primary screen in the context of three conditions: tissue culture media alone, B16F10 melanoma cells and HCT116 colon carcinoma cells, both of the latter in monolayer co-culture with the *Salmonella* reporter library. The tumor cells were grown in 96-well plate format overnight and then bacterial clones added to wells corresponding to each of the two co-culture conditions and media alone. After a two-hour

incubation, bioluminescence imaging of plates enabled identification of clones specifically up-regulating genes in the context of exposure to melanoma and/or colon carcinoma cells (**Figure 1A**). Results of the screen from co-culture with melanoma and colon carcinoma cells are shown in **Figures 1B** and **1C**, respectively. In each case, data are shown as a rank-ordered S-plot of the $\log_2$ of the normalized signal for each clone of the library, where normalized signal was the ratio of the signal in the condition of interest to the signal in media alone. The majority of data points clustered around zero, indicating that most mutants interrogated in the assay did not show tumor-specific gene regulation. However, quartile analysis with a boundary for hit selection corresponding to a high stringency targeted error rate ($\alpha = 0.0027$) identified five candidate mutants wherein the transposon reporter was specifically up-regulated during co-culture with malignant cells.

Verification and characterization of *Salmonella* gene activation events in the context of tumor cell co-culture

Following the primary screen, we utilized inverse touchdown PCR to map the specific location of each transposon in the *Salmonella* genome (15). **Table 1** documents the site of chromosomal integration for the transposon and candidate gene up-regulated in each isolate. All genes were novel in that they have not been previously reported to be involved in *Salmonella*-host interactions, nor involved in *Salmonella* colonization of neoplasia. Interestingly, the genomic insertion sites of the transposon in three of the clones inserted in a cluster in the chromosomal sequence. Mapped to three different, but closely linked genes (*STM1787*, *STM1791* and *STM1793*, respectively), two are known hydrogenases, and all three genes are likely co-regulated and involved in the same *Salmonella* function. Sequencing showed that in

one high stringency hit, the transposon had inserted into *adiY*, a *Salmonella* gene known to be involved in an acid tolerance response (16). The transposon in the fifth clone was identified to have landed in *yohJ*, a putative membrane protein (17).

To validate cancer cell co-culture-specific gene activation events identified in the primary screen, we first repeated the co-culture assay in quadruplicate in at least three independent experiments for each clone. **Figure 2A** shows the data from one representative experiment for clones verified by this assay. Again, all five clones showed statistically significant enhancement of bioluminescence in the presence of tumor cells, with a trend toward greater gene up-regulation when co-cultured with B16F10 melanoma cells. Then, to further characterize tumor cell-induced response of *Salmonella*, we utilized the tumor cells in a dose-response assay (**Figures 2B, C**). Additionally, to verify that reporter activation seen in the *Salmonella* reporter-trap clones was not an effect of differing substrate permeability due to mutations in bacterial genes, bacteria were generated that contained the original chromosomal *luxAB* insertion as well as a plasmid constitutively expressing *luxCDE*, the biosynthetic genes for the long-chain aldehyde that acts as the optical substrate of the bacterial luciferase operon. Therefore, for this assay, it was not necessary to add decanal to the media. Identical inoculations of bacteria showed greater up-regulation of the reporter when exposed to greater numbers of tumor cells in co-culture conditions, indicating that the stimuli from tumor cells instigated a graded response from the bacteria. Because expression of the *lux* operon genes fully complemented the use of exogenous decanal in the system, the data confirmed that the effect was not an artifact of exogenous decanal permeability in the primary screen.

Finally, to verify that the reporters in fact reflected mRNA transcriptional regulation in wild-type *Salmonella* during co-culture with tumor cells, we utilized semi-quantitative PCR.

Following a three-hour co-culture of wild-type (SB3001A1) bacteria with B16F10 cells or in tissue culture media alone, isolated RNA was reverse transcribed to cDNA. Semi-quantitative PCR of cDNA showed that co-culture with B16F10 melanoma cells enhanced the intensity of target gene transcripts, but not control ribosomal RNA transcripts (*rrsH*) (**Figure 2D**). The effect was generalizable, as co-culture with HeLa tumor cells produced similar results (**Figure 2D**).

Notably, of the genes identified in this screen, at least one, *adiY*, has previously been reported to be up-regulated in acidic pH conditions (16). One characteristic of tumor microenvironments *in vivo* is an abnormally acidic pH (18). In fact, due to the Warburg effect, cancer cells are constitutively glycolytic, even in high oxygen conditions, releasing lactic acid and thereby creating a particularly acidic tumor microenvironment (19). For these reasons, the *Salmonella* transposon insertion mutants were further investigated for reporter signal activation in acidic conditions. **Figure 3A** shows that reporter signals increased in acidic pH media compared to neutral media. Each of the clones up-regulated the reporter gene at pH 6.0 compared to the physiological pH of normal body tissue (pH 7.5), suggesting that the stimulus *Salmonella* responded to in the context of neoplastic cells was microenvironment acidification.

To determine whether the activated genes were required for localization to tumors or required for colonization and growth within tumors *in vivo*, *Salmonella* strains null for genes identified in the screen were constructed. Selected genes were deleted using a lambda red recombinase insertional deletion strategy, which inserted a chloramphenicol resistance cassette into the targeted genes. The deletion mutants were created from a parental *Salmonella* strain (*luxCDABE msbB*-) containing a chromosomally-integrated and constitutively-expressed bacterial luciferase operon for imaging bacterial localtization *in vivo* in real time. The strain also contained a *msbB* gene deletion, which causes a less immunogenic LPS structure and minimizes

septic shock effects when the strain is administered intravenously (20). Based on the analysis that the identified *STM1787, STM1791* and *STM1793* genes were contained in a single operon, we targeted a large region of this operon for deletion in a single mutant strain, 1789^{-}1793^{-}. The gene *adiY* also appeared to be a part of a larger operon of co-regulated genes and was therefore targeted along with the adjacent genes *adi* and *yjdE*. The gene *yohJ* was targeted individually. In a B16F10 melanoma tumor xenograft model, all bacterial strains were injected via mouse tail vein and deletion mutants compared to the parental strain for localization to and persistence within the tumor using bioluminescence imaging (**Supplementary Figure 1**). All mutant strains and the parent strain were capable of tumor localization and persistence, indicating that although the identified genes were activated by tumor cell co-culture *in vitro*, they were not essential for bacterial *colonization* of the tumor. The experiment was also performed in an HCT116 colon carcinoma xenograft model with similar results. **Supplementary Table 1** summarizes the numbers of mice with colonized tumors on or before day 10 in each experiment. Additionally, in pilot competitive infection studies, there was no significant difference between the *STM1789-1793* mutant and the parental *Salmonella* strain (*luxCDABE msbB*-) in tumor colonization (CFU/ml; data not shown).

Specificity and reversibility of the *Salmonella STM1787* promoter *in vivo*

We next sought to demonstrate the specificity of the STM1787 promoter activation in the tumor microenvironment *in vivo*. We chose this promoter because it displayed the highest acidic pH induction *in vitro* (**Figure 2A**). Here, we used the constitutively bioluminescent *Salmonella* strain Tn:27.8+p*luxCDE* or the conditionally bioluminescent strain Tn:1787+p*luxCDE*, each of which constitutively express plasmid-encoded *luxCDE*, but the latter strain will only bioluminesce upon activation of the chromosomally-encoded *luxAB* reporter. In a B16F10

melanoma tumor xenograft model, bacteria were injected via mouse tail vein or intratumorally and allowed two days to localize and adapt to tumors *in vivo*. Tumors were then excised, incubated in solutions of various pH values and imaged periodically for six hours. Initially, all tumors showed bioluminescent bacteria *ex vivo*. Over time, constitutive Tn:27.8 *Salmonella* showed a gradual increase in signal consistent with bacterial growth in the tumor explants. This behavior was also observed in the Tn:1787 *Salmonella*-infected tumor explants incubated in low pH media. By contrast, when the Tn:1787 *Salmonella*-infected tumor explants were maintained in basic media conditions throughout, the signal initially increased, but then plateaued around 4 hours and decreased in comparison to the constitutively bioluminescent Tn:27.8 strain (**Figure 3B,C**). This finding suggested that bacterial gene expression was initially engaged by the low pH conditions of the *in vivo* tumor microenvironment, but after exposure to a higher pH environment *ex vivo*, the promoter driving the reporter was repressed and signal declined. Further, this *ex vivo* effect was reversible. When the medium on the Tn:1787 *Salmonella*-infected tumor explant was changed from pH 6.0 to pH 7.5, the bioluminescent signal decreased. Conversely, when the media was changed from pH 7.5 to pH 6.0, the signal increased (**Figure 3B, C**). These effects were not seen with the constitutive Tn:27.8 *Salmonella*-infected tumor explants, and provided further evidence in support of the specificity of the trapped *Salmonella* promoter in the Tn:1787 transposon mutant for the tumor microenvironment.

Because the identified promoters were highly activated in the tumor microenvironment *ex vivo*, utilization of these promoters provided a unique opportunity to design tumor-targeting bacterial vectors subject to multiple levels of controlled specificity *in vivo*. Thus, we sought to determine if the acidic pH of the tumor microenvironment could be exploited to specifically activate a target transgene during tumor localization. As proof of principle, we constructed

Salmonella reporter strains expressing plasmids encoding the bacterial luciferase operon driven by either constitutive promoters or an inducible promoter to demonstrate tumor-mediated transgene activation *in vivo*. The plasmids p*MAAC001* and p*Lux* both encoded constitutively-expressed luciferase operons, while the p*PROMOTERLux* plasmid was engineered to contain the luciferase operon driven by the *Salmonella* candidate promoter (*STM1787*) comprising 500 base pairs upstream of the putative transcription start site of tumor-activated genes *STM1787, STM1793* and *STM1791* (which we will now refer to as the *STM1787* promoter). Bacteria expressing these plasmids were identically injected into mice bearing HCT116 tumor xenografts on each flank (**Figure 4**). We chose to utilize intratumoral injection to directly compare reporter gene activation from two different bacterial strains, one inducible and the other constitutive, over time in the same mouse. Although reporter signals from p*PROMOTERLux*-expressing bacteria were low immediately after injection into the tumor, the bacteria quickly induced a 90-fold enhanced expression of the reporter after an 8 hr exposure to the tumor microenvironment (**Figure 4A**). Concurrently, bacteria constitutively expressing p*Lux*- or p*MAAC001*-luciferase showed <20-fold or no reporter activation, respectively, after exposure to the tumor microenvironment (**Figures 4A and 4B**). These data directly demonstrated tumor-specific induction of a transgene from the *Salmonella STM1787* promoter in an *in vivo* system. Therefore, the *STM1787* promoter could be used as a platform to design tumor-targeting *Salmonella* strains capable of specifically delivering a therapeutic gene or toxin to the site of a tumor *in vivo*.

Selective anti-tumor therapy *in vivo*

We utilized the cancer cell-activated STM1787 promoter to regulate the expression of Shiga toxin 2 (Stx2), a toxic transgene of bacterial origin, in a wild type strain of *S.* typhimurium (SB300A1) to selectively induce tumor cell death *in vitro* and *in vivo.* Stx2 is a secreted AB_5

holotoxin composed of a single N-glycosidase A subunit that is directed to target eukaryotic cell membranes through interaction of the pentameric B subunits and the host receptor, glycosphingolipid globotriaosylceramide (Gb_3) (21). Once inside the host cell, the A subunit cleaves the 28S RNA of the 60S ribosomal subunit, thereby inhibiting peptide elongation and inducing apoptosis. Stx2B has been extensively studied for its tumor targeting potential as many invasive tumors display high levels of Gb_3 (22).

Using bioluminescence as a reporter of total tumor cell mass, we performed a co-culture experiment with $HeLa^{CMV\text{-}Fluc}$ cells *in vitro*. First, plated HeLa cells were grown to confluency to acidify the media and then co-cultured with strain SB300A1 transformed with P1787 (empty vector) or P7187-Stx2. Both SB300A1 transformants were also grown in media alone. The supernatant was then filtered from each of the groups and aliquoted onto separately plated $HeLa^{CMV\text{-}Fluc}$ cells in increasing volumes: 1) +media+P1787; 2) +media+P1787-Stx2; 3) +HeLa+P1787; and 4) +HeLa+P1787-Stx2. After 24 hours of treatment, major toxicity was only observed in $HeLa^{CMV\text{-}Fluc}$ cells treated with the supernatant of +HeLa+P1787-Stx2 (**Figure 5A**); a general concentration-response trend was observed (**Figure 5B**). Stx2 expression was verified using mRNA PCR amplification (**Figure 5B inset**). No overt cytotoxicity was observed in $HeLa^{CMV\text{-}Fluc}$ cells treated with supernatant from any of the other conditioned media groups.

Given the selective regulation and associated toxicity of P1787-Stx2 *in vitro*, we next desired to demonstrate the tumor-targeting potential *in vivo* using established s.c. flank $HeLa^{CMV\text{-}Fluc}$ xenograft tumors and bioluminescence imaging. In two independent proof-of-principle experiments, intratumoral injection of a single high-dose of SB300A1 transformed with P1787-Stx2 resulted in an 80% mean reduction in initial viable tumor mass five days after treatment (**Figure 6A**). Furthermore, when tumors were treated with a single low-dose of SB300A1

transformed with P1787-Stx2, a robust anti-tumoral effect was observed after two weeks (**Figure 6B**). We also observed that treatment with P1787 resulted in tumor stasis, consistent with previous reports that *S.* typhimurium alone can block tumor growth *in vivo,* while LB broth alone showed no inhibitory effect (23). To verify tumor cell death independent of bioluminescence signal, tumor H&E sections from the high-dose treatment were analyzed (**Figure 6C**). Sections through LB-treated (control) tumors showed a broad rim of viable tumor cells with focal necrotic regions centrally. In the P1787 tumors, a thin rim of viable tumor cells was present in most areas, with fibroinflammatory reaction at the periphery of the mass. The central necrotic zone was larger and contained more neutrophils than in the LB-treated tumors. In the P1787-Stx2-treated tumors, viable tumor cells were difficult to find, and in most sections, only a central necrotic zone surrounded by fibroinflammatory reaction was present. Note that mice treated with high-dose P1787-Stx2 eventually succumbed to the combined bacterial and Stx2 toxin load. However, mice receiving low-dose P1787-Stx2 were healthy for two weeks, at which point the experiment was concluded, but each still displayed a significant reduction in tumor size compared to P1787 alone (**Figure 6B**).

Discussion

Salmonella typhimurium bacteria are typically classified as human gastrointestinal pathogens and a common cause of modern food-borne illness. However, another noted characteristic of *Salmonella* is the capacity to colonize tumor tissue. In fact, in the 1800's, physicians began to intentionally use bacteria as tumor therapeutics, but due to significant toxicity and lack of consistent, reliable results, these practices were abandoned. However,

modern studies using attenuated strains and longitudinal imaging have demonstrated colonization of tumors by *Salmonella* in real time and have sparked a renewed interest in this concept using *Salmonella* (23, 24) as well as various other tumor-localizing microbes as an option for cancer treatment (25-31). These observations along with the current intense focus on developing PAMP/ TLR-based anti-cancer immunotherapies offer unique opportunities for combinatorial strategies in tumor targeting.

Both wild-type and genetically engineered *Salmonella* are capable of inducing tumor regression in mouse cancer models (4), as was observed in our experiments (**Figure 6**). A number of studies utilize bacteria as treatment vectors *per se* or as drug delivery vehicles by exploiting their potentially low toxicity and high genetic tractability to maximize therapeutic efficacy (5). In this regard, various attenuated *Salmonella* strains have been developed for use in tumor-targeting studies, including specific amino acid auxotrophs and LPS mutants (20, 32). However, the greatly reduced toxicity of *Salmonella* LPS mutants (*msbB*-) observed in swine models has not been observed in mouse models (33, 34). In more than one instance, attenuated *Salmonella* have even been used in a clinical trial to treat cancer in humans (35, 36). However, trials so far show relatively low rates of tumor colonization in human hosts, which may be due to excessive attenuation of the bacterial strains (5, 34). Indeed, one study indicates that induction of TNFα by bacteria is necessary for optimal colonization of tumors (37). Nonetheless, few studies have investigated the phenotypic and gene expression patterns of these tumor-targeting bacteria following exposure to tumor cells.

In this study, we utilized an engineered transposon to interrogate the *Salmonella* genome for genes activated during exposure to cancer cells. Toward this objective, we generated a library of greater than 7,400 independent transposon insertions, which, assuming random integration,

would predict genomic transposon insertion into each of *Salmonella'*s 4,620 genes at least once. From this library, we identified five *Salmonella* genes specifically up-regulated during co-culture with cancer cells: *STM1787*, *STM1791*, *STM1793*, *adiY* and *yohJ*. Following identification of these tumor cell-activated genes, verification in secondary assays and confirmation in wild-type *Salmonella*, we determined that the common stimulus for up-regulation of target gene expression was acidic pH. In another study aimed at identifying *Salmonella* promoters involved in tumor colonization *in vivo*, *Salmonella* genomic DNA was digested and ligated randomly upstream of a GFP reporter. In this study, the major stimulus identified in reporter activation was hypoxia, but no pH-regulated promoters were identified (38). Another recent study performed a similar *in vivo* screen utilizing a promoter-trap GFP based system and indentified a conserved 'tumor specific' DNA motif (*tusp)* in the promoters of *Salmonella* genes specifically activated in a tumor xenograft model (33). While pH and hypoxia are physiologically linked, the five genes identified herein show no overlap with the promoters identified by Leschner et al. (33) nor Arrach et al. (38). However, the STM1787 promoter located upstream of three of our own target genes (STM1787, STM1791, and STM1793) did contain the conserved *tusp* motif identified by Leschner et al. (tattttatataaa). The discrepancy in promoter identification may stem from the different bacterial strains or strategies utilized for gene identification in the two studies. Whereas Arrach et. al. utilized a plasmid-based overexpression system, the present study identified genes by chromosomal integration of a transposon. Nonetheless, hydrogenase genes are noted in some cases to be up-regulated in low oxygen conditions, indicating that hypoxia may serve as a further stimulus for the pH-induced promoters identified in the present study (39). However, in pilot studies with an incubation pouch system used for growing anaerobic bacteria, we did not observe any significant changes in transposon reporter activity under hypoxic

conditions (KF, unpublished data). While these data do not necessarily rule out oxygen-independence, pH appeared to be the dominant signal inducing responses in the promoters identified by our bioluminescent transposon reporter-trap screen. It will also be of interest in future studies to determine if in addition to hypoxia, pH is another regulator of *Salmonella* promoters that contain the largely uncharacterized *tusp* motif.

In view of the usual pathophysiology of *Salmonella*, it is not surprising that *Salmonella* strains have gained the ability to precisely regulate genes in response to different pH environments. *Salmonella* encounter low pH conditions regularly during human infection, for example, during transit through the stomach, and later during intracellular trafficking through the phagosome (40, 41). Interestingly, the acidic pH of the tumor environment *in vivo* has long been noted as an important microenvironmental condition when designing effective tumor treatments (18, 42). Additionally, the low pH environment of the tumor inhibits host defense. Cytotoxic immune cell activity and cytokine secretion has been shown to be impaired by a low extracellular pH (43). In contrast, with a bacterial-driven tumor therapeutic, low pH may become an exploitable advantage, by adding another level of selectivity to bacterial gene activation. Indeed, the utility of a low pH-activated bacterial therapeutic will avoid toxicity to the liver and spleen which are the other major off-target organ sites of bacterial colonization, but which generally have a neutral pH (33). In this case, a bacterial-based system may succeed, while both conventional therapeutics and host defenses fail.

When using bacteria as a vector for drug delivery studies, tumor-specific colonization and subsequent expression is a major concern. The genes identified herein are highly expressed in an acidic tumor environment, but are not required for bacterial tumor targeting (**Supplemental Figure 1**). Therefore, the promoters regulating these genes and further dissection of the complex

regulation of the *tusp* motif may generate ideal chromosomal insertion site candidates or synthetic promoter systems for utilization in therapeutic gene, pro-drug or toxin delivery studies. We have identified the *STM1787* promoter as an ideal bacterial sequence capable of driving tumor-specific expression of a transgene, and demonstrated this *in vivo* using bioluminescent imaging. We further applied the STM1787 promoter to conditionally regulate the expression of Stx2 in wildtype *S.* typhimurium in tumor targeting toxicity models *in vitro* and *in vivo*. In proof-of-principle studies, we observed dramatic cancer cell death in a co-culture model *in vitro* and dramatic tumor response over a relatively short time scale with a robust therapeutic effect *in vivo*. Future pharmacokinetic studies with P1787-Stx2 will be required to optimize mode of delivery, dose, and efficacy. In addition, it will be of interest to take advantage of the recent discovery that manganese treatment protects the host against lethal levels of Shiga toxin (44). Clearly, other relevant tumor toxins could be explored downstream of STM1787.

In summary, by adapting the *STM1787* promoter in *Salmonella* to drive expression of an appropriate therapeutic transgene, the resulting bacterial vector would provide two independent mechanisms for specifically targeting tumors. First, *Salmonella* specifically localize to and accumulate in primary tumors and metastases *in vivo*. Second, the *STM1787* promoter is preferentially activated in the acidic tumor microenvironment. The combined effect of these two levels of specificity provides a potential option to design more successful PAMP/ TLR-based immunotherapeutic bacterial systems in the future.

Methods

Bacterial strains and culture conditions

The *Salmonella* typhimurium strains SB300A1 (14), SB300A1FL6 (*luxCDABE)* (45), luxAB and AM3 (*luxCDABE msbB*-) were grown in LB broth with appropriate antibiotics. SB300A1FL6 is modified by chromosomal integration of *luxCDABE* and is constitutively bioluminescent. The luxAB strain consists of SB300A1FL6 with the integrated *luxE* gene disrupted. This strain does not bioluminesce without addition of exogenous decanal substrate. The AM3 strain has the SB300A1FL6 background, but also has an *msbB* gene disruption, giving it a less immunogenic LPS structure. The Tn:27.8 strain, specifically identified from the screen as a non-inducible mutant, phenocopies luxAB with constitutive bioluminescence that requires exogenous decanal.

Tissue culture cell lines and culture conditions

B16F10 murine melanoma and HeLa cells were obtained from ATCC and cultured according to ATCC directions. HCT116 human colon carcinoma cells were a gift from Bert Vogelstein and were cultured according to ATCC methods. Cell lines were not further authenticated.

Plasmids: The plasmid pMAAC001 contains the full bacterial luciferase operon *luxCDABE* driven by a T7 promoter and an ampicillin resistance cassette. The plasmid pLuxCDE consists of the pMAAC001 backbone amplified using the forward primer cccgggattggggaggttggtatgtaa and the reverse primer cccgggtgaatgatttgatgagccaaa (*XmaI* sites underlined). This product was then *XmaI* digested and re-ligated to exclude the majority of the *luxA* and *luxB* genes. pLux and pPROMOTERLux plasmids were constructed by inserting the full bacterial luciferase operon

between the *KpnI* and *BamHI* restriction sites in the vector pUC19. The pPROMOTERLux plasmid additionally had a 500 base pair promoter region (*STM1787*) from the *Salmonella* genome inserted upstream of the luciferase operon between the *SacI* and *KpnI* restriction enzyme sites. The 500 base pair sequence was amplified from the *Salmonella* genome using the forward primer aaagagctcacgccctctttcaaacagtc and the reverse primer aaaggtaccgcttgataaaaggtctcctcgt (*SacI* and *KpnI* sites underlined). To construct the P1787-based vectors, 500bp of the endogenous SB300A1 *1787* promoter was cloned into the *BglII* and *NdeI* sites of pET3a (Novagen) using the following primers: forward-gagagagaagatct gggacgccctctttcaaacagtctc, reverse- ccttcctgcccatatgaacgcgtatttttctccttttgcacc. This cloning strategy conserved the endogenous 1787 Shine-Dalgarno sequence and removed the *T7* promoter and synthetic *RBS* of pET3a. The P1787-Stx2A/B vector was constructed by inserting the *Stx2A/B* operon downstream of the *1787* promoter using *NdeI* and *BamHI* with the following primers: forward-gagagagacatatgaagtgtatattatttaaatgggtactgtgcctgttactgggtttttcttcggtatcc, reverse-ccttccttccggatccttatcaatggtgatggtgatggtgg.

Construction of a Salmonella typhimurium reporter-trap library

Salmonella strain SB300A1 was used to construct a bacterial library comprising approximately 7,400 clones of unique chromosomal integrations of our reporter transposon (14). The custom *Tn5*-based transposon was designed with the EZ-Tn5 system (Epicentre, Madison, WI) using the pMOD4 transposon construction vector. A kanamycin-resistance cassette and promoter from EZ-Tn5<KAN-2> was amplified using the forward primer acgacaaagcttggacgcgatggatatgttct and the reverse primer agcttttctagaggtggaccagttggtgattt (*HindIII* and *XbaI* restriction sites underlined) and inserted into the *HindIII* and *XbaI* restriction sites of pMOD4. The luciferase enzyme genes *luxAB* from *Photorhabdus* luminescens were amplified with the forward primer

acagtcgaattccgccgaatgagaattgagat and the reverse primer aagctgggtacctgttggctgctttcactcac (*EcoRI* and *KpnI* sites underlined) and inserted between the *EcoRI* and *KpnI* sites in pMOD4 (45). The plasmid contained an R6Kγ origin of replication and therefore was amplified in *E. coli* DH5α λpir, purified, digested with *PvuII*, and the transposon fragment recovered by gel purification. The purified transposon was combined with transposase (Epicentre). After bench top incubation for 30 minutes, followed by 48 hours at 4°C, the transposon DNA was electroporated into bacteria as per the vendor's instructions. Bacteria were plated on LB kanamycin plates to select for transformants containing the chromosomally-integrated transposon. Each clone was expanded and stored in 60% glycerol in 96-well plates at -80°C.

Screening the library

To screen for gene activation events occurring in the context of malignant cells, *Salmonella* library clones were cultured under three different conditions: co-culture with B16F10 mouse melanoma cells, co-culture with HCT116 human colon carcinoma cells and culture in media alone. Each of the two tumor cell lines were seeded into 96-well white plates at approximately 70-80% confluency in DMEM with 10% FBS. In the plate containing media alone, each well contained 100 µl of DMEM with 10% FBS only. Plates were incubated overnight to allow tumor cell adhesion to the 96-well white plates. Independently, bacterial clones were grown overnight in LB broth with kanamycin in 96-well plates and subcultured the following day 1:10 into LB broth. Five to six hours after subculturing, 30 µl of bacterial culture were added to three replicate plates, each corresponding to a separate culture condition. Bacteria were allowed to co-incubate with the malignant cells or media alone for 2 hours. Subsequently, bacteria were imaged by adding 30 µl of decanal solution, waiting 10 minutes, and imaging with an IVIS 100 imaging system (Caliper; acquisition time, 60 sec; binning, 4; filter, < 510; f stop, 1; FOV, 23 cm) (46).

Because white plates were used to maximize signal intensity, images were aquired utilizing a <510 filter to reduce phosphorescence from the plates. Three control wells were included on every plate comprising: *luxCDABE Salmonella* (SB300A1FL6), which contain the full luciferase operon inserted into the chromosome; *luxAB* strain, which contains the luciferase enzyme genes only and therefore requires addition of exogenous substrate to image reporter activity in the assay; and a blank well, which contained media, but was not inoculated with bacteria, to serve as a control for background luminescence. Imaged plates were analyzed with Living Image (Caliper) and Igor (Wavemetric) analysis software packages as described (47). Data were normalized by dividing the photon flux of experimental wells by media alone wells and presented as the $\log_2$ of the normalized photon flux data.

Identification of hits

Library screening data representing photon flux from each well of a library plate were analyzed with Image J software (48). To identify statistically significant hits from the primary screens, we utilized a set of statistical requirements. First, a threshold was set to identify active clones. Clones that did not produce photon signals greater than three standard deviations above the signal in the un-inoculated, media alone wells were not further analyzed. A quartile method of statistical analysis was then applied to the remaining clonal data (49). For quartile analysis, plates of clones were grouped by assay date into sets for data analysis. For each set, we normalized data by calculating the $\log_2$ of the fold-change of photon flux signal between the condition of interest (co-culture with B16F10 or HCT116 cells) and media alone. From this data, we calculated the median (Q2), first (Q1), and third (Q3) quartile values. The boundary for hit selection was calculated as Q3 + c(ICQ), where ICQ = Q3-Q1 and c = 1.7239, corresponding to a high stringency targeted error rate of $\alpha = 0.0027$ (49).

Verification of primary screen hits

To verify hits identified by the primary screen, clones were tested again in a similar manner, in quadruplicate. The assay followed the same steps as those in the primary screen, except each clone was tested in 4 wells under each of three conditions across a 12-well row in a black 96-well plate. Imaging was done with an IVIS 100 imaging system (acquisition time, 60 sec; binning, 4; filter, open; f stop, 1; FOV, 23 cm).

Identification of transposon insertion site

To map sites of transposon integration in the chromosome of clones of interest, an inverse touchdown PCR strategy was used (15). Genomic DNA was isolated from bacteria using DNAzol (Molecular Research Center, Cincinatti, Ohio). PCR was performed using bacterial chromosomal DNA, 20 pmols of a primer specific to the 5' end of the transposon (atggctcataacacccctttg), and 100 pmols of a degenerate primer (cggaatccggatngayksnggntc). Reactions were initiated with a 95°C preparation step for 5 minutes, followed by 25 cycles comprising denaturation at 95°C for 45 seconds, annealing at various temperatures for 45 seconds and extension at 72°C for 2 minutes. The annealing temperature started at 60°C and decreased 0.5°C per cycle for the subsequent 24 cycles. Then PCR proceeded with 25 cycles of 95°C for 45 seconds, 50°C for 45 seconds and 72°C for 2 minutes. PCR reaction products were fractionated on a 1% agarose gel, and the most prominent bands in each lane were excised and gel purified (Qiagen kit). For some reactions, PCR products were purified (Qiagen) and the resulting purified PCR product was used as a template for a second round of PCR using a different transposon-specific primer (aacatcagagattttgagacacc) before gel purification of

products. The cycling conditions and degenerate primer used in the second round of PCR were the same as round one.

Semi-quantitative RTPCR

Salmonella strains SB300A1, P1787 or P1787 transformed SB300A1 were subcultured from a stationary phase culture 1:10 and grown for 6 hours. Bacteria were then diluted 1:20 and 30 µl added to 96-well plates containing tissue culture media alone, B16F10 melanoma cells or HeLa cells, seeded 24 hours previously at 100,000 cells/well and 50,000 cells/ well, respectively. After three and a half hours of co-culture, extracellular media containing bacteria was removed from the 96-well plates and triplicates pooled. Media were centrifuged to pellet bacteria and pellets were frozen at -80°C. After thawing, pellets were resuspended in 200 µl water with 5 mg/ml lysozyme and incubated at room temperature for 5 minutes. Then, 700 µl of RLT buffer was added and bacterial RNA was purified using the Qiagen RNeasy kit (Qiagen Inc, Valencia, CA). Samples were then treated with DNase I at room temperature for 15 minutes, after which EDTA was added and samples were incubated for 10 minutes at 65°C to inactivate the DNase. Samples were then ethanol precipitated and resuspended in 30 µl water. For reverse transcriptase PCR, 1 µg of total RNA was used as a template and reverse transcribed using Superscript II Reverse Transcriptase and 300 ng random primers as per the manufacturer's instructions (Invitrogen, Carlsbad, CA). Following RTPCR, samples were treated with RNase H for 25 minutes at 37°C. To perform semi-quantitative PCR, samples were amplified using primers specific to each gene target or to ribosomal RNA: STM1787 (forward: tcggtagatcgcatgatgtc, reverse: ggttggtcataagcctgtcg), STM1791 (forward: acacgggaacatccagattc, reverse: cggcaaaggacaaatctcat), STM1793(forward: ttcggcaacctgtttttagg, reverse: acgcctccttgcataatcac), *adiY* (forward: ccttattgaccgccaactgt, reverse: gtggtcaagaaagcgggata), *yohJ* (forward:

caggcatttttcttgcatca, reverse: cgccatataacgaatcagca), *rrsH* (forward: cagccacactggaactgaga, reverse: gttagccggtgcttcttctg), Stx2A (forward: atgacgccgggagacgtgga, reverse: ggccacagtccccagtatcgct) and Stx2B (forward: gcaatggcggcggattgtgc, reverse: acaatccgccgccattgcat). PCR cycling conditions were: 95°C for 5 minutes, 30 cycles (or 20 cycles for *rrsH* reactions) of denaturation at 95°C for 45 seconds, annealing at 50°C for 45 seconds and extension at 72°C for 1 minute. PCR products were fractionated on a 1% agarose gel.

Construction of deletion mutants

Mutant strains deficient for the identified target genes were constructed in *Salmonella* strain *luxCDABE msbB*- (AM3), which contains a constitutively active, chromosomally-encoded bacterial luciferase operon as well as a mutation in *msbB* to create a less immunogenic LPS structure. Mutants were constructed using a lambda red recombinase strategy (50). First, primers were designed to amplify the chloramphenicol-resistance cassette in pKD3 with tails flanking the targeted locus of the *Salmonella* genome to be deleted. Primer sequences specifically targetting the genome for each mutant were used (*adi* forward targetting primer: atgaaagtattaattgttgaaagtgagtttctgcatcaggacacctgggtgtgtaggctggag-ctgcttc, *adi* reverse targetting primer: atcctgtttaaccggcgcatccagcggatacgggtttttgtgaatgc-ggtcatatgaatatcctccttag; *yohJ* forward targetting primer: agtaagtcactgaatattatctg-gcaatatatacgcgcttgtgtaggctggagctgcttc, *yohJ* reverse targetting primer: ttttttcgttcc-cttctgcccaaccactttacgctcaccgcatatgaatatcctccttag; STM1789-1793 forward targetting primer: atgaatgcgcaacgcgtagtggtgatggggttaggaaaccgtgtaggctggagctgcttc, STM1789-1793 reverse targetting primer: ctaataaagttcatgatcgttgcggcggagggtccccaggcatatgaa-tatcctccttag). PCR fragments were then electroporated into AM3 bacteria expressing plasmid-encoded red recombinase. Following electroporation, growth on chloramphenicol plates at 37°C selected for strains that had lost the temperature-sensitive recombinase plasmid and inserted the

chloramphenicol-resistance cassette into the targeted genomic loci. Deletion of the genes was confirmed by PCR.

Dose-response to tumor cells

To test the dose-response of hits from the screen to tumor cell co-culture, the assay was performed as described, except that either B16F10 or HCT116 cells were plated at $1x10^5$; $2 x10^5$; or $3 x10^5$ cells per well 24 hours before co-culture with bacteria. Stationary phase bacteria were diluted 1:50 and incubated for 6 hours before identical aliquots were allowed to co-culture with the malignant cells. Growth curves performed for each mutant strain at different pH values showed no significant differences. Imaging was done with an IVIS 100 imaging system (acquisition time, 10 sec; binning, 8; filter, open; f stop, 1; FOV, 20 cm). Imaged plates were analyzed with Living Image (Caliper) and Igor (Wavemetrics) analysis software packages as described (47).

Assaying promoter activation in different pH media

Stationary phase bacteria were subcultured 1:100 into LB broth. Five to six hrs after subculturing, 10 µl of bacterial culture were added to 190 µl pre-warmed HEPES-buffered media in black 96-well plates adjusted to different pH values, and allowed to incubate for three and a half hours. Bacteria were then imaged with an IVIS 100 imaging system (acquisition time, 60 sec; binning, 8; filter, open; f stop, 1; FOV, 20 cm).

Mouse imaging studies

To generate tumor xenografts, 6-week old *nu*/*nu* mice (Taconic) were injected subcutaneously in the right flank with $1 x10^6$ B16F10 cells or $2.5 x10^6$ HCT116 cells in 100 µl PBS. Tumors were

allowed to grow for two (B16F10) or three (HCT116) weeks before bacterial challenge. Saturated cultures of strain AM3 and deletion mutant bacteria were subcultured 1:100 into LB and grown for 3 hours. Bacteria were then diluted to 1 $x10^6$ bacteria/ ml (based on OD_{600} readings) and 100 µl were injected via tail vein. Mice were imaged as indicated using an IVIS 100 imaging system (acquisition time, 60 sec; binning, 8; filter, open; f stop, 1; FOV, 20 cm). Photon flux data were calculated by utilizing user-determined regions of interest (ROIs) around bioluminescent tumors with Living Image software.

For *in vivo* promoter inducibility experiments, 6-week old *nu*/*nu* mice (Taconic) were injected subcutaneously in the right and left flanks with 1 $x10^7$ HCT116 cells in 100 µl PBS. Tumors were allowed to grow for one week. Saturated cultures of *Salmonella* strain SB300A1 containing plasmids pMAAC001, pPROMOTERLux, or pLux were subcultured 1:100 into LB and grown for 3 hours. Twenty microliters of bacterial culture were injected intratumorally. Mice were imaged as indicated using an IVIS 100 imaging system (acquisition time, 180 or 60 sec; binning, 8; filter, open; f stop, 1; FOV, 25 cm). Photon flux data were calculated by utilizing software-determined regions of interest (ROIs) around bioluminescent tumors with Living Image software.

Tumor ex vivo imaging

6-week old *nu*/*nu* mice (Taconic) were injected subcutaneously in the right flank with 1 $x10^5$ B16F10 cells and tumors allowed to grow for two and a half weeks. Saturated cultures of bacteria were diluted and 5 $x10^5$ bacteria (based on OD_{600} readings) were injected intratumorally. At 24 and 48 hours following bacterial injections, mice were sacrificed, and tumors excised and dissected into 4 sections each. The bacterial-colonized tumor sections were incubated in

HEPES/Tris-buffered media at the indicated pH values and imaged using an IVIS 100 imaging system at the indicated times (acquisition time, 180 sec; binning, 8; filter, open; f stop, 1; FOV, 12 cm).

In vitro toxicity assays

Confluent HeLa cells or mock media alone (DMEM + 10% FBS) were inoculated at 1:100 with a stationary culture of SB300A1 transformed with P1787 or P1787-Stx2A/B and cultured at 37 °C for 18 hours. The cultured media was then separately filtered through a 0.22 μm filter to remove the bacteria and subsequently aliquoted at various volumes onto HeLa$^{CMV\text{-}FLuc}$ cells pre-plated in a 96 well plate in quintuplicate. 24 hours later, bioluminescence of the conditioned media-treated HeLa$^{CMV\text{-}FLuc}$ cells was imaged using an IVIS 100. Phase contrast microscopy (TMS-F, Nikon) was used in parallel to qualitatively confirm loss of cell viability.

In vivo toxicity assays

6 week old male homozygous CrTac:NCr-*Foxn1*^{nu} mice (Taconic) were subcutaneously injected in the right flank with of 4.5 x 10^6 HeLa$^{CMV\text{-}FLuc}$ cells in 20 μL DMEM. When tumor volumes reached approximately 100 mm^2 (5 days later), mice were injected i.p. with 150mg/ kg of D-luciferin and 10 minutes later imaged using an IVIS 100. Immediately following imaging, mice were injected intratumorly with LB broth, or SB300A1 transformed with P1787, or SB300A1 transformed with P1787-STx2A/B at either 2.5 x10^5 (low-dose) or 2 x 10^6 (high-dose) CFU/ injection. Mice (n= 9-14 in each group) were weighed and imaged for bioluminescence every five days for 2 weeks. Viable tumor mass is presented as fold-initial photon flux (pre-treatment/ post-treatment).

Histology

Tumors were excised and immediately frozen at -80°C. Frozen tumors were fixed in 10% neutral buffered formalin for 24 hours. Prior to paraffin embedding, histology sectioning and H&E staining, fixed tumors were washed with 30%, 50% and then 70% ethanol for 5 minutes each.

Statistics: Error bars represent the standard error of the linearly regressed data or the standard error of the mean where noted.

Acknowledgements

The authors thank colleagues of the Molecular Imaging Center for helpful discussions and Reece Goiffon for statistical assistance and David Haslam for the Stx2 plasmid. This study was supported in part by a grant from the National Institutes of Health to the Molecular Imaging Center at Washington University (P50 CA94056), NIH Training Grants T32 GM007067 for stipend support to K.F. and T32 CA113275 for stipend support to B.K., and The Siteman Cancer Center supported in part by a NCI Cancer Center Support Grant (P30 CA91842).

B.3 References

1. Ellis, M., Ding, L., Shen, D., Luo, J., Suman, V., Wallis, J., et al. Whole genome sequencing to characterise breast cancer response to aromatase inhibition Nature, 2012, in press.

2. Cairns, R., Papandreou, I., and Denko, N. Overcoming physiologic barriers to cancer treatment by molecularly targeting the tumor microenvironment. Mol Cancer Res, *4:* 61-70, 2006.

3. Hanahan, D. and Weinberg, R. A. Hallmarks of cancer: the next generation. Cell, *144:* 646-674, 2011.

4. Gardlik, R., Behuliak, M., Palffy, R., Celec, P., and Li, C. J. Gene therapy for cancer: bacteria-mediated anti-angiogenesis therapy. Gene Ther, *18:* 425-431, 2011.
5. Forbes, N. S. Engineering the perfect (bacterial) cancer therapy. Nat Rev Cancer, *10:* 785-794, 2010.

6. Forbes, N. S., Munn, L. L., Fukumura, D., and Jain, R. K. Sparse initial entrapment of systemically injected Salmonella typhimurium leads to heterogeneous accumulation within tumors. Cancer Res, *63:* 5188-5193, 2003.

7. Zhao, M., Yang, M., Li, X. M., Jiang, P., Baranov, E., Li, S., et al. Tumor-targeting bacterial therapy with amino acid auxotrophs of GFP-expressing Salmonella typhimurium. Proc Natl Acad Sci U S A, *102:* 755-760, 2005.

8. Ganai, S., Arenas, R. B., Sauer, J. P., Bentley, B., and Forbes, N. S. In tumors Salmonella migrate away from vasculature toward the transition zone and induce apoptosis. Cancer Gene Ther, *18:* 457-466, 2011.

9. Kasinskas, R. W. and Forbes, N. S. Salmonella typhimurium lacking ribose chemoreceptors localize in tumor quiescence and induce apoptosis. Cancer Res, *67:* 3201-3209, 2007.

10. Martinon, F., Mayor, A., and Tschopp, J. The inflammasomes: guardians of the body. Annu Rev Immunol, *27:* 229-265, 2009.

11. Garaude, J., Kent, A., van Rooijen, N., and Blander, J. M. Simultaneous targeting of toll- and nod-like receptors induces effective tumor-specific immune responses. Sci Transl Med, *4:* 120ra116, 2012.

12. O'Neill, L. A. and Bowie, A. G. The family of five: TIR-domain-containing adaptors in Toll-like receptor signalling. Nat Rev Immunol, *7:* 353-364, 2007.

13. Pawelek, J. M., Low, K. B., and Bermudes, D. Bacteria as tumour-targeting vectors. Lancet Oncol, *4:* 548-556, 2003.

14. McKinney, J., Guerrier-Takada, C., Galan, J., and Altman, S. Tightly regulated gene expression system in Salmonella enterica serovar Typhimurium. J Bacteriol, *184:* 6056-6059, 2002.

15. Levano-Garcia, J., Verjovski-Almeida, S., and da Silva, A. C. Mapping transposon insertion sites by touchdown PCR and hybrid degenerate primers. Biotechniques, *38:* 225-229, 2005.

16. Kieboom, J. and Abee, T. Arginine-dependent acid resistance in Salmonella enterica serovar Typhimurium. J Bacteriol, *188:* 5650-5653, 2006.

17. The universal protein resource (UniProt). Nucleic Acids Res, *36:* D190-195, 2008.
18. Tannock, I. F. and Rotin, D. Acid pH in tumors and its potential for therapeutic exploitation. Cancer Res, *49:* 4373-4384, 1989.

19. Vander Heiden, M. G., Cantley, L. C., and Thompson, C. B. Understanding the Warburg effect: the metabolic requirements of cell proliferation. Science, *324:* 1029-1033, 2009.

20. Low, K. B., Ittensohn, M., Le, T., Platt, J., Sodi, S., Amoss, et al. Lipid A mutant Salmonella with suppressed virulence and TNFalpha induction retain tumor-targeting in vivo. Nat Biotechnol, *17:* 37-41, 1999.

21. O'Loughlin, E. V. and Robins-Browne, R. M. Effect of Shiga toxin and Shiga-like toxins on eukaryotic cells. Microbes Infect, *3:* 493-507, 2001.

22. Engedal, N., Skotland, T., Torgersen, M. L., and Sandvig, K. Shiga toxin and its use in targeted cancer therapy and imaging. Microb Biotechnol, *4:* 32-46, 2011.

23. Pawelek, J. M., Low, K. B., and Bermudes, D. Tumor-targeted Salmonella as a novel anticancer vector. Cancer Res, *57:* 4537-4544, 1997.

24. Yu, Y. A., Shabahang, S., Timiryasova, T. M., Zhang, Q., Beltz, R., Gentschev, I., et al. Visualization of tumors and metastases in live animals with bacteria and vaccinia virus encoding light-emitting proteins. Nat Biotechnol, *22:* 313-320, 2004.

25. Dang, L. H., Bettegowda, C., Huso, D. L., Kinzler, K. W., and Vogelstein, B. Combination bacteriolytic therapy for the treatment of experimental tumors. Proc Natl Acad Sci U S A, *98:* 15155-15160, 2001.

26. Dang, L. H., Bettegowda, C., Agrawal, N., Cheong, I., Huso, D., Frost, P., et al. Targeting vascular and avascular compartments of tumors with C. novyi-NT and anti-microtubule agents. Cancer Biol Ther, *3:* 326-337, 2004.

27. Weibel, S., Stritzker, J., Eck, M., Goebel, W., and Szalay, A. A. Colonization of experimental murine breast tumours by Escherichia coli K-12 significantly alters the tumour microenvironment. Cell Microbiol, *10:* 1235-1248, 2008.

28. Stritzker, J., Weibel, S., Hill, P. J., Oelschlaeger, T. A., Goebel, W., and Szalay, A. A. Tumor-specific colonization, tissue distribution, and gene induction by probiotic Escherichia coli Nissle 1917 in live mice. Int J Med Microbiol, *297:* 151-162, 2007.

29. Agrawal, N., Bettegowda, C., Cheong, I., Geschwind, J. F., Drake, C. G., Hipkiss, E. L., et al. Bacteriolytic therapy can generate a potent immune response against experimental tumors. Proc Natl Acad Sci U S A, *101:* 15172-15177, 2004.

30. Bettegowda, C., Foss, C. A., Cheong, I., Wang, Y., Diaz, L., Agrawal, N., et al. Imaging bacterial infections with radiolabeled 1-(2'-deoxy-2'-fluoro-beta-D-arabinofuranosyl)-5-iodouracil. Proc Natl Acad Sci U S A, *102:* 1145-1150, 2005.

31. Hajitou, A., Trepel, M., Lilley, C. E., Soghomonyan, S., Alauddin, M. M., Marini, F. C., 3rd, et al. A hybrid vector for ligand-directed tumor targeting and molecular imaging. Cell, *125:* 385-398, 2006.

32. Zhao, M., Yang, M., Ma, H., Li, X., Tan, X., Li, S., et al. Targeted therapy with a Salmonella typhimurium leucine-arginine auxotroph cures orthotopic human breast tumors in nude mice. Cancer Res, *66:* 7647-7652, 2006.

33. Leschner, S., Deyneko, I. V., Lienenklaus, S., Wolf, K., Bloecker, H., Bumann, D., et al. Identification of tumor-specific Salmonella Typhimurium promoters and their regulatory logic. Nucleic Acids Res, 2011.

34. Leschner, S. and Weiss, S. Salmonella-allies in the fight against cancer. J Mol Med (Berl), *88:* 763-773, 2010.

35. Toso, J. F., Gill, V. J., Hwu, P., Marincola, F. M., Restifo, N. P., Schwartzentruber, D. J., et al. Phase I study of the intravenous administration of attenuated Salmonella typhimurium to patients with metastatic melanoma. J Clin Oncol, *20:* 142-152, 2002.

36. Heimann, D. M. and Rosenberg, S. A. Continuous intravenous administration of live genetically modified salmonella typhimurium in patients with metastatic melanoma. J Immunother, *26:* 179-180, 2003.

37. Leschner, S., Westphal, K., Dietrich, N., Viegas, N., Jablonska, J., Lyszkiewicz, M., et al. Tumor invasion of Salmonella enterica serovar Typhimurium is accompanied by strong hemorrhage promoted by TNF-alpha. PLoS One, *4:* e6692, 2009.

38. Arrach, N., Zhao, M., Porwollik, S., Hoffman, R. M., and McClelland, M. Salmonella promoters preferentially activated inside tumors. Cancer Res, *68:* 4827-4832, 2008.

39. Hayes, E. T., Wilks, J. C., Sanfilippo, P., Yohannes, E., Tate, D. P., Jones, B. D., et al. Oxygen limitation modulates pH regulation of catabolism and hydrogenases, multidrug transporters, and envelope composition in Escherichia coli K-12. BMC Microbiol, *6:* 89, 2006.

40. Ibarra, J. A. and Steele-Mortimer, O. Salmonella--the ultimate insider. Salmonella virulence factors that modulate intracellular survival. Cell Microbiol, *11:* 1579-1586, 2009.

41. Foster, J. W. and Spector, M. P. How Salmonella survive against the odds. Annu Rev Microbiol, *49:* 145-174, 1995.

42. Gerweck, L. E. and Seetharaman, K. Cellular pH gradient in tumor versus normal tissue: potential exploitation for the treatment of cancer. Cancer Res, *56:* 1194-1198, 1996.

43. Muller, B., Fischer, B., and Kreutz, W. An acidic microenvironment impairs the generation of non-major histocompatibility complex-restricted killer cells. Immunology, *99:* 375-384, 2000.

44. Mukhopadhyay, S. and Linstedt, A. D. Manganese blocks intracellular trafficking of Shiga toxin and protects against Shiga toxicosis. Science, *335:* 332-335, 2012.

45. Flentie, K. N., Qi, M., Gammon, S. T., Razia, Y., Lui, F., Marpegan, L., et al. Stably integrated *luxCDABE* for assessment of *Salmonella* invasion kinetics. Mol Imaging, *7:* 222-233, 2008.

46. Pfeifer, C. G., Marcus, S. L., Steele-Mortimer, O., Knodler, L. A., and Finlay, B. B. Salmonella typhimurium virulence genes are induced upon bacterial invasion into phagocytic and nonphagocytic cells. Infect Immun, *67:* 5690-5698, 1999.

47. Gross, S. and Piwnica-Worms, D. Real-time imaging of ligand-induced IKK activation in intact cells and in living mice. Nat Methods, *2:* 607-614, 2005.

48. Rasband, W. ImageJ. 1.3.1_03 edition. Bethesda, Maryland: National Institutes of Health, 2005.

49. Zhang, X. D., Yang, X. C., Chung, N., Gates, A., Stec, E., Kunapuli, P., et al. Robust statistical methods for hit selection in RNA interference high-throughput screening experiments. Pharmacogenomics, *7:* 299-309, 2006.

50. Datsenko, K. A. and Wanner, B. L. One-step inactivation of chromosomal genes in Escherichia coli K-12 using PCR products. Proc Natl Acad Sci U S A, *97:* 6640-6645, 2000.

B.4 Figures

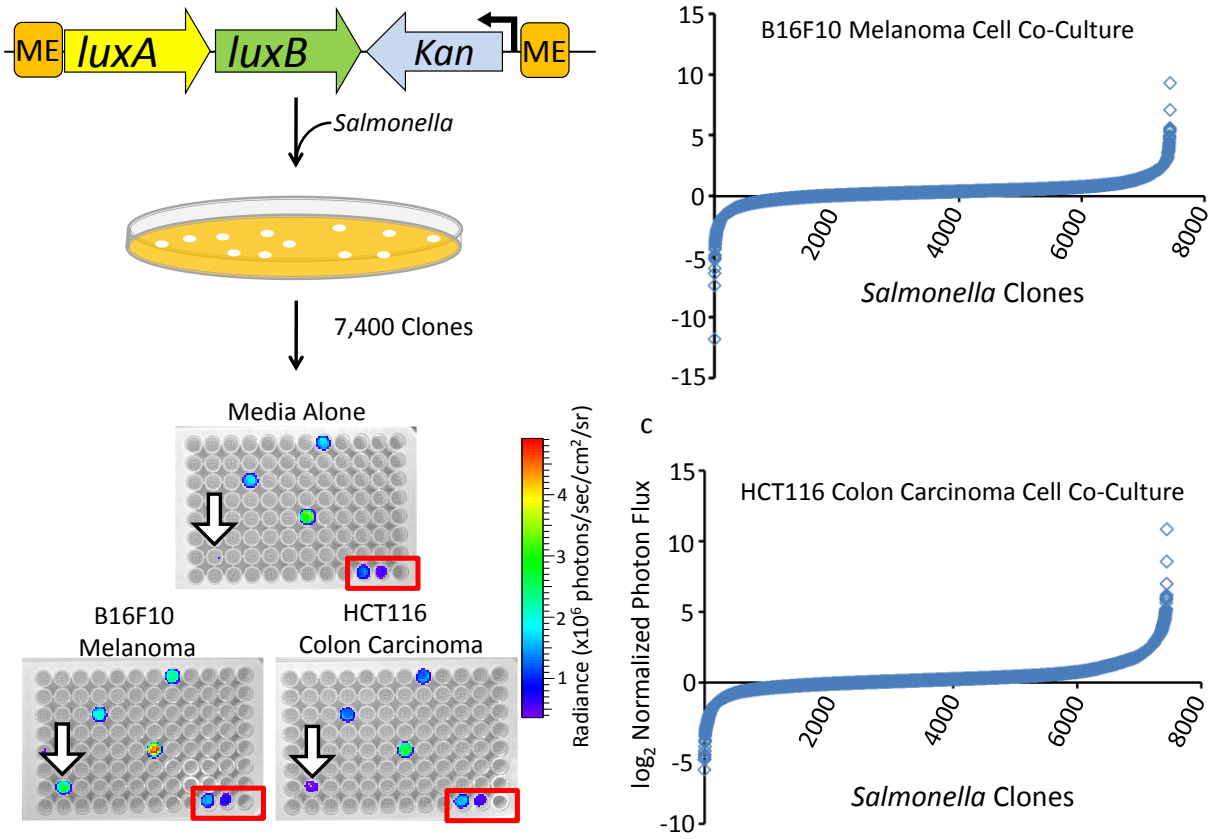

Figure 1. **Design and utilization of a high throughput screen to identify tumor cell-induced gene activation events in *Salmonella*.** (A) A schematic of the promoter trap system using Tn5-based *luxAB* chromosomal integration. Expression of the promoterless *luxAB* reporter vector, and resulting *Salmonella* bioluminescence, is dependent on "trapping" an active promoter upstream of the chromosomal integration site. The transposon was randomly integrated into strain SB300A1, and kanamycin-resistant colonies were selected and arrayed into 96-well plates for library screening. *Continued on next page*

Representative primary screening plates in triplicate show responses of *Salmonella* library strains to three separate co-culture conditions: media alone (top), B16F10 melanoma cells (bottom left), HCT116 colon carcinoma cells (bottom right). Hit 47.74, showing selective activation in co-culture with cancer cells, is indicated by the black open arrowhead, while the signals in the upper and central wells represent non-selective activation of clones. In each plate, wells H10, H11, and H12 (red box) contain media and bacteria constitutively expressing *luxCDABE*, bacteria constitutively expressing *luxAB*, and no bacteria, respectively, as controls. Primary library screening data from *Salmonella* promoter trap clones co-cultured with B16F10 melanoma cells (B) or HCT116 colon carcinoma cells (C). Data are reported as the $\log_2$ of the normalized signal for each library clone, where normalized signal was the ratio of the signal in the condition of interest to the signal in media alone.

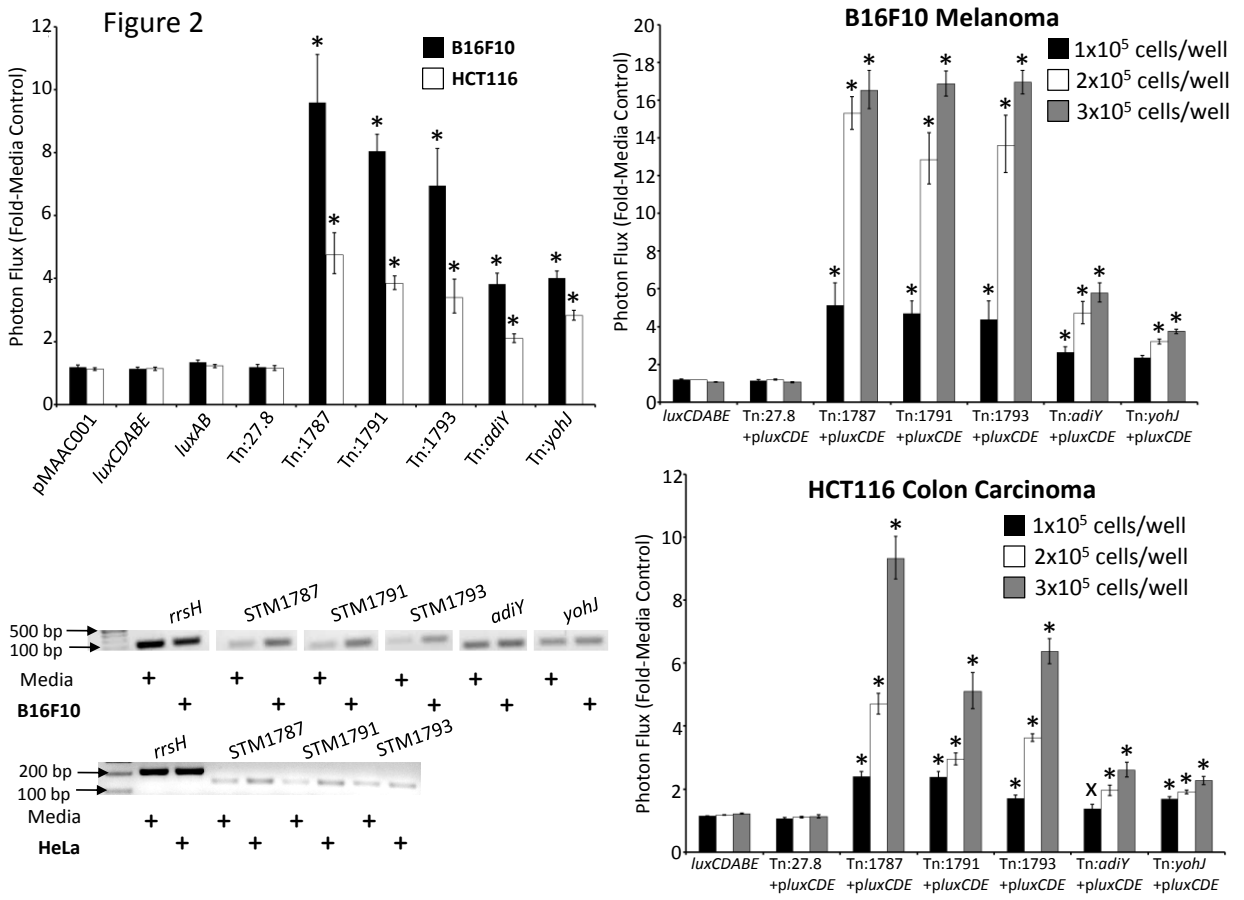

Figure 2. Verification of *Salmonella* gene activation events in the context of tumor cell co-culture. (A) *Salmonella* reporter clones displaying gene activation signals during co-culture with tumor cell lines (black bars, B16F10 cells; open bars, HCT116 cells). *Salmonella* strains *luxAB* and Tn:27.8 contain chromosomal *luxAB* genes under constitutive promoter control; *luxCDABE* *Salmonella* contain the full luciferase operon inserted into the chromosome; pMAAC001 constitutively expresses plasmid-encoded *luxCDABE*. (B, C) *Salmonella* reporter clones display dose-responsive gene activation in co-culture with B16F10 and HCT116 cells. Bacteria were co-cultured with $1x10^5$, $2x10^5$, or $3x10^5$ B16F10 or HCT116 cells/well. Data were normalized as the ratio of the signal in the condition of interest to signal in media alone. (*Continued on next page*)

Error bars correspond to SEM. All *p* value calculations are between *luxCDABE* and the group indicated by the symbol: * $p \leq 1x10^{-7}$; $^{x}p \leq 0.06$. (D) Semi-quantitative reverse transcriptase PCR with wild-type SB300A1 bacteria verifies that genes identified by the reporter transposon screen in *Salmonella* are activated during co-culture with B16F10 melanoma and HeLa tumor cells. *rrsH* = ribosomal RNA.

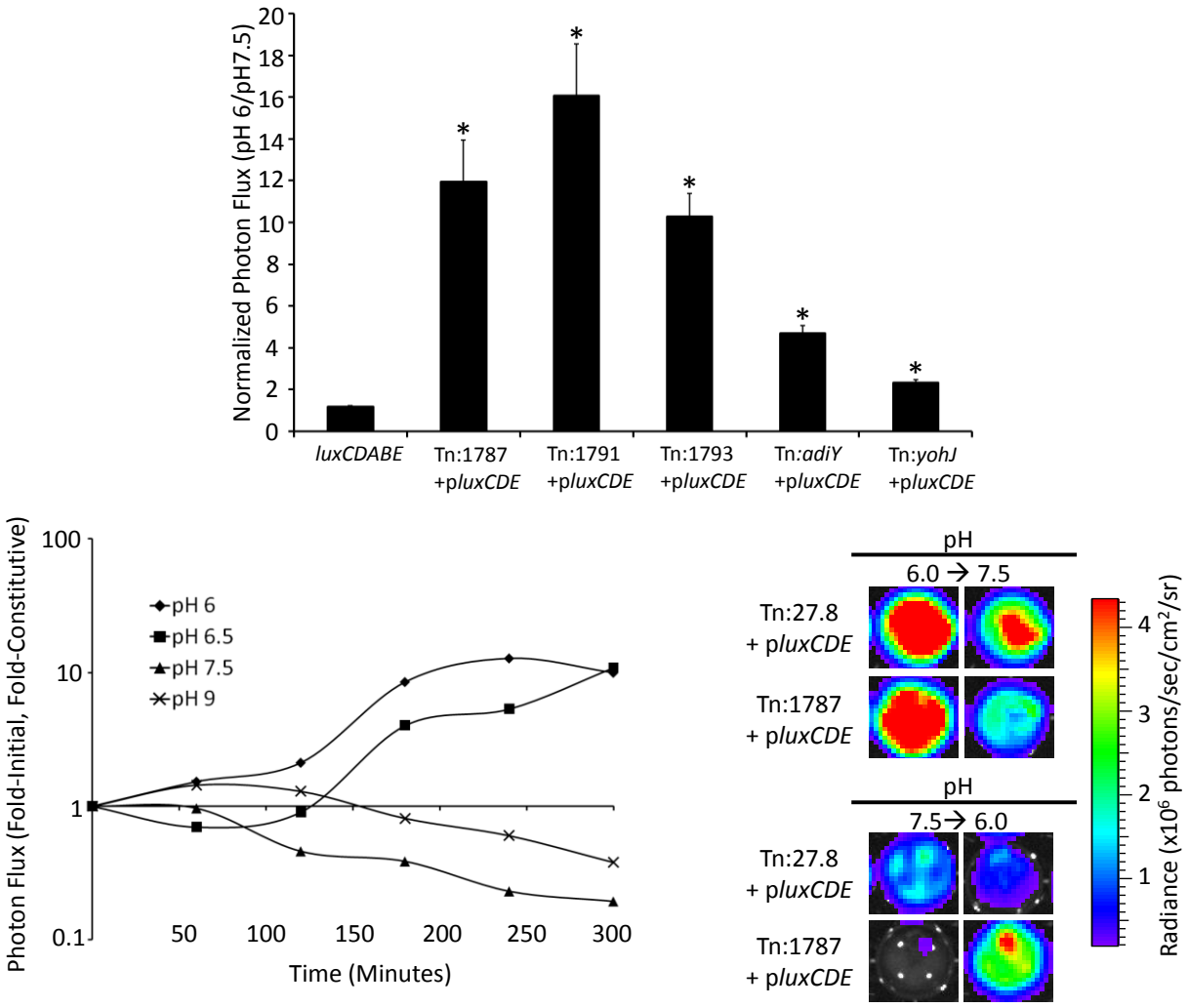

Figure 3. Acidic pH specifically and reversibly stimulates the Tn:1787 trapped promoter. (A) Bacteria were cultured in media of different pH values and reporter activation by *Salmonella* library clones in low pH media (pH 6) were compared to reporter activation in normal pH (7.5). Genes identified in the tumor cell co-culture screen were activated in the context of acidic pH compared to pH 7.5. pMAAC001 and *luxCDABE* constitutively express plasmid-encoded and chromosomally-encoded *luxCDABE*, respectively. Data were normalized as the ratio of the signal in media pH 6.0 to signal in media pH 7.5. Error bars correspond to standard error. (*Continued on next page*)

The data show one representative experiment with 4 replicates per condition tested. All *p*-value calculations are between *luxCDABE* and the group indicated by the asterisk, $*p \leq 2x10^{-14}$. (B) Mice bearing B16F10 flank tumor xenografts were injected intratumorally with tumor-activated (Tn:1787+p*luxCDE*) or constitutively bioluminescent (Tn:27.8+p*luxCDE*) *Salmonella*. The excised tumors were imaged hourly and data are presented as the normalized signal at each time point. The normalized signal represents the ratio of the mean of the fold-initial signal of two Tn:1787+p*luxCDE*-colonized tumors to the mean of the fold-initial signal of two constitutive Tn:27.8+p*luxCDE*-colonized tumors. The data presented are from a representative experiment; the experiment was performed independently two times, each with two mice per bacterial treatment group. (C) Representative *ex vivo* tumor imaging shows reversibility of the bioluminescent signal in the tumor-activated *Salmonella*. Images on the left show *Salmonella*-infected tumor explants after 6 hours of incubation at the indicated pH (pH 6.0, top; pH 7.5, bottom). Two hours later (8 hours total), media was removed and replaced with media of the indicated pH (pH 7.5, top; pH 6.0, bottom). Images on the right show *Salmonella*-infected tumor explants 4 hours after the pH of the media was changed.

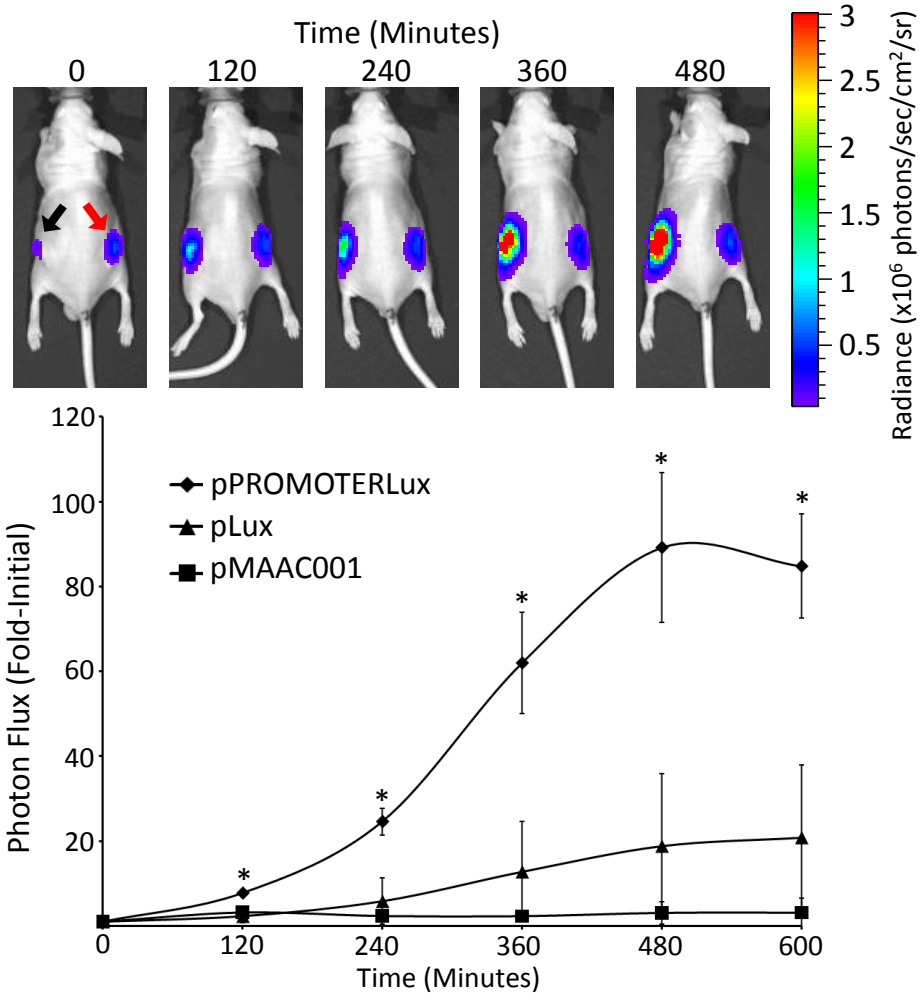

Figure 4. The *STM1787* promoter in *Salmonella* is rapidly activated *in vivo* by the tumor microenvironment. (A) A representative mouse with two HCT116 flank tumor xenografts. The left tumor (black arrow) was injected with *STM1787* p*PROMOTERLux*-expressing *Salmonella*, while the right tumor (red arrow) was injected with constitutive p*MAAC001*-expressing *Salmonella*, and the mouse imaged at the indicated times post-injection. (B) The mean photon flux for each set of *Salmonella*-injected tumors, normalized to the initial signal in each tumor, plotted as a function of time. Error bars represent SEM; p*PROMOTERLux* (n=6); p*Lux* (n=3); p*MAAC001* (n=3), *p<0.025

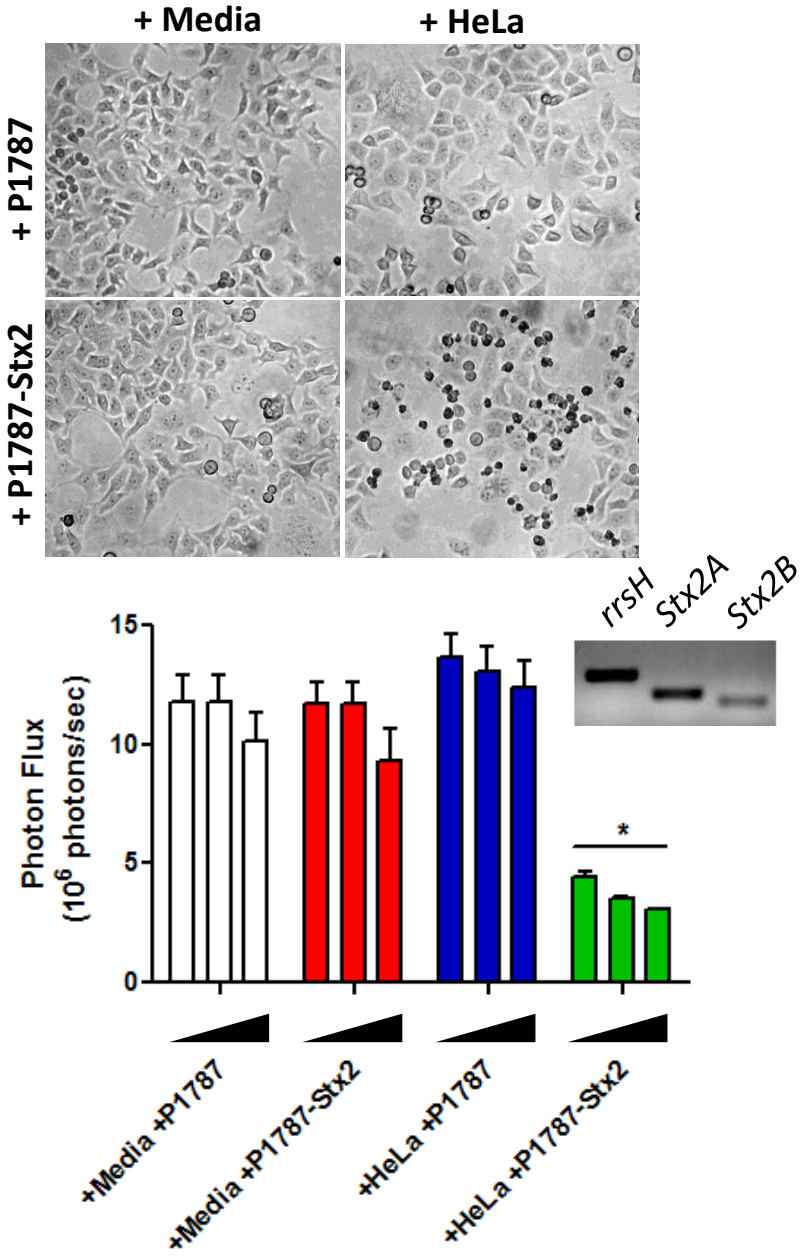

Figure 5. P1787-driven Stx2 cytoxicity is selectively activated by the cancer cell environment *in vitro*. (A) Representative brightfield microscopy of HeLa$^{CMV\text{-}FLuc}$ cells treated with 4 different conditioned, filtered media for 24 hours (+media+P1787; +media+P1787-Stx2; +HeLa+P1787; and +HeLa+P1787-Stx2). (*Continued on next page*)

Note the dramatic membrane blebbing and apoptotic morphology of +HeLa+P1787-Stx2 conditioned media-treated cells. (B) Bioluminescence imaging of HeLa$^{CMV\text{-}FLuc}$ cells treated with increasing amounts of 4 different conditioned, filtered media for 24 hours (bar groups, left to right: 17%, 29%, 44% of total volume per well). *$p<0.0005$ compared to all other treatments. *Inset* represents PCR amplification of *Stx2A/B* mRNA from P1787-Stx2 transformed SB300A1 co-cultured with HeLa cells.

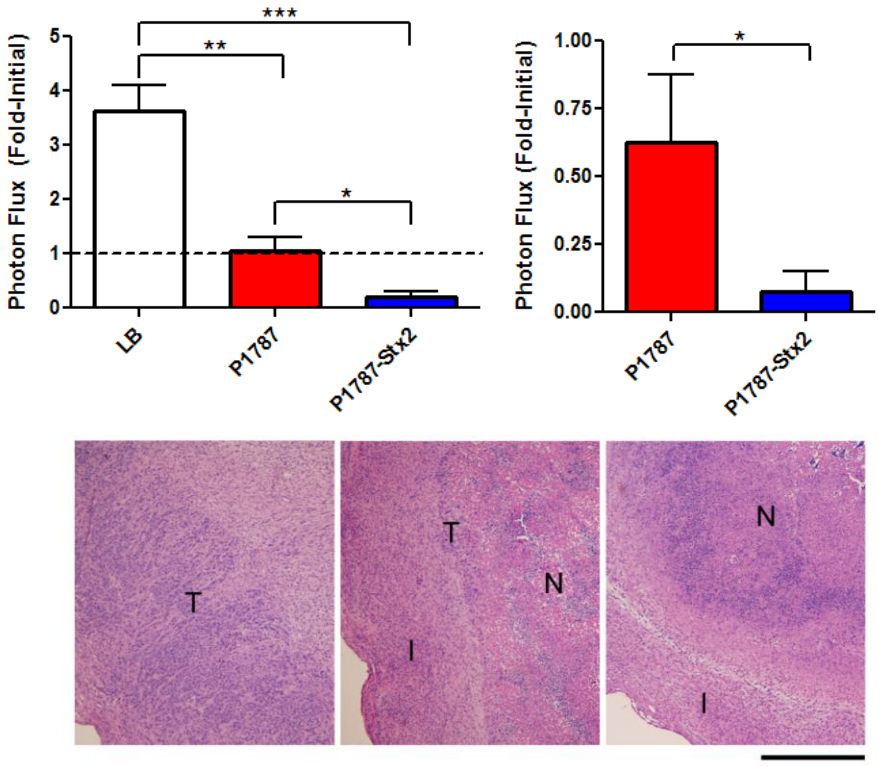

Figure 6. Enhanced anti-tumor response with P1787-Stx2 *in vivo*. (A) Viable cell mass of HeLa$^{CMV\text{-}FLuc}$ tumors from mice treated with LB (n = 14), or high-dose SB300A1 transformed with P1787 (n= 12) or P1787-Stx2 (n = 9) at five days post treatment. Results are combined from two independent experiments and presented as fold-initial photon flux. Dotted line demarks lack of fold-change in tumor bioluminescence. Error bars indicate standard error of the mean ***p<0.0002,**p<0.0003, *p<0.007). (B) Fold-initialized photon flux of HeLa$^{CMV\text{-}FLuc}$ tumors from mice treated with low-dose SB300A1 transformed with P1787 (n= 7) or P1787-Stx2 (n = 7) at 14 days post treatment. Error bars indicate standard error of the mean.*p <0.04. (C) H&E staining of HeLa$^{CMV\text{-}FLuc}$ tumors from mice treated with LB (left), or high-dose SB300A1 transformed with P1787 (middle) or SB300A1 transformed with P1787-Stx2 (right) after five days. Regions of tumor are denoted as tumor (T), fibroinflammatory reaction (I), and necrotic zone (N). Scale bar, 500 µm.

B.5 Table

Table 1. Transposon chromosomal insertion locations in *Salmonella* reporter mutants.

Strain Name	**Transposon Insertion Location**	**Base pairs Downstream of Start Codon**	**Function (Putative) (17)**
Tn:1787	*STM1787*	1,189	Hydrogenase
Tn:1791	*STM1791*	505	Hydrogenase
Tn:1793	*STM1793*	661	Cytochrome oxidase
Tn:adiY	*adiY*	439	araC-like transcriptional activator; arginine-dependent acid tolerance
Tn:yohJ	*yohJ*	205	Hypothetical membrane protein

B.6 Supplementary Figure

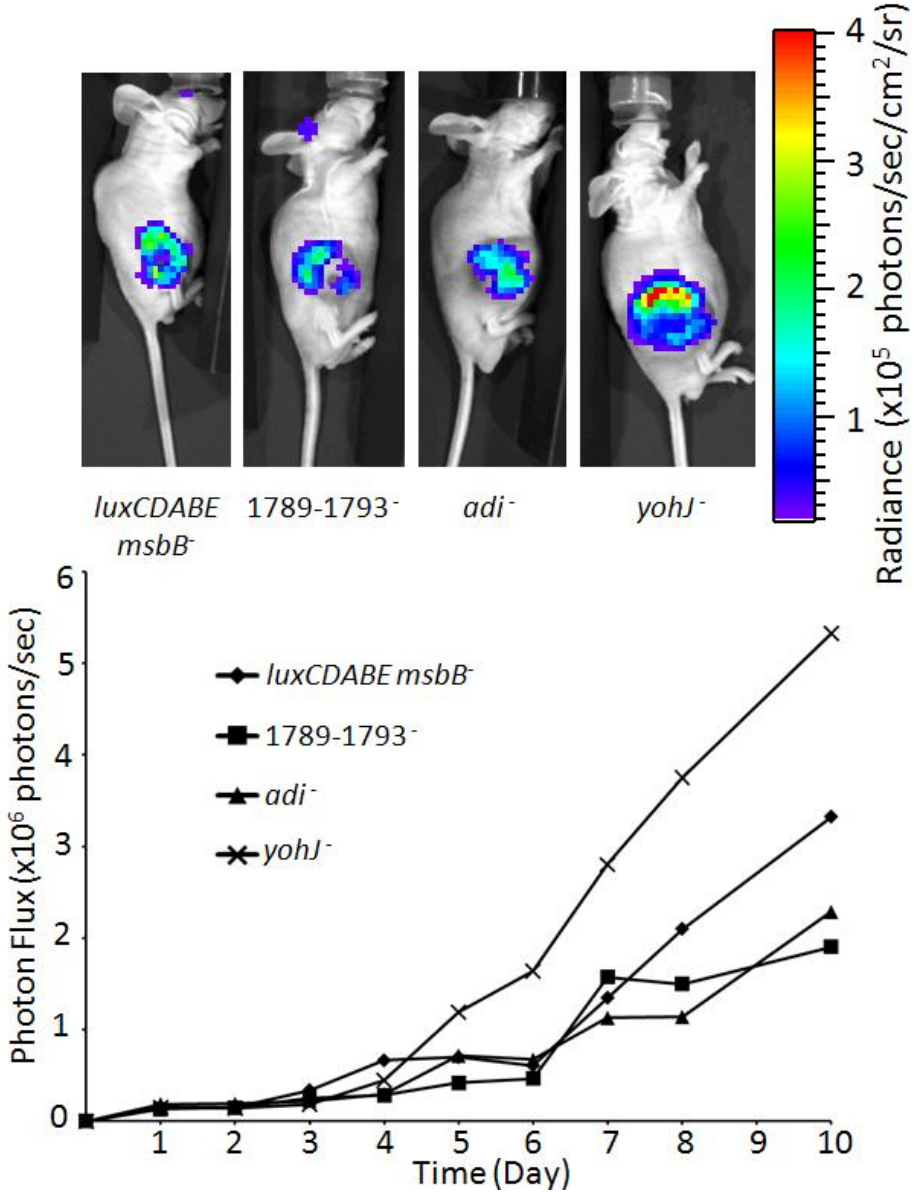

Supplemental Figure 1. Activated genes are not essential for *Salmonella* tumor localization. Mice bearing B16F10 flank tumor xenografts were injected intravenously with constitutively bioluminescent gene-deleted *Salmonella*. (A) Representative mice on day 10 post *Salmonella* injection. (B) Bioluminescent photon flux of the four mice depicted in (A) as a function of time following intravenous injection of bacteria.

B.7 Supplementary Table

Supplementary Table I. Tumor localization of constitutively bioluminescent *Salmonella* mutants.

Mutant	**Number of Mice with Bioluminescent, Colonized Tumors/Total Mice Injected (HCT116 Tumors)**	**Number of Mice with Bioluminescent, Colonized Tumors/Total Mice Injected (B16F10 Tumors)**	**Totals**
luxCDABE	2/3	3/4	5/7
STM1789-1793	2/3	2/5	4/8
adi	1/2	4/5	5/7
yohJ	3/3	3/5	6/8